

# Black-hole binaries, gravitational waves, and numerical relativity

Joan Centrella\* and John G. Baker†

*Gravitational Astrophysics Laboratory, NASA/GSFC, 8800 Greenbelt Road, Greenbelt, Maryland 20771, USA*

Bernard J. Kelly‡ and James R. van Meter§

*CRESST and Gravitational Astrophysics Laboratory, NASA/GSFC, 8800 Greenbelt Road, Greenbelt, Maryland 20771, USA and*

*Department of Physics, University of Maryland, Baltimore County, 1000 Hilltop Circle, Baltimore, Maryland 21250, USA*

(Dated: November 30, 2010)

Understanding the predictions of general relativity for the dynamical interactions of two black holes has been a long-standing unsolved problem in theoretical physics. Black-hole mergers are monumental astrophysical events, releasing tremendous amounts of energy in the form of gravitational radiation, and are key sources for both ground- and space-based gravitational-wave detectors. The black-hole merger dynamics and the resulting gravitational waveforms can only be calculated through numerical simulations of Einstein's equations of general relativity. For many years, numerical relativists attempting to model these mergers encountered a host of problems, causing their codes to crash after just a fraction of a binary orbit could be simulated. Recently, however, a series of dramatic advances in numerical relativity has allowed stable, robust black-hole merger simulations. This remarkable progress in the rapidly maturing field of numerical relativity, and the new understanding of black-hole binary dynamics that is emerging is chronicled. Important applications of these fundamental physics results to astrophysics, to gravitational-wave astronomy, and in other areas are also discussed.

## Contents

<b>I. Prelude</b>	2	<b>G. Numerical Approximation Methods</b>	15
<b>II. Black-Hole Binaries and Gravitational Waves</b>	2	<b>H. Extracting the Physics</b>	15
A. Basic Properties	3	<b>V. Black-Hole Merger Dynamics and Waveforms</b>	16
1. Black-Hole Basics	3	A. First Glimpses of the Merger: The Lazarus Approach	16
2. Gravitational Wave Primer	3	B. Mergers of Equal-Mass, Nonspinning Black Holes	17
B. Astrophysical Black Holes	4	1. The First Merger Waveforms	17
C. Gravitational Waves from Black-Hole Binaries	5	2. Universal Waveform	18
<b>III. Historical Overview</b>	5	3. Longer Waveforms	20
A. Setting the Stage	5	C. Mergers of Unequal-Mass, Nonspinning Black Holes	22
B. Numerical Relativity Milestones	6	1. Mode Analysis and Gravitational Waveforms	22
C. Breakthroughs and the Gold Rush	7	2. A Qualitatively New Feature: Kicks	23
<b>IV. Numerical Development</b>	8	D. Mergers of Spinning Black Holes	24
A. Einstein's Equations	8	1. Gravitational Waveforms	25
B. The Cauchy Problem	8	2. Spinning Binary Mergers and Spin Flips	25
C. Representing Black Holes in Numerical Spacetimes	9	3. Kicks from Mergers of Spinning Black Holes	26
D. Initial Data	10	<b>VI. Interaction of Numerical Relativity with Post-Newtonian Theory</b>	27
E. Numerically Friendly Formulations of the Evolution Equations	11	A. Independent Post-Newtonian Dynamics and Waveforms	28
1. Hyperbolicity and Well-Posedness	12	B. Analytic Full-Waveform Models	30
2. Harmonic Formulations	12	C. Post-Newtonian Models for Numerical Initial Data.	32
3. ADM-based Formulations	12	D. Post-Newtonian Theory for Interpretation of Numerical Results.	32
F. Gauge Conditions	13	<b>VII. Applications to Gravitational Wave Data Analysis</b>	33
1. Choosing the Slicing and Shift	13	A. The Direct Impact of Merger Waveforms in Data Analysis	35
2. Moving Punctures	13	B. Developing Analytic Inspiral-Merger-Ringdown Gravitational Waveform Templates	37
3. Generalized Harmonic Coordinates	14	C. Using Numerical Waveforms in Data Analysis Applications	38
4. Other Coordinate Techniques	14	<b>VIII. Impact on Astrophysics</b>	39
		A. Recoiling Black Holes	39
		1. Predicting the Recoil	39
		2. Consequences of Black Hole Recoil	40
		B. The Spin of the Final Black Hole	40

\*Electronic address: Joan.Centrella@nasa.gov

†Electronic address: John.G.Baker@nasa.gov

‡Electronic address: Bernard.J.Kelly@nasa.gov

§Electronic address: James.R.vanMeter@nasa.gov

C. Electromagnetic Counterparts of Black Hole Mergers	41
1. Astrophysical Considerations	41
2. Simulations with Magnetic Fields or Gas near the Merging Holes	41
<b>IX. Frontiers and Future Directions</b>	43
A. Gravitational-Wave Astronomy	43
B. Other Astrophysics	43
C. Other Physics	44
D. Strong Gravity as Observational Science	44
<b>Acknowledgments</b>	45
<b>References</b>	45

## I. PRELUDE

The final merger of two black holes in a binary system releases more power than the combined light from all the stars in the visible Universe. This vast energy comes in the form of gravitational waves, which travel across the Universe at the speed of light, bearing the waveform signature of the merger. Today, ground-based gravitational-wave detectors stand poised to detect the mergers of stellar black-hole binaries, the corpses of massive stars. In addition, planning is underway for a space-based detector that will observe the mergers of massive black holes, awesome behemoths at the centers of galaxies, with masses of  $\sim (10^4 - 10^9)M_\odot$ , where  $M_\odot$  is the mass of the Sun. Since template matching forms the basis of most gravitational-wave data analysis, knowledge of the merger waveforms is crucial.

Calculating these waveforms requires solving the full Einstein equations of general relativity on a computer in three spatial dimensions plus time. As you might imagine, this is a formidable task. In fact, numerical relativists have attempted to solve this problem for many years, only to encounter a host of puzzling instabilities causing the computer codes to crash before they could compute any sizable portion of a binary orbit. Remarkably, in the past few years a series of dramatic breakthroughs has occurred in numerical relativity (NR), yielding robust and accurate simulations of black-hole mergers for the first time.

In this article, we review these breakthroughs and the wealth of new knowledge about black-hole mergers that is emerging, highlighting key applications to astrophysics and gravitational-wave data analysis. We focus on comparable-mass black-hole binaries, with component mass ratios  $1 \leq q \leq 10$ , where  $q = M_1/M_2$  and  $M_1, M_2$  are the individual black-hole masses. We will frequently also refer to the *symmetric mass ratio*

$$\eta \equiv \frac{M_1 M_2}{(M_1 + M_2)^2} = \frac{q}{(1+q)^2}. \quad (1)$$

For simplicity, we choose to set  $c = 1$  and  $G = 1$ ; with this, we can scale the dynamics and waveforms for black-hole binaries with the total system mass  $M$ . In particular, we can express both length and time scales in terms of the mass, giving  $M \sim 5 \times 10^{-6} M/M_\odot \sim 1.5 M/M_\odot \text{ km}$ .

We begin by setting both the scientific and historical contexts. In Sec. II we provide a brief overview of astrophysical black-hole binaries as sources for gravitational-wave detectors. We next turn to a historical overview in Sec. III, surveying efforts to evolve black-hole mergers on computers, spanning more than four decades and culminating with the recent triumphs. Having thus set the stage, we focus on more in-depth discussions of the key components underlying successful black-hole merger simulations, discussing computational methodologies in Sec. IV, including numerical-relativity techniques and black-hole binary initial data. Section V is the heart of this review. Here we discuss the key results from numerical relativity simulations of black-hole mergers, following a historical development and concentrating on the merger dynamics and the resulting gravitational waveforms. These results have opened up a variety of exciting applications in general relativity, gravitational waves, and astrophysics. We discuss synergistic interactions between numerical relativity and analytic approaches to modeling gravitational dynamics and waveforms in Sec. VI, and applications of the results to gravitational-wave data analysis in Sec. VII. The impact of merger simulations on astrophysics is presented in Sec. VIII, which includes discussions of recoiling black holes and potential electromagnetic signatures of the final merger. We conclude with a look at the frontiers and future directions of this field in Sec. IX.

Before we begin, we mention several other resources that may interest our readers. The review articles by Lehner (2001) and Baumgarte and Shapiro (2003) provide interesting surveys of numerical relativity several years before the breakthroughs in black-hole merger simulations. The article by Pretorius (2009) is an early review of the recent successes, covering some of the same topics that we discuss here. Hannam (2009) reviewed the status of black-hole simulations producing long waveforms (including at least ten cycles of the dominant gravitational-wave mode) and their application to gravitational-wave data analysis. Finally, the text books by Bona and Palenzuela (2005) and Alcubierre (2008) provide many more details on the mathematical and computational aspects of numerical relativity than we can include here, and serve as useful supplements to our discussions.

## II. BLACK-HOLE BINARIES AND GRAVITATIONAL WAVES

Black holes and gravitational waves are surely among the most exotic and amazing predictions in all of physics. These two offspring of Einstein's general relativity are brought together in black-hole binaries, expected to be among the strongest emitters of gravitational radiation.

## A. Basic Properties

We begin by presenting some basic properties of black holes and gravitational waves. For fuller discussions and more details, see Misner *et al.* (1973) and Schutz (2009).

### 1. Black-Hole Basics

A black hole forms when matter collapses to infinite density, producing a singularity of infinite curvature in the fabric of spacetime. Each black hole is surrounded by an event horizon, at which the escape velocity is the speed of light. The event horizon is a global property of the spacetime, since it is defined by the paths of “outgoing” photons that are the boundary between photon trajectories that must fall inward, and those that can escape to infinity. The photons defining the event horizon hover at finite radius at the surface of the black hole. Since, in principle, mass (energy) can fall into the event horizon at late times – which will move the location at which photon paths can hover – we must know the entire future development of the system to locate the event horizon.

When black holes merge, a single event horizon forms whose area is at least as large as the sum of the individual horizons. Since numerical relativists want to know when this occurs during the course of a calculation, they rely on a related concept known as an *apparent horizon*, whose location depends only on the properties of the spacetime at any given time (Poisson, 2004). For quiescent black holes, the apparent and event horizons coincide; for more general holes, the apparent horizon is always inside the event horizon (with restrictions on the behavior of the matter involved). So, in terms of causality in a numerically-generated spacetime, any physical phenomenon found inside an apparent horizon should not leak out and affect the spacetime outside.

The simplest black hole is nonrotating and is described by the spherically symmetric Schwarzschild solution to the Einstein equations of general relativity in vacuum (i.e., with no “matter” sources in the spacetime). A Schwarzschild black hole is fully specified by one quantity, its mass  $M$ . The horizon is located at coordinate  $r = 2M$  (in Schwarzschild coordinates); its area is  $4\pi(2M)^2$ .

More general black holes can have both charge and spin. Since a charged black hole in astrophysics will generally be neutralized rapidly by any surrounding plasma, we can consider only rotating, uncharged black holes. Stationary (i.e., time independent) black holes are described by the axisymmetric Kerr solution. A Kerr black hole is fully specified by two quantities, its mass  $M$  and its angular momentum per unit mass  $a$ . The event horizon is located at the Boyer-Lindquist (Misner *et al.*, 1973) radius  $r_+$ , where

$$r_+ = M + (M^2 - a^2)^{1/2}. \quad (2)$$

The area of the event horizon is  $8\pi Mr_+$ .

Equation (2) requires  $a \leq M$ ; when  $a = M$  the black hole is said to be maximally rotating or “extremal”. Notice that  $r_+ = 2M$  when  $a = 0$ , and that  $r_+$  decreases as  $a$  increases, thus bringing the location of the horizon deeper into the potential well as the black-hole spin increases.

Photons and test particles in the vicinity of a single black hole can experience either stable or unstable orbits. For a Schwarzschild black hole of mass  $M$ , the *innermost stable circular orbit* (ISCO) occurs at  $r = 6M$  for massive test particles. In the case of a Kerr black hole, the ISCO is closer in for co-rotating test particles, and farther out for counter-rotating particles.

While the concept of an ISCO is strictly defined only for massive test particles, it has proven useful for studies of the spacetime around two black holes spiralling together on quasicircular orbits. Imagine that you put the two black holes on an *instantaneously* circular orbit around each other; at that moment they have neither nonzero radial velocity nor nonzero radial acceleration. At any given separation, the black holes have some angular momentum. The ISCO is the separation where that angular momentum is a minimum, in analogy to the test particle definition. Black holes at closer separations would be expected to fall inward, toward the center, even without radiating angular momentum via gravitational radiation.

### 2. Gravitational Wave Primer

Gravitational waves are ripples in the curvature of spacetime itself. They carry energy and momentum and travel at the speed of light, bearing the message of disturbances in the gravitational field.

As with electromagnetic waves, gravitational waves can be decomposed into multipolar contributions that reflect the nature of the source that generates them. Recall that electromagnetic radiation has no monopole contribution due to the conservation of total charge. By analogy, conservation of total mass-energy guarantees that there can be no monopole gravitational radiation. Since dipolar variations of charge and currents are possible, electromagnetic waves can have a dipole character. However, conservation of linear and angular momenta removes any possibility of dipolar gravitational waves, so the leading-order contribution to gravitational radiation is quadrupolar.

Gravitational waves are thus generated by systems with time-varying mass quadrupole moments (Flanagan and Hughes, 2005; Misner *et al.*, 1973). In the wave zone, a gravitational wave is described as a perturbation  $h$  to a smooth underlying spacetime. The wave amplitude is

$$h \sim \frac{G}{c^4} \frac{\ddot{Q}}{r} \sim \frac{GM_{\text{quad}}}{rc^2} \frac{v^2}{c^2}, \quad (3)$$

where  $Q$  is the quadrupole moment of the source,  $r$  is

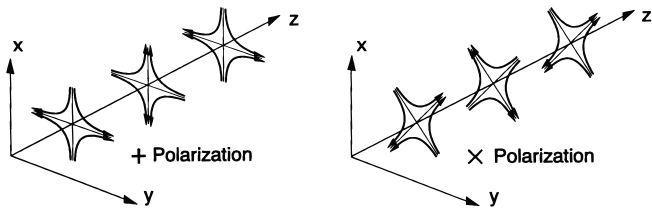


FIG. 1 Lines of force for plane gravitational waves propagating along the  $z$  axis. The wave on the left is purely in the  $+$  polarization state, and the one on the right is purely in the  $\times$  polarization state. The gravitational waves produce tidal forces in planes transverse to the propagation direction. From (Abramovici *et al.*, 1992). Reprinted with permission from AAAS.

the distance from the source, and  $M_{\text{quad}}$  is the mass in the source that is undergoing quadrupolar changes. This shows that the strongest gravitational waves will be produced by large masses moving at high velocities, such as binaries of compact stars and black holes.

A gravitational wave is purely transverse, acting tidally in directions perpendicular to its propagation direction. When a gravitational wave impinges on a detector of length scale  $L$ , it produces a length change in that detector  $\delta L/L \sim h/2$ . By substituting in typical values for compact objects in the Universe into Eq. (3), one can see that astrophysical sources typically yield wave amplitudes of  $h \lesssim 10^{-21}$  at the Earth. Consequently, precision measurements are needed to make detections.

Gravitational waves have two polarization components, known as  $h_+$  and  $h_\times$  for a linearly polarized wave. Figure 1 shows the corresponding lines of force for sinusoidal gravitational waves propagating along the  $z$  axis. In the purely  $+$  polarization on the left, the wave stretches along one axis and squeezes along the other, alternating sinusoidally as the wave passes. The  $\times$  polarization wave on the right acts similarly, stretching and squeezing along axes rotated by  $45^\circ$ . In general, a gravitational wave is a superposition of these two states, conveniently written as a complex waveform strain  $h$ , where

$$h = h_+ + ih_\times. \quad (4)$$

## B. Astrophysical Black Holes

Astronomers have found evidence for black holes throughout the Universe on a remarkable range of scales. The smallest of these, stellar black holes, have masses in the range  $\sim (3 - 30)M_\odot$  and form as the end-products of massive star evolution. There is good observational evidence for the existence of stellar black holes, based on dynamical measurements of the masses of compact objects in transient systems that undergo X-ray outbursts. Since neutron stars cannot have masses  $\gtrsim 3M_\odot$ , compact objects more massive than this must be black holes (Remillard and McClintock, 2006).

Intermediate-mass black holes (IMBHs) have masses in the range  $\sim (10^2 - 10^4)M_\odot$ . IMBHs may form as the result of multiple mergers of smaller objects in the centers of dense stellar clusters in the present Universe (Miller and Colbert, 2004; Portegies Zwart and McMillan, 2002), assuming mass loss from stellar winds is not significant (Glebbeek *et al.*, 2009). They may also arise from the evolution of very massive stars early in the history of the Universe, forming black-hole “seeds” in the centers of massive halos (the precursors of the galaxies we see today) early in the history of the Universe, to redshifts  $z \gtrsim 10$  (Madau and Rees, 2001). Currently the best observational evidence for IMBHs comes from models of ultra-luminous X-ray sources (Colbert and Miller, 2005).

Finally, massive black holes (MBHs) have masses in the range  $\sim (10^4 - 10^9)M_\odot$  and are found at the centers of galaxies, including our own Milky Way galaxy. The observational case for the existence of MBHs is quite strong, based on dynamical models of stars and gas believed to be moving in the potential well of the central MBH (Desroches *et al.*, 2009; Ferrarese and Ford, 2005; Kormendy and Richstone, 1995; Richstone *et al.*, 1998).

Black-hole binaries are binary systems in which each component is a black hole. As mentioned above, we focus here on comparable-mass binaries, which are expected to produce the strongest gravitational-wave signals. Stellar black-hole binaries may form as the result of binaries composed of two massive stars; see Bulik and Belczynski (2009) and references therein. Stellar black-hole binaries may also arise from dynamical processes in which a black hole is captured into an orbit around another black hole in dense stellar environments (Miller and Lauberg, 2009; O’Leary *et al.*, 2007). IMBH binaries can also form through dynamical processes in stellar clusters (Gürkan *et al.*, 2006) and from mergers of massive halos at high redshifts. Since both stellar and IMBH binaries are “dark” – that is, they are generally not surrounded by gas which might produce electromagnetic radiation – we have few observational constraints on these types of black-hole binaries. This situation will change dramatically, however, with the detection of gravitational radiation from these systems (Bulik and Belczynski, 2009; Miller, 2009), as gravitational waves bring direct information about the dynamical behavior of the orbiting masses and do not rely on electromagnetic emissions from nearby matter.

Since essentially all galaxies are believed to contain an MBH at the center and to undergo a merger with another galaxy at least once during the history of the Universe, MBH binaries can arise when their host galaxies merge (Begelman *et al.*, 1980); see also Djorgovski *et al.* (2008) and references therein. However, due to the vast cosmic distances involved, and the small angular separations on the sky expected for MBH binaries, only a few candidates are currently known through electromagnetic observations (Komossa, 2003; Komossa *et al.*, 2003; Rodriguez *et al.*, 2006). When they form, MBH bina-

ries typically have relatively wide separations, and the gravitational radiation they emit is very weak and insufficient to cause the binary to coalesce within the age of the Universe. However, various processes such as gaseous dissipation and  $N$ -body interactions with stars can remove orbital energy from the binary and cause the black holes to spiral together (Armitage and Natarajan, 2002; Gould and Rix, 2000); see also Berentzen *et al.* (2009) and Colpi *et al.* (2009) and references therein. Eventually, the black holes reach separations at which gravitational radiation reaction becomes the dominant energy-loss mechanism, leading to the final coalescence of the black holes and the emission of strong gravitational waves (Sesana *et al.*, 2009b).

### C. Gravitational Waves from Black-Hole Binaries

Mergers of comparable-mass black-hole binaries are expected to be among the strongest sources of gravitational waves. This final death spiral of a black-hole binary encompasses three stages: inspiral, merger, and ringdown (Flanagan and Hughes, 1998; Hughes, 2009).

In the early stages of the inspiral, the orbits of most astrophysical black-hole binaries will circularize due to the emission of gravitational radiation (Peters, 1964; Peters and Mathews, 1963). During the inspiral, the orbital time scale is much shorter than the time scale on which the orbital parameters change; consequently, the black holes spiral together on quasicircular orbits. Since the black holes have wide separations, they can be treated as point particles. The inspiral dynamics and waveforms can be calculated using post-Newtonian (PN) equations, which result from a systematic expansion of the full Einstein equations in powers of  $\epsilon \sim v^2/c^2 \sim GM/Rc^2$ , where  $R$  is the binary separation (Blanchet, 2006). The inspiral phase produces gravitational waves in the characteristic form of a *chirp*, which is a sinusoid with both frequency and amplitude increasing with time.

As the black holes spiral inward, they eventually reach the strong-field, dynamical regime of general relativity. In this merger stage, the orbital evolution is no longer quasi-adiabatic; rather, the black holes plunge together and coalesce into a single, highly distorted remnant black hole, surrounded by a common horizon. Since the point-particle and PN approximations break down, numerical relativity simulations of the Einstein equations in three dimensions are needed to calculate the merger. Due to the difficulty of these simulations, the resulting gravitational waveforms were completely unknown until recently.

Finally, the highly distorted remnant black hole settles down into a quiescent rotating Kerr black hole by shedding its nonaxisymmetric modes through gravitational-wave emission. We call this process the “ringdown,” in analogy to how a bell that has been struck sheds its distortions as sound waves. Various analytic techniques of black-hole perturbation theory (Regge and Wheeler,

1957; Teukolsky, 1973; Zerilli, 1970) form the basis of ringdown calculations, producing gravitational waveforms in the shape of exponentially damped sinusoids (Berti *et al.*, 2009; Leaver, 1986).

The characteristic gravitational-wave frequency of a quasicircular black-hole binary, produced by the dominant (highest-order) quadrupole component, is

$$f_{\text{GW}} \sim 2f_{\text{orb}} \sim (M/R^3)^{1/2}, \quad (5)$$

where  $f_{\text{orb}}$  is the orbital frequency. Astrophysical black-hole binaries produce gravitational waves that span three frequency regimes, depending on the black-hole masses (Flanagan and Hughes, 2005). Stellar black-hole binaries and the lower mass end of the IMBH binaries radiate in the high frequency band,  $f_{\text{GW}} \sim (10 - 10^4)\text{Hz}$ , which is already being observed by ground-based laser interferometer detectors such as LIGO (Abbott *et al.*, 2009b), and will be observed by the advanced detectors by  $\sim 2016$  (Smith, 2009). Low frequency gravitational waves cover the band  $f_{\text{GW}} \sim (10^{-5} - 1)\text{Hz}$  and will be observed by the space-based laser interferometer LISA, currently under development (Jennrich, 2009). MBH binaries with masses  $M \sim (10^{4.5} - 10^7)M_{\odot}$  will be very strong sources for LISA, with the lower mass systems visible out to redshifts  $z \gtrsim 10$  (Arun *et al.*, 2009a); the inspirals of IMBH binaries will also be detectable (Miller, 2009). Finally, the very low frequency band  $f_{\text{GW}} \sim (10^{-9} - 10^{-7})\text{Hz}$  will be observed by pulsar timing arrays (Verbiest *et al.*, 2009). This band is expected to be dominated by gravitational waves from a very large population of unresolved MBH binaries (Sesana *et al.*, 2008) with possibly a few discrete sources (Sesana *et al.*, 2009a).

## III. HISTORICAL OVERVIEW

The quest to calculate the gravitational-wave signals from the merger of two black holes spans more than four decades and encompasses key developments in theoretical and experimental general relativity, astrophysics, and computational science. In this section, we begin by delineating these threads in general terms, and then turn to a more detailed account of select milestones along the path toward successful simulations of black-hole mergers.

### A. Setting the Stage

At the end of the 18th century Michell (1784) and Laplace (1796) first speculated, using Newtonian gravity, that a star could become so compact that the escape velocity from its surface would exceed the speed of light. In the 20th century, scientists realized that such black holes could form as the final state of total gravitational collapse in general relativity (Harrison *et al.*, 1965; Oppenheimer and Snyder, 1939); John Wheeler would later popularize the term “black hole” to describe such an object (Misner *et al.*, 2009; Ruffini and Wheeler, 1971).

Beginning in the 1960s, many highly energetic astrophysical phenomena were discovered with physical properties pointing to extremely strong gravitational fields as underlying mechanisms; among these are quasars and X-ray binaries such as Cygnus X-1 (Overbeck and Tananbaum, 1968; Overbeck *et al.*, 1967), the first credible black-hole candidate. As discussed in Sec. II.B, today astrophysical black holes are believed to exist on a vast range of scales throughout the Universe, and black-hole binaries are considered to be strong sources of gravitational waves.

Einstein’s equations of general relativity form a coupled set of nonlinear partial differential equations, in which dynamic curved spacetime takes the role of Newton’s gravitational field and interacts nonlinearly with massive bodies. Gravitational waves were first recognized as solutions to the linearized, weak-field Einstein equations early in the past century. By mid-century, gravitational waves were recognized as real physical phenomena, carrying energy and being capable of producing a response when impinging on a detector. This development spawned a major branch of experimental general relativity, with concepts for the first gravitational-wave detectors appearing in the 1960s; see Camp and Cornish (2004) for a review. The discovery of two neutron stars in a binary system by Hulse and Taylor (1975) provided an astrophysical laboratory for the first *indirect* detection of gravitational radiation. Decades of observation revealed the binary orbit to be shrinking by precisely the amount expected if the system were emitting gravitational waves according to general relativity (Weisberg and Taylor, 2005); Hulse and Taylor were awarded the Nobel Prize in 1993. Today, the prognosis for *direct* detection of gravitational waves is excellent, with the first events expected from the advanced ground-based interferometers around the middle of this coming decade.

As you might expect, Einstein’s equations pose formidable obstacles to anyone who would dare to probe the physics within. Throughout most of the 20th century, relativists uncovered a fairly small number of exact solutions by exploiting symmetries, and made progress toward more general problems using various perturbative expansions. By the 1960s, computers had become powerful enough to encourage attempts at solving Einstein’s equations numerically, to uncover physics beyond the realm of perturbation theory. The subsequent development of numerical relativity has been made possible in part by continued increases in computer power and advances in algorithms and computational methods.

Most numerical-relativity simulations start with the idea of decomposing four-dimensional spacetime into a stack of curved three-dimensional spacelike slices threaded by a congruence of timelike curves (York Jr., 1979). Arnowit, Deser, and Misner (ADM) pioneered this “3+1” approach as the basis for a canonical formulation of the dynamics of general relativity (Arnowitt *et al.*, 1962). In this Hamiltonian formulation, the three-metric  $\gamma_{ij}$  on the spatial slices takes the role of the “configura-

tion variables.” Quantities based on the extrinsic curvature  $K_{ij}$ , which is roughly the time derivative of  $\gamma_{ij}$ , play the role of “conjugate momenta.” Variation of an action with respect to  $\gamma_{ij}$  produces a set of six first-order evolution equations for the conjugate momenta; varying the momenta gives six first-order evolution equations for  $\gamma_{ij}$ . ADM also introduced four Lagrange multipliers as freely specifiable gauge or coordinate conditions, representing the four coordinate degrees of freedom in general relativity. Variation of these Lagrange multipliers yields four equations that must hold on each slice: a Hamiltonian constraint, and three momentum constraints.

Originally intended as a tool for quantizing gravity, the ADM formalism later became the basis for most work in numerical relativity. As we discuss in Sec. IV below, key elements in this approach are solving the Cauchy problem, beginning with the initial data on a spacelike slice, and then evolving that data forward in time. The constraint equations form the basis for this initial value problem. Appropriate choices for the gauge conditions are crucial ingredients for today’s successful black-hole merger simulations.

## B. Numerical Relativity Milestones

Hahn and Lindquist (1964) made the first known attempt to simulate the head-on collision of two equal-mass black holes on a computer in 1964, using a two-dimensional axisymmetric approach. Their simulation ran for 50 timesteps to a duration of  $\sim 1.8M$ ; at this point, they decided that the simulation was no longer accurate enough to warrant continued evolution, and stopped the code. Smarr and Eppley (Eppley, 1975; Smarr, 1975, 1977; Smarr *et al.*, 1976) returned to this problem in the mid-1970s, again employing two-dimensional axisymmetry but now using the ADM formalism, specialized coordinates, and improved coordinate conditions. Although they encountered problems with instabilities and large numerical errors, they managed to evolve the collision and extract information about the emitted gravitational waves. Smarr and Eppley had used the most powerful computers of their day. Going to the next step, orbiting black holes in three dimensions, was deemed to be not feasible at the time, due to unresolved questions about the instabilities and insufficient computer power. Consequently, the black-hole merger problem lay dormant for over a decade.

In the 1990s, attention returned to black-hole mergers as the LIGO project began to move forward, and black-hole mergers were recognized as the strongest sources for this detector. Since the signal-to-noise ratio for such ground-based detectors is fairly modest, having a template for the merger waveform is a key part of the data analysis strategy. Numerical relativists revisited the problem of colliding two black holes head-on with modern techniques and more powerful computers (Anninos *et al.*, 1993; Bernstein *et al.*, 1994). In the mid-1990s, the

National Science Foundation funded a Computational Grand Challenge grant for a large multi-institution collaboration aimed at evolving black-hole mergers in three dimensions and calculating the resulting gravitational waveforms. Around the same time, a large and very active numerical relativity group arose at the newly-formed Albert-Einstein Institut (AEI) in Potsdam, Germany. During the late 1990s and into the early 2000s, two developments on the experimental side further increased the desire for black-hole merger simulations: the ground-based gravitational-wave detectors started taking data, and interest grew in LISA and its potential for observing gravitational waves from massive black-hole binary mergers.

While no one expected the task at hand – developing computer codes to solve the full Einstein equations in three dimensions for the final few orbits and merger of two black holes – to be simple, numerical relativists found that the problem was far more difficult than anticipated. Producing a waveform useful for gravitational-wave detection purposes typically would require running a simulation for a duration of several hundred  $M$ . However, a variety of instabilities plagued the codes, causing them to crash well before any significant portion of an orbit could be achieved.

Nevertheless, during a period encompassing a little over a decade, much important work was accomplished that laid the foundations for later success. Key milestones include these developments:

- initial data for binary black holes near the ISCO (Baumgarte, 2000; Cook, 1994, 2002; Cook and Pfeiffer, 2004);
- new methods for representing black holes on computational grids such as punctures (Brandt and Brügmann, 1997) and excision (Alcubierre and Brügmann, 2001; Anninos *et al.*, 1995b; Seidel and Suen, 1992; Shoemaker *et al.*, 2003);
- recognition of the importance of hyperbolicity in formulating the Einstein equations for numerical solution (Abrahams *et al.*, 1997; Anderson *et al.*, 1997; Bona and Massó, 1992; Friedrich and Rendall, 2000);
- improved formulations of the Einstein equations (Baumgarte and Shapiro, 1998; Nakamura *et al.*, 1987; Shibata and Nakamura, 1995);
- fully three-dimensional evolution codes and their use in evolving distorted black holes (Brandt *et al.*, 2003; Camarda and Seidel, 1999), boosted black holes (Cook *et al.*, 1998), head-on collisions (Sperhake *et al.*, 2005), and grazing collisions (Alcubierre *et al.*, 2001a; Brandt *et al.*, 2000; Brügmann, 1999);

- coordinate conditions that keep the slices from crashing into singularities and the spatial coordinates from falling into the black holes as the evolution proceeds (Alcubierre *et al.*, 2003; Bona *et al.*, 1995);
- the Cactus Computational Toolkit<sup>1</sup>, which provided a framework for developing numerical-relativity codes and analysis tools used by many groups;
- modern adaptive mesh refinement finite-difference (including Carpet<sup>2</sup> with Cactus, BAM (Brügmann, 1999), and Paramesh (MacNeice *et al.*, 2000)), and multi-domain spectral (Pfeiffer *et al.*, 2003) infrastructures for numerical relativity.

Throughout this period, the length of black-hole evolutions gradually increased. Improvements in the formalisms allowed simulations of single black holes and, later, two black holes to increase in duration to  $\gtrsim 10M$ . The addition of new slicing and shift conditions again increased the evolution times to  $\gtrsim 30M$ . The Lazarus project took a novel approach to combine these relatively short-duration binary simulations with perturbation techniques for the late-time behavior to produce a hybrid model for a black-hole merger (Baker *et al.*, 2000, 2001, 2002a,b). By late 2003, Brügmann *et al.* (2004) carried out the first complete orbit of two equal-mass, nonspinning black holes. While this simulation lasted  $\sim 100M$ , the code crashed shortly after the orbit was completed and the gravitational waves were not extracted. Overall, progress was slow, difficult, and incremental. However, the situation was about to change dramatically.

### C. Breakthroughs and the Gold Rush

In early 2005, Frans Pretorius electrified the relativity community when he achieved the first evolution of an equal-mass black-hole binary through its final orbit, merger, and ringdown using techniques very different from those employed by the rest of the community (Pretorius, 2005a). Later in 2005 the groups at the University of Texas at Brownsville (UTB) and NASA’s Goddard Space Flight Center independently and simultaneously discovered a new method, called “moving punctures,” that also produced successful black-hole mergers (Baker *et al.*, 2006b; Campanelli *et al.*, 2006a). Their presentations were given back-to-back at a workshop on numerical relativity, to the amazement of each other and the assembled participants.

Since the moving-puncture approach was based on underlying techniques used by several other groups, it was

<sup>1</sup> <http://www.cactuscode.org/>

<sup>2</sup> <http://www.carpetcode.org/>

rapidly and readily adopted by most in the community, producing a growing avalanche of results. 2006 was a year of many firsts: the first simulations of unequal-mass black holes and the accompanying recoil of the remnant hole (Baker *et al.*, 2006c), the first mergers of spinning black holes (Campanelli *et al.*, 2006d), the first long waveforms ( $\sim 7$  orbits) (Baker *et al.*, 2007c), the first comparisons with PN results (Baker *et al.*, 2007d; Buonanno *et al.*, 2007a), and the first systematic parameter study in numerical relativity (González *et al.*, 2007b). The year 2007 opened with the discovery of “superkicks” – recoil velocities exceeding  $1000 \text{ km s}^{-1}$  (Campanelli *et al.*, 2007b; González *et al.*, 2007a), and in 2008 a black-hole binary merger with mass ratio  $q = 10$  was accomplished (González *et al.*, 2009), while Campanelli *et al.* (2009) carried out the first long-term evolution of generic spinning and precessing black-hole binaries. As this article was being written in 2009 the state of the art continues to advance, with the first simulations of black-hole mergers using spectral numerical techniques (Chu *et al.*, 2009; Scheel *et al.*, 2009; Szilágyi *et al.*, 2009), and the first steps towards modeling the flows of gas around the merging black holes (van Meter *et al.*, 2010b). Applications of the merger results in areas such as comparisons with PN expressions for the waveforms, astrophysical computations of black-hole merger rates, and the development of templates for gravitational-wave data analysis have accompanied these technical developments in the simulations. The study of black-hole mergers using numerical relativity is thriving indeed.

#### IV. NUMERICAL DEVELOPMENT

In this section, we discuss the mathematical and numerical foundations underlying current black-hole merger simulations, highlighting the key issues involved in achieving successful evolutions. For more detailed treatments, we direct the interested reader to Alcubierre (2008) or (Gourgoulhon, 2007).

##### A. Einstein’s Equations

The central task of numerical relativity is solving Einstein’s field equations

$$G_{\mu\nu} = 8\pi T_{\mu\nu}, \quad (6)$$

where Einstein’s tensor  $G_{\mu\nu}$  represents the curvature of spacetime, the energy-momentum tensor  $T_{\mu\nu}$  contains the matter sources, and  $\mu, \nu = 0, 1, 2, 3$ . By convention, an index  $\mu = 0$  selects a “time” component, and  $\mu = 1, 2, 3$  selects a “space” component.  $G_{\mu\nu}$  depends on the first and second derivatives of the metric tensor  $g_{\mu\nu}$ . For vacuum black-hole spacetimes,  $T_{\mu\nu} = 0$ . Note that all of the tensor fields discussed here are symmetric in the indices, e.g.  $g_{\mu\nu} = g_{\nu\mu}$ .

The metric characterizes the geometry of spacetime by giving the infinitesimal spacetime interval  $ds$  through the following definition:

$$ds^2 = g_{\mu\nu} dx^\mu dx^\nu, \quad (7)$$

where we use the Einstein summation convention which implies summation over all values of a given index that appears twice in an expression. Many physical implications of the metric are immediately apparent from Eq. (7). For example, when  $ds^2 = 0$ , the resulting metric-determined relationship between the time and space coordinates yields the paths that light rays must follow in this spacetime.

The dependence of Einstein’s tensor on the metric can be simply illustrated in coordinates known as “harmonic”; in vacuum Eq. (6) takes the form:

$$\square g_{\mu\nu} - t_{\mu\nu} = 0, \quad (8)$$

where  $\square$  is the flat-space wave-operator and  $t_{\mu\nu}$  represents all terms nonlinear in the metric. If  $t_{\mu\nu}$  is interpreted as an effective source term, this is a simple wave equation. The familiar form of this equation suggests that its Cauchy problem can be solved by specifying the metric and its first derivative on an initial, spatial surface and then integrating in time, as for an ordinary wave equation.

Einstein’s equations admit various formulations and coordinate conditions, which should be tailored to the problem at hand – in this case, numerical simulation of black-hole spacetimes. Regardless of these choices, current numerical practices universally involve an initial three-dimensional slice of spacetime that is evolved forward in time. Here, we review the history and current most common choices of initial data, black-hole representations, formulation, coordinate conditions, and some details of the numerics. The impetus, and most important outcome, of all these developments is the ability to generate gravitational waveforms from black-hole binary sources over many cycles.

##### B. The Cauchy Problem

The Cauchy problem concerns solution of the field equations given initial data specified on an initial (typically spatial) hypersurface. In practice, the Cauchy problem is more conveniently investigated in a “3+1” formulation, explicitly based on a foliation of the spacetime into three-dimensional spatial slices parametrized by a time coordinate. A common 3+1 formulation inspired by ADM (Arnowitt *et al.*, 1962) divides up the components of the metric according to their relationships with space and time, such that the line element takes the form:

$$ds^2 = (-\alpha^2 + \beta^i \beta_i) dt^2 + 2\beta_i dt dx^i + \gamma_{ij} dx^i dx^j, \quad (9)$$

where  $\alpha$  is called the lapse function,  $\beta^i$  the shift vector, and  $\gamma_{ij} = g_{ij}$  is the spatial three-metric. We write the



time coordinate  $x^0 = t$  and the spatial coordinate indices  $i, j = 1, 2, 3$ . Note that contraction with  $g_{\mu\nu}$  or its inverse  $g^{\mu\nu}$  is used to lower or raise indices of four-dimensional tensors, respectively, while  $\gamma_{ij}$  or its inverse  $\gamma^{ij}$  is used to lower or raise indices of three-dimensional tensors. The lapse and shift represent coordinate freedom in the metric; we can choose these quantities arbitrarily. However, since the three-metric  $\gamma_{ij}$  (and its first and second spatial derivatives) determines the intrinsic curvature of the slice, it carries the information about the gravitational field and thus is constrained by the physics.

The meaning of the lapse and shift can be understood by considering two successive spatial slices separated by an infinitesimal time interval  $dt$  (Fig. 2). An observer along a vector normal to the first slice will measure an elapsed proper time of  $d\tau = \alpha dt$  in evolving to the second slice, and a change in spatial coordinate of  $dx^i = -\beta^i dt$ .

Since Einstein's equations are second order in time, we must also specify the initial time derivative of the three-metric. Rather than specifying this derivative directly, we define a new quantity:

$$K_{ij} = -\frac{1}{2\alpha} (\partial_t \gamma_{ij} - D_i \beta_j - D_j \beta_i), \quad (10)$$

where  $\partial_t = \partial/\partial t$  is an ordinary partial derivative and  $D_i$  is the spatial covariant derivative. Note that the space-time covariant derivative  $\nabla_\mu$  is a partial derivative with a correction such that it transforms as a vector and satisfies  $\nabla_\lambda g_{\mu\nu} = 0$ .  $D_i$  is the projection of  $\nabla_\mu$  onto the spatial slice and is equivalent to a three-dimensional covariant derivative formed from  $\gamma_{ij}$ . For the case of Euclidean normal coordinates,  $\alpha = 1$  and  $\beta^i = 0$ , Eq. (10) reduces to the simple expression  $K_{ij} = -(1/2)\partial_t \gamma_{ij}$ .

If we define a unit vector  $n_\mu$  normal to the spatial slice, we can show that Eq. (10) is equivalent to  $K_{ij} = -D_i n_j$ . As suggested by this expression,  $K_{ij}$  is a measure of the change of the normal vector as it is transported along the slice. In this way  $K_{ij}$  gives an extrinsic measure of the curvature of a three-dimensional spatial slice with respect to its embedding in four-dimensional spacetime. It is therefore called the extrinsic curvature. Depending on the formulation, the extrinsic curvature might or might not come into the evolution equations; however,  $K_{ij}$  is almost universally utilized when calculating initial data.

Of the ten component equations of Eq. (6), six determine the time-evolution of the metric, while four must be satisfied on a spatial slice at any given time, and are thus constraint equations. With an appropriate choice of time coordinate, and assuming vacuum spacetime, these four constraint equations are equivalent to the condition  $G_{0\nu} = 0$ . The time-time component  $G_{00} = 0$  is called the *Hamiltonian constraint*, and the time-space components  $G_{0i} = 0$  are called the *momentum constraint*. These take the form of conditions on the extrinsic curvature:

$${}^{(3)}R + K^2 - K_{ij}K^{ij} = 0 \quad (11)$$

$$D_j(K^{ij} - \gamma^{ij}K) = 0 \quad (12)$$

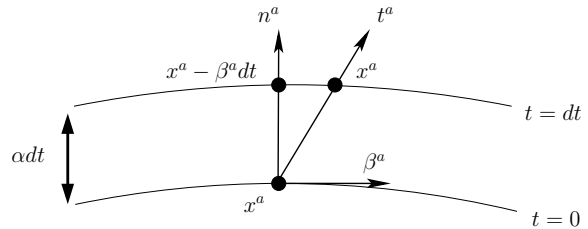


FIG. 2 The 3+1 split into space and time. Two spatial slices at  $t = 0$  and  $t = dt$  are depicted.  $\alpha$  is the lapse, and  $\alpha dt$  represents the proper time lapse between slices.  $\beta^a$  is the shift, and  $\beta^a dt$  represents the amount by which the spatial coordinates shift between slices.  $n^a$  is normal to the slice at  $t = 0$ . If a ray parallel to  $n^a$  intersects the  $t = 0$  slice at a point  $x^a$ , then it will intersect the  $t = dt$  slice at  $x^a - \beta^a dt$ .  $t^a \equiv \alpha n^a + \beta^a$  is a coordinate time vector. If a ray parallel to  $t^a$  intersects the  $t = 0$  slice at point  $x^a$ , then it will also intersect the  $t = dt$  slice at  $x^a$ .

where  ${}^{(3)}R$  is the three-dimensional Ricci scalar associated with the three-metric  $\gamma_{ij}$ , and  $K \equiv \text{trace} K_{ij} = \gamma^{ij} K_{ij}$ , sometimes called the *mean curvature*. These constraint equations must be solved in order to obtain an initial spatial slice consistent with Einstein's equations.

### C. Representing Black Holes in Numerical Spacetimes

How does one represent an exotic object such as a black hole in a numerical simulation? In particular, how can one use finite computational methods repeatedly to model an object which, analytically, contains physical and/or coordinate singularities? Fortunately, two successful strategies have emerged to meet this challenge.

The unusual topology of black holes offers one way out. As Einstein and Rosen (1935) originally showed, a black hole can be considered a “bridge” or “wormhole” connecting one Universe or “worldsheet”, to a second worldsheet (see Fig. 3). Exploiting this topology, a continuous spatial slice which avoids the physical singularity contained within the event horizon of each black hole can be constructed as follows. Starting with a spatial slice of Schwarzschild spacetime, remove the interior of the event horizon. Identify the resulting spherical boundary with the spherical boundary of an identical copy of this space. The two-dimensional analog would be to take two sheets of paper, cut out a disk from each, and then glue the resulting circular edges together. Each sheet, or copy of Schwarzschild spacetime in this example, is called a worldsheet. The identified spherical boundaries connecting the worldsheets form what is referred to as the “throat” of the wormhole.

To complete this construction, we require an appropriate coordinate system to continuously cover both world-

sheets. Brill and Lindquist discovered coordinates that will prove convenient, in which the three-metric of a particular spatial slice of Schwarzschild spacetime is given by (Brill and Lindquist, 1963)

$$\gamma_{ij} = \left(1 + \frac{m}{2r}\right)^4 \delta_{ij}, \quad (13)$$

where  $r$  is a radial coordinate. In these coordinates, the event horizon is at  $r = m/2$ . We can consider each of the worldsheets described above as being separately labeled by such coordinates. Designate one worldsheet as  $A$  and the other as  $B$ , and call their radial coordinates  $r_A$  and  $r_B$  respectively. Since the interior of the event horizon has been removed from each worldsheet, assume that  $r_A \geq m/2$  and  $r_B \geq m/2$ . The metric on each worldsheet has the form of Eq. (13). As noted by Brill and Lindquist, this form of the metric is unchanged by the transformation  $r' = m^2/4r$ , and  $r' = r$  when  $r = m/2$ . So if we define a new coordinate  $r'$  by

$$r_A = r' \text{ for } r' \geq \frac{m}{2}, \quad r_B = \frac{m^2}{2r'} \text{ for } r' \leq \frac{m}{2}, \quad (14)$$

mapping spatial infinity on worldsheet  $B$  to  $r' = 0$ , we obtain a single continuous coordinate system that applies to worldsheet  $A$  for  $r' \geq m/2$  and worldsheet  $B$  for  $r' \leq m/2$ .

This avoidance of the physical singularity comes at the expense of a coordinate singularity in the metric at  $r' = 0$ , called a “puncture”. However, it turns out this coordinate singularity can be confined to a single scalar variable, as suggested in Eq. (13). With a suitable change of variables and other means, numerical simulations haven proven capable of handling this irregular scalar field. Thus the “puncture” method is one way to represent a black hole that is amenable to computation.

Another strategy is excision, first proposed by Unruh (Thornburg, 1993). Given that no physical information can escape an event horizon to influence the exterior, the interior of a black hole can in principle be excised from the computational domain<sup>3</sup>. This relies on the fact that all physical information propagates inwards from the event horizon towards the physical singularity, i.e. light-cones tilt inwards, and nothing physical propagates outward from the horizon. Extrapolation can be used for the boundary condition of the excised region, and any non-physical numerical error that escapes the horizon should be negligible. This approach is not constrained to the particular coordinates required by the puncture method, but it can be more difficult due to the need for precise positioning of the excision boundary and accurate extrapolation. Excision was used successfully for orbiting binary simulations by Pretorius (2005a) and continues to

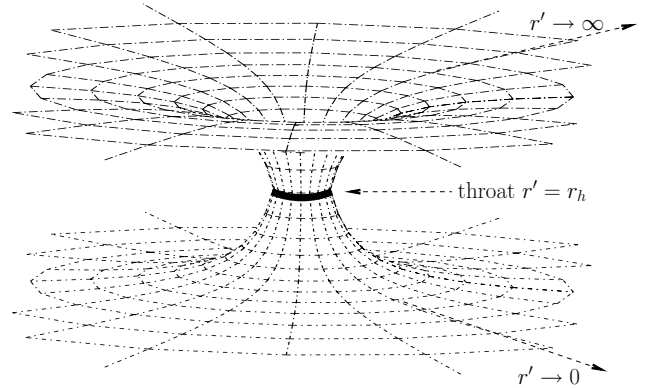


FIG. 3 In the wormhole representation of a black hole, the initial slice typically just touches the horizon. The upper “sheet” represents the exterior space, while the lower sheet is a duplicate, joined to the upper sheet by a “throat”.

be used by the Caltech-Cornell dual-coordinate spectral code (Scheel *et al.*, 2009, 2006).

Either of these methods can be useful in representing black holes on the initial data slice. Surprisingly, we will also see that either of these representations can be made robust enough to persist as the black holes evolve.

#### D. Initial Data

The starting point for successful simulations of black-hole mergers is finding initial data for astrophysically realistic inspiralling black holes. If we were simulating the orbits of stars in Newtonian gravity, this would be a simple procedure. For example, we could simply specify the masses and spins of the stars, along with their positions and velocities on orbits derived from the dynamics of point particles, and then evolve the system numerically to allow it to “relax” into orbits appropriate for bodies of finite size. In general relativity, however, the initial data must satisfy the constraint equations (11) - (12), which are cast in terms of the 3-metric  $\gamma_{ij}$  and the extrinsic curvature  $K_{ij}$ . Since there is no obvious, or natural, connection between these field variables and the astrophysical properties of inspiralling black holes, obtaining suitable initial data is a major challenge.

Building on the earlier work of Lichnerowicz (1944), York developed a general procedure for solving the constraint equations to produce initial data for the Cauchy problem in the 1970s (see York Jr. (1979) for a review). This approach generally requires solving a coupled elliptic system of four nonlinear field equations. We can break this problem down into more manageable pieces with some simplifying assumptions. While these choices

<sup>3</sup> As unphysical coordinate “gauge modes” may couple to physical modes, we also assume no superluminal coordinate effects are present.

do come at the cost of some loss of generality and astrophysical realism in the initial data for two black holes, it has been seen that for sufficiently long evolutions the final orbits and waveform signatures from the black-hole evolution are largely insensitive to this level of detail in the initial data, at least in the case of equal-mass non-spinning black holes.

The first simplification is to choose traceless extrinsic curvature,  $K = 0$ . With this, the Hamiltonian constraint is decoupled from the momentum constraints, and can be solved separately. To find solutions corresponding to multiple black holes, we generally further assume that the initial slice is conformally flat. That is, the three-metric is the product of a scalar conformal factor with a flat metric,

$$\gamma_{ij} = \psi^4 \delta_{ij}. \quad (15)$$

With this, the problem reduces to solving a (typically nonlinear) equation for the scalar field  $\psi$ .

Brill and Lindquist (1963) found a simple solution, representing  $N$  black holes momentarily at rest, which gives

$$\psi = 1 + \sum_i^N \frac{m_i}{2r_i} \quad (16)$$

where  $m_i$  is the mass associated with the  $i$ th black hole and  $r_i$  represents its coordinate center. Each  $r_i$  corresponds to the location of a puncture, as described in the last section. This is a valuable solution, but not generally useful, because these black holes lack momentum and spin.

An explicit solution by Bowen for the momentum constraint was the last crucial step in defining a procedure for calculating initial data for multiple black holes with specified linear and angular momenta (Bowen and York Jr., 1980). The Bowen-York prescription employed a two-sheeted topology found by Misner for the black-hole interiors (Misner, 1963). Later Brandt and Brügmann generalized the procedure for the Brill-Lindquist topology (Brandt and Brügmann, 1997). The Brandt-Brügmann puncture data for arbitrary momenta and spin is now widely used because of its ease of implementation.

More recently York developed another modeling ansatz, known as the Conformal-Thin-Sandwich (CTS) approach (Pfeiffer and York Jr., 2005; York Jr., 1999), which has certain additional advantages. For example, it turns out the conventional Brandt-Brügmann puncture cannot yield a spin parameter ( $a/M$ ) greater than  $\sim 0.93$  (Dain *et al.*, 2002), while CTS data can go higher (Lovelace *et al.*, 2008). As discussed above, the spatial metric is chosen to be conformally flat, then instead of providing an ansatz for the extrinsic curvature  $K_{ij}$ , the initial time-derivative of the conformal metric is specified (generally to vanish). In addition, a condition can be imposed on the slicing (see below). The result is a coupled system of elliptic equations which is solved to

enforce the constraints and optionally the choice of slicing condition. Boundary conditions may additionally be supplied to enforce rotational motion.

Either approach provides an ansatz for constructing three-dimensional binary black-hole initial *field* data for a specified choice of particle-like parameters, masses, positions, momenta, and spins. Inevitably there are differences from the nearly quiescent evolving systems that we seek to represent. Generally there is some level of spurious radiation generated from a period of initial transient dynamics through which the system relaxes to become quiescent on sub-orbital time scales. In particular, extraneous radiation content is an unavoidable consequence of conformal flatness, which post-Newtonian analysis has shown must deviate from the physically relevant inspiralling binary solution (Damour *et al.*, 2000). This spurious radiation is seen in plots of the gravitational waveforms produced by mergers; see Fig. 9 and other waveform plots in Sec. V.B.2. Often the simulations will also undergo a period of initial gauge-evolution which, though physically inconsequential, may affect the quality of the simulation numerically. For puncture initial data Hannam *et al.* (2009b) analyzed some of these gauge dynamics, and developed a promising approach (“trumpet” data) to mitigate it (see Sec. IV.F.2 for related gauge issues). However, for simulations lasting for several orbits these modest transient effects are generally negligible.

Most black-hole binary simulation studies are designed to represent the astrophysical population of systems, which have circularized before the gravitational radiation becomes observationally significant. These simulations begin with circularly inspiralling initial data configurations. Even before reliable numerical relativity simulations were possible, considerable attention had been given to prescribing initial data for these near-circular configurations (see Cook (2000) for a review). Within the CTS approach, it is particularly natural to impose initially circular motion upon the system, resulting in an initial data prescription for quasicircular orbits (Caudill *et al.*, 2006; Cook, 2002; Cook and Pfeiffer, 2004). For either the CTS or Brandt-Brügmann data, quasicircular parameters may be chosen by constraints on either an effective gravitational potential or total energy of the system (Caudill *et al.*, 2006; Cook, 1994;ourgoulhon *et al.*, 2002). For more realistic inspiralling trajectories, the PN approximation may be used (Husa *et al.*, 2008b), or, for higher accuracy, an iterative procedure involving short numerical evolutions (Pfeiffer *et al.*, 2007).

## E. Numerically Friendly Formulations of the Evolution Equations

The Einstein evolution equations, which determine the time-development of the initial data, form a set of at least six coupled, nonlinear propagation equations. The exact formulation of these equations depends on the choice of

evolved variables as well as how constraint identities are incorporated. Although many formulations are possible, not all are equivalent from a numerical point of view. The choice of formulation can affect how numerical errors grow in time, and whether these errors can converge to zero as the resolution of the computational grid is increased.

### 1. Hyperbolicity and Well-Posedness

An ideal formulation is well-posed, meaning that: (i) for a given set of initial data, a unique solution exists, and (ii) solutions depend continuously on perturbations of the initial data. To determine whether a given formulation has the desirable property of well-posedness, we first consider it as a matrix equation:

$$\partial_t \mathbf{u} = \mathbf{A} \mathbf{u} + f(\mathbf{u}, \partial_i \mathbf{u}) \quad (17)$$

where  $\mathbf{u}$  is a vector, the components of which represent the evolved variables such as components of the metric; the linear operator  $\mathbf{A}$  is the principal part, containing the highest-order spatial derivatives; and  $f(\mathbf{u}, \mathbf{u}_{,i})$  contains additional terms which may be nonlinear. Certain conditions on the eigenvalues and eigenvectors of the operator  $\mathbf{A}$  in Eq. (17) are used to characterize the equations, typically as either “strongly hyperbolic” or “weakly hyperbolic” (Calabrese *et al.*, 2002b; Nagy *et al.*, 2004; Reula, 2004).

If the eigenvalues are real and the eigenvectors form a complete set (so any solution can be written as a linear combination of them), the equations are strongly hyperbolic. Then, assuming adequate boundary conditions, the equations are well-posed and all solutions are bounded by a function that grows (at most) exponentially at a rate independent of the initial data. Strong hyperbolicity is a key ingredient for successful black-hole merger simulations.

On the other hand, if the eigenvalues are real but the eigenvectors are not complete, the equations are weakly hyperbolic. In this case the equations are not well-posed, and they permit solutions which grow at rates that depend on the initial data. Weak hyperbolicity implies that small numerical errors in the initial data may grow at a rate which depends on the resolution. It then becomes difficult to show that the numerical solution converges to a well-defined continuum solution, and at high resolutions the simulation may become unstable (Calabrese *et al.*, 2002a).

### 2. Harmonic Formulations

The quest for workable formulations of Einstein’s equations has proceeded along two parallel lines of development. One originated with consideration of “harmonic coordinates”, so called because the coordinates satisfy

the wave equation  $\square_g x^\mu = 0$ , where  $\square_g$  is the curved-space wave operator. In these coordinates, Einstein’s equations can be written such that the principal part resembles a wave equation in terms of the metric as in Eq. (8). In this form, Einstein’s equations are manifestly hyperbolic (Choquet-Bruhat, 1962). However, the harmonic coordinate condition is too restrictive for numerical purposes, so generalized harmonic coordinates were eventually developed by introducing a source term into the coordinate condition, i.e.  $\square_g x^\mu = H^\mu$  (Friedrich, 1985; Garfinkle, 2002), a suitable choice for which preserves strong hyperbolicity. The subsequent introduction of *constraint-damping* terms, which tend to drive the constraints towards zero, further ensured stability (Gundlach *et al.*, 2005). This formulation is manifestly second-order in both time and space, and has been implemented numerically as such (Pretorius, 2006), but for more efficient numerical integration a first-order-in-time formulation was also developed (Lindblom *et al.*, 2006), and is currently being used by some groups.

### 3. ADM-based Formulations

A second line of development originated with the invention of the ADM formulation of Einstein’s equations (Arnowitt *et al.*, 1962). This formulation was refined by York Jr. (1979), who suggested evolving the specific quantity of the extrinsic curvature (Eq. (10)). The associated evolution equations specify the first-order time-derivatives for the three-metric  $\gamma_{ij}$  and the extrinsic curvature  $K_{ij}$ , as well as for the gauge variables  $\alpha$  and  $\beta^i$ . However, the ADM formulation is weakly hyperbolic (see, e.g., Chapter 5 of Alcubierre (2008)), and attempts at stable numerical evolutions with it were not successful.

There are essentially two ways to modify the ADM equations that may affect their hyperbolicity (while keeping them first-order in time and maintaining their 3+1 character). One way is to add the constraints, which may change the principal part of the equations without changing the associated physics. The other is to define new independent variables. Simple addition of constraints failed to give a strongly hyperbolic formulation however. Eventually it was found that strongly hyperbolic versions could be constructed from the ADM equations by the promotion of certain derived quantities to the status of independently evolved variables (Bona *et al.*, 1995; Kidder *et al.*, 2001; Nagy *et al.*, 2004).

Although strong hyperbolicity is important for a stable formulation, it is not the only property critical for accurate evolution. Of the various strongly hyperbolic 3+1 formulations, one eventually emerged as more successful than the rest. Its development began with the observation that the numerical accuracy of  $\gamma$ , the determinant of the three-metric, and  $K$ , the trace of the extrinsic curvature, could best be preserved by evolving these two quantities independently (Nakamura *et al.*, 1987). Subsequently, to remove the redundancy in evol-

ing the full three-metric and extrinsic curvature, the conformal three-metric

$$\tilde{\gamma}_{ij} \equiv \gamma^{-1/3} \gamma_{ij} \quad (18)$$

and conformal traceless extrinsic curvature

$$\tilde{A}_{ij} \equiv \gamma^{-1/3} (K_{ij} - \frac{1}{3} K \gamma_{ij}) \quad (19)$$

were substituted (Shibata and Nakamura, 1995). To eliminate certain terms with second derivatives (which contribute to the principal part of this system), a new independently evolved variable

$$\tilde{\Gamma}^i \equiv -\partial_j \tilde{\gamma}^{ij} \quad (20)$$

was also introduced (Shibata and Nakamura, 1995). Further improvements were made shortly afterwards, such as the addition of constraints to eliminate more second-derivative terms (Baumgarte and Shapiro, 1998). The resulting formulation, now commonly known as BSSN, proved to be robustly stable and accurate for numerical purposes. Note that the above choices which comprise its form were empirically motivated, by identifying and eliminating terms which tended to compromise numerical accuracy. Some analytic justification for its success was later found by Alcubierre *et al.* (2000), who showed that the BSSN formulation avoids exponentially growing modes and most zero-speed modes, which accumulate numerical error. Finally Sarbach *et al.* (2002) and Gundlach and Martín-García (2006) proved that BSSN is also strongly hyperbolic, given an appropriate choice of gauge.

A few noteworthy refinements of the BSSN formulation followed. (Yo *et al.*, 2002) and Duez *et al.* (2004) suggested adding specific terms proportional to the “Gamma constraint” ( $\tilde{\Gamma}^i$  minus its definition) and the Hamiltonian constraint into the evolution equations. These terms have the effect of damping the constraints and thereby improving stability.

Later, for evolution of punctures specifically, Campanelli *et al.* (2006a) evolved the conformal factor in the form  $\chi = \gamma^{-1/3}$ , which vanishes at the puncture (an improvement in accuracy over the previous standard of  $\phi = \ln(\gamma)/12$ , which is singular at the puncture). This change of variables, however, introduces the potentially singular factor  $1/\chi^2$  into the evolution equations, necessitating an arbitrary restriction on the minimum value of  $\chi$ . An alternative variable  $\chi' = \gamma^{-1/6}$  was subsequently suggested because resulting appearances of  $1/\chi'^2$  mostly cancel with factors of  $\gamma^{1/3}$  (Marronetti *et al.*, 2008; Tichy and Marronetti, 2007; van Meter, 2006).

## F. Gauge Conditions

The choice of gauge or coordinate conditions, like the choice of formulation, has important consequences on the

numerics, especially the stability of the simulation. Important considerations include how to deal with the extreme conditions of black holes such as the physical singularities, the possible coordinate singularities, the strong-field gradients, and the dynamical, surrounding space-time. The coordinates must accommodate these features in a way that is numerically tractable.

### 1. Choosing the Slicing and Shift

An early consideration was how to avoid the physical singularity of a black hole through an appropriate slicing condition. One such choice, *maximal slicing*, required solution of a numerically expensive elliptic equation (Estabrook *et al.*, 1973; Lichnerowicz, 1944; Smarr and York Jr., 1978). Later, an interest in constructing a hyperbolic evolution system led to a generalization of harmonic slicing known as the Bona-Massó family (Bona *et al.*, 1995). One particular member of this family, called 1+log slicing, was found to also be singularity-avoiding, like maximal slicing, but at less numerical cost (Aninos *et al.*, 1995a; Bernstein, 1993).

Meanwhile, it was recognized that a shift vector was required to counter the large field gradients, or “slice-stretching”, incurred in the presence of a black hole (Alcubierre and Brügmann, 2001). A hyperbolic shift condition called the “Gamma driver” was introduced that fulfilled this requirement (Alcubierre and Brügmann, 2001; Alcubierre *et al.*, 2003, 2001b):

$$\partial_t B^i = \partial_t \tilde{\Gamma}^i - \eta_\beta B^i, \quad (21)$$

$$\partial_t \beta^i = F B^i, \quad (22)$$

where  $\tilde{\Gamma}^i = -\partial_j \tilde{\gamma}^{ij}$  depends on a conformal three-metric  $\tilde{\gamma}_{ij}$  of the evolving spatial slice,  $B^i$  is an auxiliary variable,  $\beta^i$  is the shift, and  $F$  is some scalar field.  $\eta_\beta$  is a damping parameter that fine-tunes the growth of the shift, which affects the coordinate size of the black-hole horizons, which in turn has bearing on the required numerical resolution (Brügmann *et al.*, 2008b; González *et al.*, 2009). This shift condition also has the desirable tendency to drive the coordinates to quiescence in synchrony with the physics, for example after a binary merges into a stationary black hole. Clearly if  $\tilde{\Gamma}^i$  vanishes,  $B^i$  is damped to zero and  $\beta^i$  approaches a (typically small) constant.

### 2. Moving Punctures

Initially these conditions were intended for use with punctures that remained at fixed coordinate positions (i.e. comoving coordinates), by choosing  $F$  to vanish at the punctures. However, this led to large gradients between the merging black holes since there the metric had

to vanish as the physical distance contracted. Pathologies also arose from the twisting of the coordinates as the black holes orbited each other.

These issues, which resulted in large numerical errors and instabilities, were eventually resolved with the breakthrough discovery that slight modifications of the 1+log and Gamma-driver conditions allowed arbitrary motion of the punctures with robust stability (Baker *et al.*, 2006b; Campanelli *et al.*, 2006a). In particular, in the shift condition, a critical alteration was “unpinning” the puncture by no longer requiring the factor  $F$  to vanish at the puncture but rather to remain constant. These modifications were subsequently refined to eliminate zero-speed modes, thus preventing the possibility of error build-up (van Meter *et al.*, 2006a). This was accomplished in part by the addition of advection terms:

$$\partial_t B^i = \partial_t \tilde{\Gamma}^i - \beta^j \partial_j \tilde{\Gamma}^i - \eta_\beta B^i + \beta^j \partial_j B^i, \quad (23)$$

$$\partial_t \beta^i = \frac{3}{4} B^i + \beta^j \partial_j \beta^i. \quad (24)$$

It is noteworthy that these particular gauge choices, coupled with the BSSN equations, also result in strong hyperbolicity (Gundlach and Martín-García, 2006; Sarbach *et al.*, 2002). A further refinement resulted from the observation that, assuming that  $\beta^i = B^i = \tilde{\Gamma}^i = 0$  initially, Eqs. (23) and (24) can be integrated to yield  $B^i = \tilde{\Gamma}^i - \frac{4}{3} \eta_\beta \beta^i$ ; this substitution allows the removal of the equation for  $B^i$ , leaving only a single shift equation (van Meter *et al.*, 2006a):

$$\partial_t \beta^i = \frac{3}{4} \tilde{\Gamma}^i + \beta^j \partial_j \beta^i - \eta_\beta \beta^i. \quad (25)$$

Use of this or similar gauge conditions became known as the “moving puncture” method, and proved to be very successful as it became increasingly widespread among the numerical-relativity community. Analysis has verified that moving punctures are valid black-hole solutions, although the initial character of the punctures changes significantly during the course of evolution. The second worldsheet shown in Fig. 3, for example, invariably becomes disconnected in numerical simulations, at a point within the horizon near the throat, due to the action of the shift vector effectively shifting computational grid points onto the first worldsheet. Meanwhile the spatial coordinates evolve such that the  $r^{-1}$  singularities in the conformal factor  $\psi$  become  $r^{-1/2}$  singularities. For a single nonspinning black hole, the numerical result rapidly asymptotes to an exact form of the Schwarzschild solution called a “trumpet”, recently investigated by Brown (2008); Hannam *et al.* (2007a, 2009b, 2008b, 2007b) and Baumgarte and Naculich (2007), which turns out to be a type of solution first considered by Estabrook *et al.* (1973).

### 3. Generalized Harmonic Coordinates

Development of generalized harmonic coordinates initially proceeded independently of the above 3+1-

formulated conditions. As mentioned, in harmonic coordinates the D’Alembertian of each coordinate vanishes. In generalized harmonic coordinates, the wave equation for each coordinate is allowed a source term, i.e.

$$\square x^\mu = H^\mu. \quad (26)$$

These “gauge driving” source terms  $H^\mu$  can be either algebraically specified or evolved such that hyperbolicity is preserved (Friedrich, 1985; Garfinkle, 2002; Lindblom *et al.*, 2006; Pretorius, 2006).

The first successful numerical orbit of black holes involved a source term for the time coordinate that effectively kept the lapse close to its Minkowski value of unity, while the spatial coordinates remained harmonic (Pretorius, 2006). This was accomplished by evolving the source term itself, according to

$$\square H_0 = [-\xi_1(\alpha - 1) + \xi_2(\partial_t - \beta^i \partial_i) H_0] \alpha^{-1} \quad (27)$$

where  $\xi_1$  and  $\xi_2$  are constants. More recently, to dampen extraneous gauge dynamics during the inspiral and merger of generic binaries, Szilágyi *et al.* (2009) found the following gauge driver to be successful:

$$H_0 = \mu_0 \left[ \log \left( \frac{\sqrt{g}}{\alpha} \right) \right]^3 \quad (28)$$

$$H_i = -\mu_0 \left[ \log \left( \frac{\sqrt{g}}{\alpha} \right) \right]^2 \frac{\beta_i}{\alpha} \quad (29)$$

where  $\mu_0$  is a specified function of time that starts at zero and eventually increases monotonically to unity.

### 4. Other Coordinate Techniques

Additional noteworthy advances in coordinate conditions were developed for the generalized harmonic formulation to facilitate spectral methods (see Sec. IV.G below) but are in principle generalizable to other frameworks. One of these is the use of multiple coordinate patches, where the coordinates are chosen according to the local physical geometry for optimal accuracy. In the generalized harmonic formulation, characteristic speeds are readily available for use in constructing physical boundary conditions between patches (Lindblom *et al.*, 2006; Pazos *et al.*, 2009; Scheel *et al.*, 2006).

The other advance is that of “dual coordinates”. Because moving punctures involve irregular fields, they are not easily made compatible with spectral methods, which are sensitive to irregularities. An alternative, that of a moving, excised region, can leave a large trail of interpolation error in its wake. The remaining option is to use comoving coordinates (Brügmann *et al.*, 2004), but these can result in instabilities due to the steep field gradients and other pathologies mentioned in Sec. IV.F. Dual coordinates were invented to exploit the advantages of both comoving and non-comoving coordinates while avoiding their disadvantages. This is accomplished by computing

all tensor field components in the non-comoving coordinate system (thus avoiding steep gradients), yet evolving them as functions of the comoving coordinates (thus allowing stationary excision boundaries) (Scheel *et al.*, 2006).

### G. Numerical Approximation Methods

The initial data, formulation, and gauge are all, in principle, analytic choices applicable to an infinite, continuous manifold. One must finally make choices pertaining explicitly to the finite, discrete mechanics of the computations that will numerically approximate the above analytic specifications. An immediate consideration is the fact that the simulated domain must have finite extent. Various conformal compactification schemes which map spatial or null infinity to a finite boundary have been tested (Pretorius, 2006; Rinne, 2010; van Meter *et al.*, 2006b), but currently it is more common to impose artificial boundaries at finite spatial coordinates and apply some form of either radiative boundary condition (Alcubierre *et al.*, 2003) or constraint-preserving boundary condition (Lindblom *et al.*, 2006).

To mitigate the effect of inward-propagating errors from the outer boundaries, some form of mesh refinement is typically employed to push the outer boundaries as far away as possible from regions of interest (e.g. wave sources and extraction regions). With a limited number of grid points available, their density is judiciously chosen to be highest near the strong field gradients of the black holes, moderate throughout regions where wave propagation is studied, and coarser beyond that. If the simulated black holes are very dynamic then some algorithm for automatically adapting the mesh refinement is necessary. Meanwhile the interfaces between refinement regions require interpolation.

On this grid, spatial derivatives are computed in one of two ways. They may be computed with finite differencing stencils across uniformly spaced grid points, derived from Taylor expansions, currently up to eighth-order accurate (Lousto and Zlochower, 2008; Pollney *et al.*, 2009). Alternatively, the spectral approach may be used, in which coefficients of an expansion in basis functions are computed to some order, on a number of collocation points comparable to the number of basis modes, from which the derivatives are then obtained analytically (Boyle *et al.*, 2007b). In the former case, dissipative terms are often added to the evolution equations to reduce noise (Kreiss and Olinger, 1973). In the latter case, spectral methods often include a smoothing step for a similar end.

Last, time must be advanced in discrete steps. Various explicit time-integration algorithms have been tested, for example the iterated Crank-Nicholson scheme, but the fourth-order Runge-Kutta algorithm has become most widely used, due to its superior accuracy and efficiency. In some codes the timestep size is made to vary with spatial resolution, for even greater efficiency, albeit at the

expense of the complication of time-interpolation. Implicit timestepping schemes are also being investigated as a means to greatly increase the timestep size (Lau *et al.*, 2009).

### H. Extracting the Physics

One of the most important end-results of a simulation of merging black holes is a computation of the emitted gravitational radiation. For this purpose, it is useful to calculate the “Weyl tensor”,  $C_{abcd}$ . The Weyl tensor, like the Einstein tensor, is constructed from derivatives of the metric. Unlike the Einstein tensor, the Weyl tensor has degrees of freedom that do not necessarily depend on a massive source; it can be nonzero while the Einstein tensor vanishes.

Certain components of the Weyl tensor form a complex quantity called  $\Psi_4$ , one of five “Weyl scalars” used to classify spacetimes (Newman and Penrose, 1962). In a special, “transverse-traceless”, spherical coordinate system,  $\Psi_4$  can be expressed as follows:

$$\Psi_4 = C_{\hat{r}\hat{\theta}\hat{r}\hat{\theta}} - C_{\hat{r}\hat{\phi}\hat{r}\hat{\phi}} - 2iC_{\hat{r}\hat{\theta}\hat{r}\hat{\phi}}, \quad (30)$$

where the subscripts  $\{\hat{r}, \hat{\theta}, \hat{\phi}\}$  denote orthonormal tetrad components. In a spacetime with gravitational radiation this quantity typically falls off as  $\sim 1/r$  (Newman and Penrose, 1962), and can be associated with outgoing radiation at spatial infinity ( $r \rightarrow \infty$ ) in asymptotically flat spacetimes (Szekeres, 1965). In terms of the strain introduced in the last section, this can be written

$$\lim_{r \rightarrow \infty} (r\Psi_4) = \lim_{r \rightarrow \infty} \left[ -r(\ddot{h}_+ - i\ddot{h}_\times) \right], \quad (31)$$

where, in terms of a metric perturbation  $h_{\mu\nu} = g_{\mu\nu} - \eta_{\mu\nu}$ ,

$$h_+ = \frac{1}{2}(h_{\hat{\theta}\hat{\theta}} - h_{\hat{\phi}\hat{\phi}}), \quad (32)$$

$$h_\times = h_{\hat{\theta}\hat{\phi}}. \quad (33)$$

What makes  $\Psi_4$  a particularly useful measure of the radiation is that to first order in  $h_{\mu\nu}$  it is coordinate-invariant.

Although the linearized radiation interpretation for  $\Psi_4$  is only strictly valid in the limit as  $r \rightarrow \infty$ , in numerical simulations it is often extracted on a sphere of large but finite radius. This will approximate the expected radiative behavior if  $|h_{\mu\nu}| \ll 1$ ; if spheres of multiple radii are used then it is also possible to extrapolate the results to infinity. Typically  $\Psi_4$  is computed on the computational grid points from the metric variables and then interpolated onto the spherical extraction surface. Recently, Cauchy-characteristic extraction methods have been applied to allow direct evaluation of radiation at future null infinity (Reisswig *et al.*, 2009).

The product of  $\Psi_4$  with a spherical harmonic function is then integrated over the sphere, as it is useful

to extract specific modes of the field. The structure of the gravitational field is such that it is convenient to expand in spin-weight -2 spherical harmonics  ${}_{-2}Y_{\ell m}(\theta, \phi)$  (Newman and Penrose, 1966; Teukolsky, 1972) (just as, analogously, it proves convenient to use the spin-weighted -1 harmonics in expanding the electromagnetic field). Thus:

$$\Psi_4 = \sum_{\ell=2}^{\infty} \sum_{m=-\ell}^{m=\ell} \Psi_{4,\ell m} {}_{-2}Y_{\ell m} \quad (34)$$

Unlike electrodynamics, there is no dipole moment of the gravitational field in conventional general relativity, so the dominant contribution is the  $\ell = 2$  quadrupole moment.

Other information that is important in analyzing spacetimes relates to the properties of the black holes themselves. This is commonly taken from apparent horizons, surfaces from which all light rays must go inward. It is useful to compute this during a simulation, for example by finding surfaces on which the expansion of light rays are minimized (Thornburg, 2004). When a black hole is sufficiently isolated, it is possible to define a mass and spin magnitude from data evaluated on the horizon (Campanelli *et al.*, 2009, 2006c; Dreyer *et al.*, 2003), as well as linear momentum (Krishnan *et al.*, 2007). These quantities can be used to characterize the physical properties of the black holes, and to label the spacetimes when comparing with PN theory.

## V. BLACK-HOLE MERGER DYNAMICS AND WAVEFORMS

The final merger of a black-hole binary takes place in the dynamical, strong-field regime of general relativity. For many years, numerical relativists wondered what they would find when they probed this arena using black-hole merger simulations. What would the merger waveforms look like? How strongly might artifacts in the initial data affect the mergers? How might the effects of unequal masses and spins change the picture obtained by studying the simplest case of nonspinning, equal-mass mergers? Would they uncover any unexpected phenomena? Recent breakthroughs in black-hole merger simulations are providing important tools for addressing such questions.

In this section we explore the dynamics of black-hole mergers and the resulting gravitational waveforms. We start with a look at the Lazarus approach, which provides hybrid waveforms by combining analytic methods with brief numerical simulations. We then begin a more comprehensive discussion of black-hole merger physics, starting with mergers of nonspinning, equal-mass black holes. Next we consider mergers of unequal-mass holes, followed by mergers with spin. Throughout this discussion we aim to provide a historical context while highlighting the key physical results.

### A. First Glimpses of the Merger: The Lazarus Approach

In the late 1990s, numerical relativity had advanced sufficiently to allow brief simulations of two black holes in three dimensions. By “brief” we mean here durations of  $\sim 10M$ , which is a small fraction of the estimated binary orbital period of  $\gtrsim 100M$  near the ISCO. While most of the community focused on technical developments aimed at extending the duration of these simulations, a small band of collaborators took a different approach (Baker *et al.*, 2000).

Their novel idea was to use full numerical-relativity simulations to calculate the strong-field approach to merger during  $\sim 10M$  of simulation time, and then to calculate the remaining evolution using perturbative techniques (Baker *et al.*, 2002a). They began with traditional puncture black holes (which remain fixed in the grid) on quasicircular orbits near the ISCO, and evolved them towards merger. Then, just before the simulation became unstable, they stopped the calculation and extracted the physical data for the merging black holes and the emerging gravitational waves. This data was then interpreted as initial data for a highly distorted single black hole, and evolved using techniques of black-hole perturbation theory. They called this method of reviving a (nearly) dead calculation the *Lazarus* approach.

The hybrid waveforms produced by the Lazarus collaboration gave the first indications of what might be expected from the final merger of black-hole binaries (Baker *et al.*, 2001, 2002b). They ran a suite of simulations, varying the initial black-hole separations and the time at which they stopped the calculation and made the transition from the fully numerical evolution to the perturbed black hole evolution. Figure 4 shows the dominant quadrupole  $\ell = 2, m = 2$  component of  $\text{Re}(\Psi_4)$ , which corresponds to the + polarization, for the case of equal-mass, nonspinning black holes. Note the simple shape of the waveform smoothly tying together what might be the end of an (inspiral) chirp with a damped (ringdown) sinusoid.

By tuning the mass and spin of the background hole for the perturbative evolution, Baker *et al.* (2002b) also determined that the merger remnant was a Kerr (spinning) hole of mass  $M_{\text{Kerr}} \approx 0.97M_{\text{initial}}$ , and spin  $a_{\text{Kerr}} \approx 0.7M_{\text{Kerr}}$ .

The Lazarus method was also applied to mergers of black holes with spins either aligned or anti-aligned with the orbital angular momentum (Baker *et al.*, 2004); in all cases, a similar waveform shape was seen. How generic was this simple shape and, in particular, would it also arise in situations where the black holes complete one or more orbits before merging?



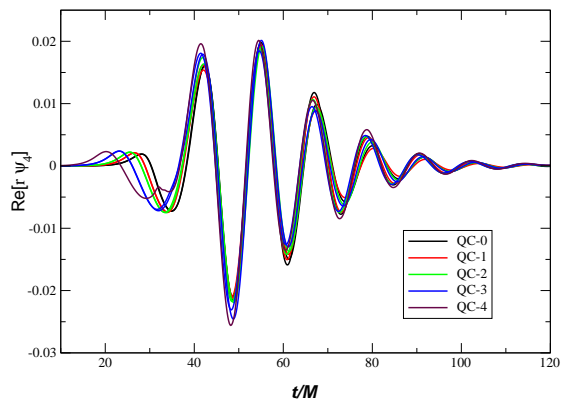


FIG. 4 Lazarus waveforms for equal-mass, nonspinning black-hole mergers, from Baker *et al.* (2002b). The real,  $\ell = 2, m = 2$  part of  $r\Psi_4$ , corresponding to the  $+$  polarization (measured on the system’s axis), is shown for ten simulations: five different initial black-hole separations (designated QC-0, etc.), each with two transition times to perturbative evolution.

## B. Mergers of Equal-Mass, Nonspinning Black Holes

### 1. The First Merger Waveforms

Early in 2005, Frans Pretorius stunned the community by achieving the first robust simulation of two equal-mass black holes through a single plunge orbit, merger, and ringdown (Pretorius, 2005a). The resulting gravitational waveforms are shown in Fig. 5, where  $r\text{Re}(\Psi_4)$  is plotted versus  $t/M_0$ . Here  $r$  is the coordinate distance from the center of the grid to the sphere on which the waveform is extracted (see Sec. IV.H), and  $M_0 \sim 0.5M$  is the mass of a single black hole. (Note that the time axes for all other waveform plots in this paper are scaled by either the total system mass  $M$  or the mass of the final, remnant black hole  $M_f$ ). Here curves are plotted for waveforms extracted on four spheres with successively larger radii. The curves have been shifted in time so that the waveforms overlap. Note that the overall waveform shape is simple. The merger yields a single black hole that is spinning, with spin parameter  $a_f \sim 0.70M_f$ , where  $M_f$  is the mass of the final black hole that forms.

To carry out these mergers, Pretorius (Pretorius, 2005b, 2006) used techniques that are very different from the more traditional approach based on BSSN and punctures, used by nearly all other numerical relativists. As discussed in Sec. IV.E.2, he used a generalized harmonic formulation in which the Einstein equations are written with second-order time and space derivatives. The spatial domain was compactified, so that the outer boundary of each slice was mapped to spatial infinity. Moreover, he excised the black holes (each formed from the collapse of scalar field “blobs”) and evolved their motion across the grid using adaptive mesh refinement (see Secs. IV.C and IV.G).

Pretorius had clearly developed a robust method for evolving black-hole binary mergers. In the wake of his

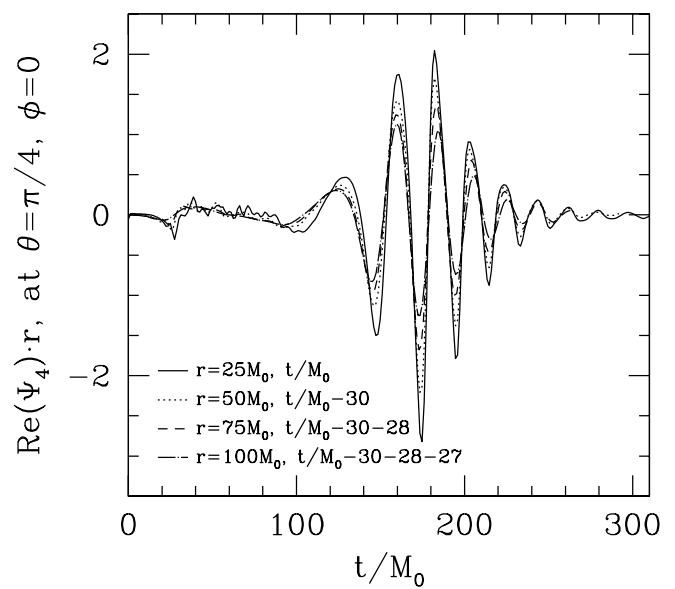


FIG. 5 The first gravitational waveform for black holes evolving through a single plunge orbit, merger, and ringdown, achieved by Pretorius (2005a). The waves were extracted at four radii, and shifted in time to overlap for comparison. Note the amplitudes decrease for larger  $r$ , due to lower resolution in the outer regions

remarkable success, many numerical relativists began studying his methods. However, another surprise was soon to emerge.

In the autumn of 2005 two research groups, one at UTB and the other at Goddard, independently developed a powerful technique for evolving mergers of puncture black holes within the traditional BSSN approach (Baker *et al.*, 2006b; Campanelli *et al.*, 2006a). As discussed in Sec. IV.F.2, the standard puncture method requires the black holes to remain fixed on the numerical grid. In this new “moving puncture” approach, simple but novel gauge conditions allow the punctures to move across the grid, producing accurate and stable merger evolutions (van Meter *et al.*, 2006a).

Although the UTB and Goddard codes were both based on the BSSN approach, they were independently written and featured somewhat different implementations of moving punctures. In addition, the Goddard code used second-order finite differencing (standard in the community at the time). They employed a box-in-box fixed mesh refinement to produce the high resolution in the region around the black holes needed to compute the dynamics accurately, while maintaining adequate resolution in more distant regions and a large enough computational domain to allow accurate extraction of the gravitational waves. The UTB code used fourth-order finite differencing, and the “fish-eye” coordinate transformation to produce higher resolution around the black-hole orbits and lower resolution in the wave extraction regions.

Both groups successfully evolved an equal-mass, non-

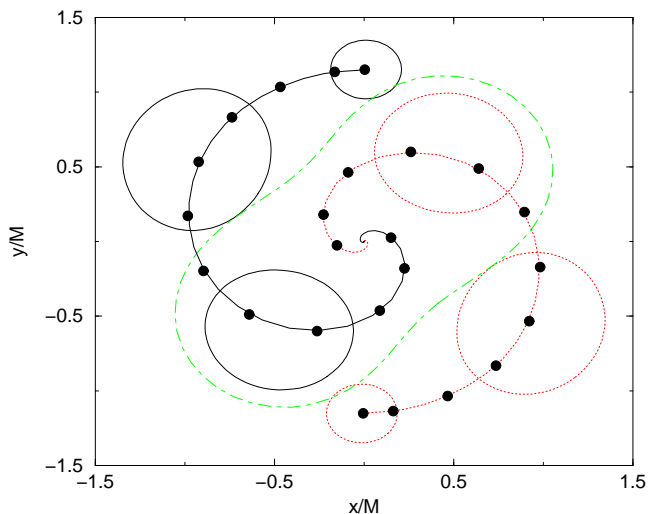


FIG. 6 The trajectories of the black-hole punctures from a run by Campanelli *et al.* (2006a). The individual apparent horizons are shown at times  $t = 0, 10M$  and  $18.8M$ . The solid circles denote the centroids of the apparent horizons every  $2.5M$  during the evolution. The first common horizon, marking the time of merger, forms at  $18.8M$ , just before the punctures complete  $1/2$  orbit.

spinning binary through the final plunge orbit, merger, and ringdown, and extracted the gravitational waveforms. In these simulations, the black holes completed  $\sim 1/2$  orbit before merger, defined as the time at which a single apparent horizon was formed. Figure 6 shows the tracks traced by the black-hole punctures, with the apparent horizons superimposed, for the UTB run (Campanelli *et al.*, 2006a). These simulations produced plunge waveforms with a simple shape similar to that found by Pretorius; compare Fig. 5 from Pretorius’s simulations with Fig. 7, which shows waveforms from the Goddard simulation plus a corresponding Lazarus waveform.

## 2. Universal Waveform

In most cases, astrophysical black-hole binaries spiral together over many orbits, radiating away any orbital eccentricity in the form of gravitational waves. By the time the black holes reach the final inspiral, their orbits will be quasicircular. All mergers of such equal-mass non-spinning binaries should thus produce the same waveform signature, subject only to rescaling with the total system mass  $M$ .

Over the years, concerns had been raised within the relativity community about the effects of deviations from astrophysical initial conditions on the waveforms. For example, spurious eccentricity in the orbits could arise from starting conditions that did not approximate quasicircular inspiral accurately. Moreover, the commonly-used conformal flatness prescription (see Sec. IV.D) for the

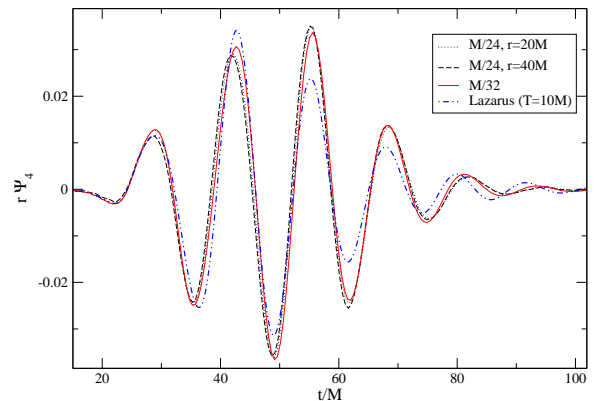


FIG. 7 Gravitational waveforms from the black-hole merger simulations by Baker *et al.* (2006b). The real part of the  $\ell = 2$ ,  $m = 2$  mode of  $r\Psi_4$  was extracted from the numerical simulation on spheres of radii  $r = 20M$ , and  $40M$  for the medium- and high-resolution runs. The waveforms extracted at different radii have been rescaled by  $r$ , and shifted in time to account for the wave propagation time between the two extraction spheres. Curves are shown for medium ( $M/24$  in the finest grid) and high ( $M/32$ ) resolutions. A waveform from a Lazarus calculation starting with the same initial data is shown for comparison (Baker *et al.*, 2002b). The Lazarus waveform shown in this figure is scaled differently from those in Fig. 4.

initial data is different from the conditions experienced by an astrophysical binary; these differences would result in spurious gravitational radiation being present in the initial conditions for the binary simulations. How would factors such as these influence the merger waveforms?

Having developed robust techniques for evolving black-hole mergers, numerical relativists eagerly pursued longer simulations with the black holes starting at wider separations, completing more orbits, and producing longer wavetrains. The UTB group ran a simulation in which the black holes completed nearly 1.5 orbits before the formation of a single apparent horizon (Campanelli *et al.*, 2006b). They observed that the resulting waveform was quite similar to those produced by their earlier simulation that started near the plunge (Campanelli *et al.*, 2006a), with a brief oscillatory signal at the beginning. (Campanelli *et al.*, 2006b) anticipated “that the plunge waveform, when starting from quasicircular orbits, has a generic shape that is essentially independent of the initial separation of the binary.”

The Goddard group, simultaneously pursuing this same goal, produced the first “universal” waveform for the merger of equal-mass, nonspinning black holes (Baker *et al.*, 2006a). Using approximately quasicircular initial conditions, they ran a series of four simulations, starting the black holes at increasingly wider separations. In all, the binaries completed  $\sim 1.8, 2.5, 3.6,$  and  $4.2$  orbits before forming a common apparent horizon; the systems emitted just under 4% of their energy as gravitational radiation, and the final black holes were spinning with  $(a/M)_f \sim 0.69$ . To compare the results

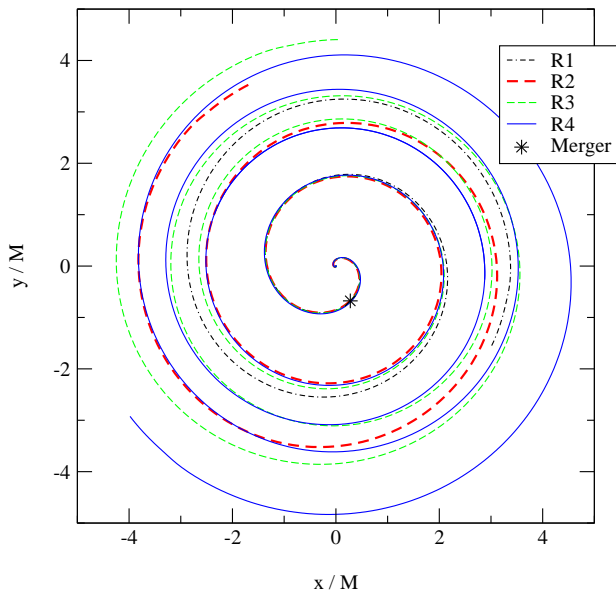


FIG. 8 Puncture tracks from equal-mass, nonspinning black-hole merger simulations starting at increasingly larger separations by Baker *et al.* (2006a). For clarity, the trajectory of only one black hole in each run is shown. The tracks lock on to a universal trajectory  $\sim 1$  orbit before merger (denoted by \*).

of these models, they chose the fiducial time  $t = 0$  to be the moment of peak amplitude in the gravitational radiation; this typically occurs within a few  $M$  of merger. It is worth noting how close these results are to those obtained from the Lazarus approach to the same system (see Sec. V.A).

The binary orbital dynamics of these runs is clearly seen in Fig. 8, which shows the tracks of the black-hole punctures. Here only one puncture track is shown for each binary, with the trajectories oriented to superpose at the fiducial  $t = 0$ . The tracks show the effects of eccentricity in the early stages of each run; plots of the separation  $r$  versus time show that the initial eccentricity decreases as the initial separation increases. As the holes spiral together into the strong-field regime, the eccentricity diminishes. The puncture tracks lock on to a single universal trajectory, independent of the initial conditions, through the final orbit, plunge, and merger.

Figure 9 shows the corresponding universal gravitational waveform for equal-mass, nonspinning black holes. Specifically, it shows the real part of the  $\ell = 2$ ,  $m = 2$  mode of  $r\Psi_4$  versus time; for this case, the quadrupole ( $2, \pm 2$ ) modes strongly dominate all other modes. Here the signals produced by each run have been shifted in time so that  $t = 0$  marks the moment of peak radiation amplitude. Starting from  $t \sim -50M_f$ , the waveforms for the final burst of radiation show nearly perfect agreement, with differences at the level of  $\sim 1\%$ . For the preceding few orbits, the waveforms agree in amplitude and phase to  $\sim 10\%$ , except for the brief initial bursts of spurious radiation (see Sec. IV.D). Overall, the merger

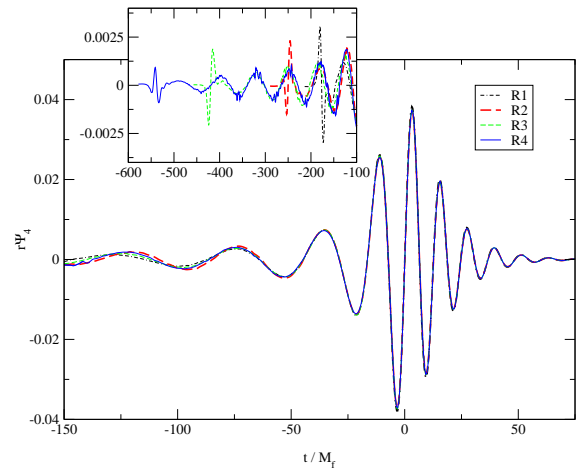


FIG. 9 The universal waveform ( $\ell = 2$ ,  $m = 2$  mode) produced by the four simulations whose puncture tracks are shown in Fig. 8 (Baker *et al.*, 2006a). The signals have been shifted in time so that the peak radiation amplitude occurs at  $t = 0$ . The agreement among the waveforms is excellent, with differences  $\sim 1\%$  for the final burst of radiation starting at  $t \sim -50M_f$ .

stage lasts  $\sim 100M$ , converting  $\sim 4\%$  of the initial total mass  $M$  into gravitational-wave energy. The gravitational wave released during this burst has a luminosity  $L \sim 10^{23}L_\odot$ , which is greater than the total luminosity of all the stars in the visible Universe. For stellar black-hole binary mergers, this luminosity will last for a few milliseconds, while for MBH binaries it will last for several minutes.

Note that this universal waveform has a simple shape. The signal starts with a short inspiral chirp, increases smoothly in amplitude during the plunge and merger, and then transitions to the damped ringdown sinusoid. Overall, the frequency increases monotonically, reaching a maximum value that stays constant during the ringdown (Baker *et al.*, 2006a).

Since black-hole-merger waveforms will be used to help find signals in data from gravitational-wave detectors, it was important to verify that various groups consistently achieve the same results. Figure 10 provides a comparison of waveforms computed by Pretorius and the groups at UTB and Goddard for equal-mass, nonspinning black-hole mergers (Baker *et al.*, 2007b); here the real part of  $r\Psi_4$ 's dominant  $\ell = 2$ ,  $m = 2$  mode is shown, with all three waveforms aligned in time so that the moment of peak gravitational radiation amplitude occurs at  $t = 0$ . All three simulations evolved through the last  $\sim 1.8 - 2.5$  orbits before merger; the Goddard run is R1 from Baker *et al.* (2006a) and shown in Figs. 8 and 9. Note that all evolutions produce the same overall waveform shape. The Goddard and UTB groups evolved black holes with zero spin starting on similar quasicircular initial orbits, and produced nearly identical waveforms. Pretorius used co-rotating initial conditions which impart a small spin  $(a/M)_{1,2} = 0.08$  to each black hole.

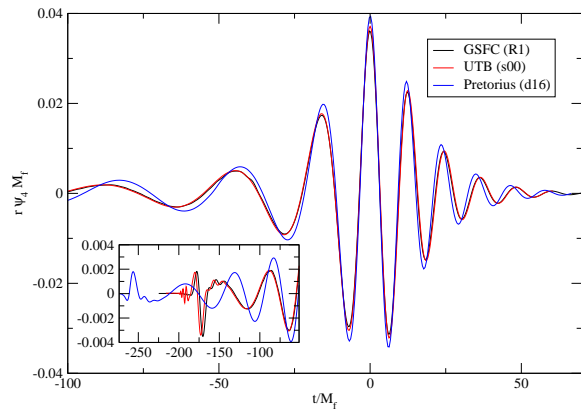


FIG. 10 Comparison of three waveforms from simulations of equal-mass black-hole mergers computed by Pretorius and the UTB and Goddard groups (Baker *et al.*, 2007b). The UTB and Goddard simulations used nonspinning black holes, whereas Pretorius’ initial conditions produced co-rotating black holes, each with a small spin  $(a/M)_{1,2} = 0.08$ . The differences between Pretorius’ waveform and the others during the ringdown,  $t/M_f \gtrsim 25$ , are consistent with his simulation producing a slightly faster rotating final black hole due to these initial spins. Reproduced by permission of the Institute of Physics.

This difference is consistent with the slightly higher frequencies seen in Pretorius’ results during the ringdown,  $t \gtrsim 25M_f$ .

How robust is this universal waveform to larger amounts of orbital eccentricity and gravitational radiation in the initial data? Hinder *et al.* (2008) studied a series of equal-mass, nonspinning binaries starting from roughly the same initial orbital period and having varying amounts of initial orbital eccentricity  $e$ . For  $e \lesssim 0.4$ , the initial eccentricity is radiated away, and the binaries circularize and begin a universal plunge at  $t \sim 50M_f$  before the time of peak radiation amplitude, producing a final black hole with  $a \sim 0.69M_f$ . For  $e \gtrsim 0.5$ , the black holes do not complete any orbits, but rather plunge together and merge; the final black hole spin reaches a maximum value  $a \sim 0.72M_f$  around  $e \sim 0.5$ . Figure 11 shows the puncture tracks, and Fig. 12 shows the real part of the strain’s  $\ell = 2$ ,  $m = 2$  mode, for two nonspinning, equal-mass black-hole mergers with nonzero eccentricity from this study; in both cases, Hinder *et al.* (2008) show quantitatively that the waveform for the final burst of radiation is the same as the universal waveform.

In a complementary study, Sperhake *et al.* (2008a) found that the final spin of the remnant black hole is essentially insensitive to the eccentricity for binaries that do not plunge immediately. Bode *et al.* (2008) examined the effects of spurious gravitational waves by superposing a tunable packet of gravitational radiation on an equal-mass, nonspinning binary. They found the binary evolution and the spin of the remnant black hole to be robust to modest amounts of added gravitational radiation.

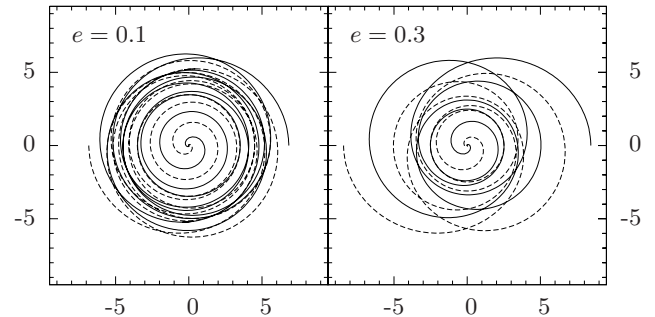


FIG. 11 Puncture tracks for equal-mass black-hole mergers with initial orbital eccentricity  $e = 0.1$  (left) and  $e = 0.3$  (right) from Hinder *et al.* (2008). In these cases, the initial eccentricity is radiated away and the binaries circularize before merger.

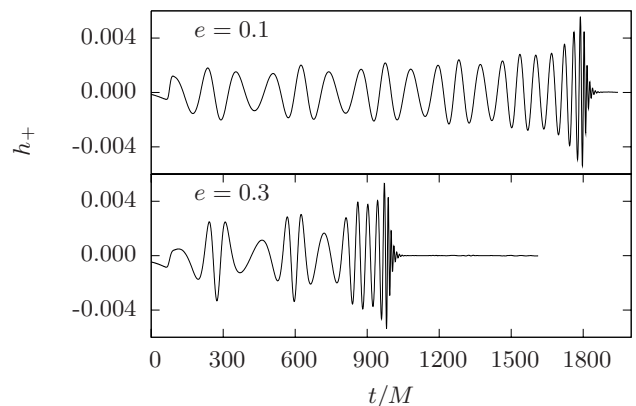


FIG. 12 Real part of  $(2,2)$  strain mode (labeled  $h_+$  here) for black-hole mergers shown in Fig. 11 from Hinder *et al.* (2008). These runs have initial orbital eccentricity  $e = 0.1$  (top) and  $e = 0.3$  (bottom) and enter a universal plunge by  $t \sim 50M_f$  before the gravitational radiation reaches its peak value.

### 3. Longer Waveforms

The black-hole simulations discussed so far cover the last  $\lesssim$  four orbits before merger. These achievements marked the triumph of solving a long-standing problem of fundamental importance to general relativity: the two-body problem for the final merger of equal-mass Schwarzschild black holes driven by gravitational radiation reaction. These simulations provided the first look at the dynamics and waveforms of black holes evolving and merging in the nonlinear, strong-field regime. They also pointed the way towards applications in detecting the final gravitational-wave burst from black-hole mergers (Baumgarte *et al.*, 2008). However, for more advanced applications to gravitational-wave data analysis and comparisons with PN analytical treatments, longer

waveforms that start many cycles before merger are essential.

The Goddard group (Baker *et al.*, 2007c,d) produced the first such long waveforms for equal-mass, nonspinning black holes starting  $\sim 7$  orbits or  $\sim 14$  gravitational-wave cycles before merger. They used improved initial conditions with low eccentricity  $e < 0.01$ , and focused on improving accuracy while the black holes traversed the relatively long inspiral. They investigated the observability of black-hole mergers with ground- and space-based gravitational-wave detectors (Baker *et al.*, 2007c) (see Sec.VII.A) and successfully applied their long waveforms to comparisons with PN results, focusing on the waveform phases (Baker *et al.*, 2007d).<sup>4</sup>

Shortly thereafter, the Jena group simulated a binary inspiralling for nine orbits (18 gravitational-wave cycles) before merger (Hannam *et al.*, 2008c). With this, they made the first quantitative comparisons with both the PN phase *and* amplitude, and quantified the level of error in the quadrupole approximation. They used higher-order finite differencing (Husa *et al.*, 2008a) and initial binary parameters calculated using the PN approximation to reduce the initial eccentricity significantly (Husa *et al.*, 2008b), enabling a precise measurement of the waveform phase.

The Caltech-Cornell group currently holds the record for the longest and most accurate black-hole binary evolution, starting 16 orbits and 32 gravitational-wave cycles before merger (Scheel *et al.*, 2009). Using their spectral code (see Sec. IV.G), they begin with a very small initial orbital eccentricity  $e \sim 5 \times 10^{-5}$  and evolve with very high accuracy through a relatively long inspiral, then merger and ringdown. The impressive trajectories of their black holes are shown in Fig. 13 and the accompanying gravitational waveforms in Fig. 14.

Comparison of waveforms from different groups remains important in the push for higher accuracy and use in gravitational-wave data analysis. The Samurai project (Hannam *et al.*, 2009a) sets the current state of the art for studying the consistency of black-hole binary waveforms. This effort focuses on comparing waveforms from equal-mass, nonspinning binaries, starting with at least six orbits (or 12 gravitational-wave cycles) before merger and continuing through the ringdown. They focus on comparing the amplitude  $A(t)$  and phase  $\phi(t)$  for the  $\ell = 2, m = 2$  mode of  $r\Psi_4$ , defined as

$$r\Psi_{4,22}(t) = A(t)e^{-i\phi(t)}; \quad (35)$$

the gravitational-wave frequency of this mode is then

<sup>4</sup> Recall that the PN approximation is an expansion in powers  $\epsilon = v^2/c^2$  and applies when the black holes are far enough apart that the black hole speeds remain well below the speed of light. We refer to PN results by the order at which the series is truncated. For example, “2 PN” means that terms of order  $\epsilon^2 = v^4/c^4$  are retained. See Sec. VI for a deeper discussion of the PN approximation in the context of numerical relativity.

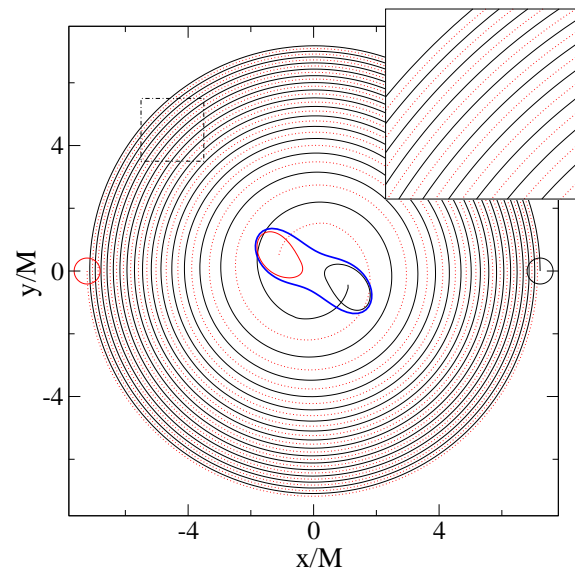


FIG. 13 Trajectories for the merger of equal-mass, nonspinning black holes computed by the Caltech-Cornell group using their spectral evolution code (Scheel *et al.*, 2009). The red and black circles/ellipses are the initial/final coordinate locations of the apparent-horizon surfaces, and the blue thick contour is the common apparent horizon just after it appeared. The black holes complete 16 orbits before merging. Figure kindly provided by H. Pfeiffer.

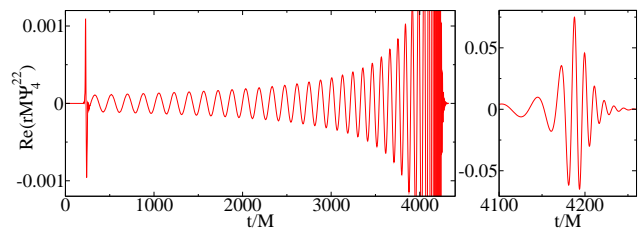


FIG. 14 Gravitational waveforms from the Caltech-Cornell merger simulation seen in Fig. 13 showing the  $\ell = 2, m = 2$  component of  $\text{Re}(r\Psi_4)$  (Scheel *et al.*, 2009). The left panel shows a zoom of the inspiral waveform, and the right panel a zoom of the merger and ringdown.

$\omega(t) = \dot{\phi}(t)$ . They compare the results from five independent numerical codes: the moving-puncture codes from the AEI, Goddard, Jena, and Penn State groups, and the Caltech-Cornell spectral code. Figure 15 compares the gravitational-wave amplitudes and Fig. 16 the gravitational-wave phases as a function of frequency for the five waveforms. Qualitatively, the results appear to be quite consistent. Quantitatively, they concluded that these waveforms have sufficient accuracy to be used for detection with all current and planned ground-based detectors.

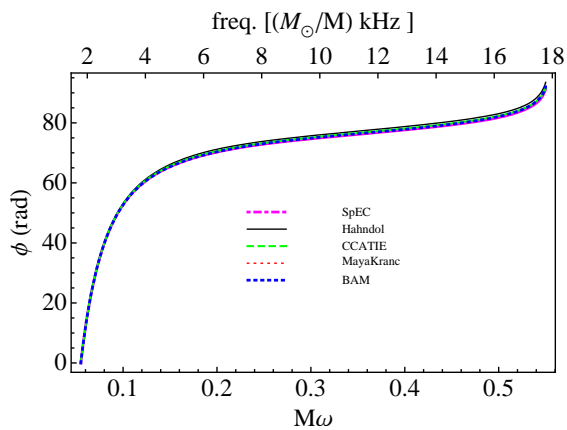


FIG. 15 The gravitational-wave phase  $\phi$  as a function of the dimensionless frequency  $M\omega$  for the five codes from the Samurai comparison (Hannam *et al.*, 2009a). The scale along the top of the panel labels the frequency in kHz scaled with respect to the total binary mass in solar units.

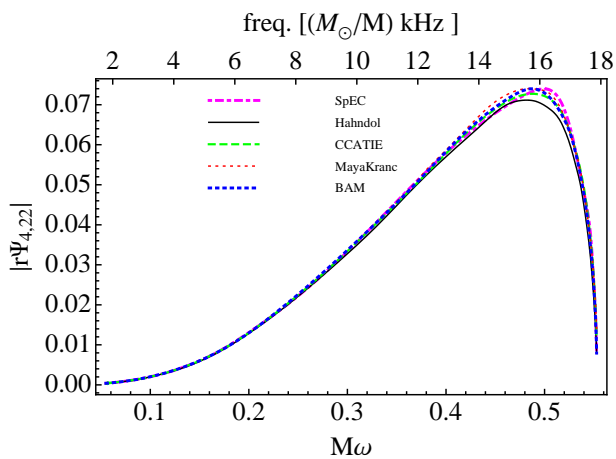


FIG. 16 Amplitudes of the  $\ell = 2$ ,  $m = 2$  component of the gravitational waves produced by the five codes in the Samurai comparison (Hannam *et al.*, 2009a) are shown as a function of frequency.

### C. Mergers of Unequal-Mass, Nonspinning Black Holes

Early in 2006, numerical relativists took the next step in opening up the parameter space of binary black-hole mergers by simulating nonspinning binaries with unequal masses. This added a new parameter, the mass ratio  $q$ , to the problem and brought an additional need for adaptive mesh refinement to achieve adequate resolution around the smaller black hole. As shown in Fig. 17, the smaller black hole also moves faster, completing an orbit around the center of mass in the same time as the larger hole and thus requiring smaller timesteps for its evolution. These factors combine to make simulations of unequal-mass binaries more technically challenging; currently, numerical relativists are able to simulate mass ratios up to  $q = 10$  (González *et al.*, 2009).

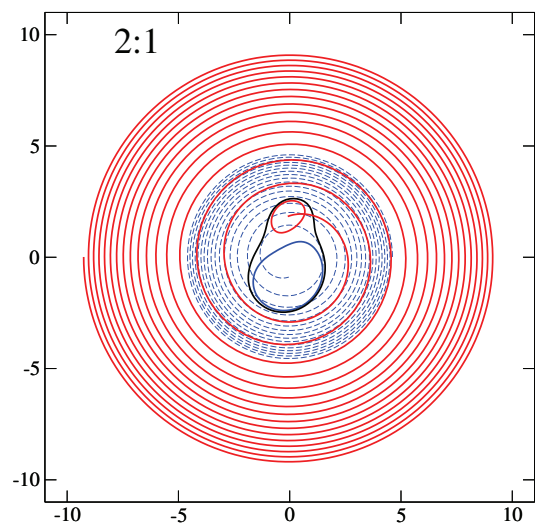


FIG. 17 Puncture tracks for an unequal-mass nonspinning binary with  $q = 2$  produced by the Caltech-Cornell spectral code; figure kindly provided by H. Pfeiffer. The solid (red) curve gives the trajectory of the smaller black hole, and the dotted (blue) curve the path of the larger one. The red and blue contours are the final coordinate locations of the apparent-horizon surfaces, and the black contour is the common apparent horizon just after it appeared.

### 1. Mode Analysis and Gravitational Waveforms

Decomposition into spin-weighted spherical harmonic modes (see Sec. IV.H) provides the basis for an in-depth study of black-hole mergers. For the equal-mass case  $q = 1$ , the  $\ell = 2$ ,  $m = \pm 2$  quadrupole mode is dominant and the odd- $m$  modes are suppressed by symmetry. As  $q$  increases, the sub-dominant modes become more important, affecting both the evolution of the source and the emitted radiation.

Berti *et al.* (2007b) carried out a set of unequal-mass mergers with mass ratios in the range  $1 \leq q \leq 4$ . They found that, to leading order, the total energy emitted during merger scales  $\sim \eta^2$  while the spin of the final black hole scales  $\sim \eta$ , where  $\eta$  is the symmetric mass ratio (1). They also studied the multipolar structure of the gravitational waves. Figure 18 shows several  $(\ell, m)$  modes of the radiation produced in their simulations for the case  $q = 2$ . They demonstrated that the higher modes carry larger fractions of the total energy as  $q$  increases; in particular, the  $\ell = 3$  mode generally carries  $\sim 10\%$  of the emitted energy for  $q > 2$ .

The Goddard group (Baker *et al.*, 2008b) performed a complementary study of nonspinning unequal-mass mergers for mass ratios  $1 \leq q \leq 6$ . They found that the overall simple waveform shape first discovered for equal-mass mergers extends to the cases with  $q > 1$ ; this is easily seen when the gravitational waves are scaled by  $\eta$ . Figure 19 shows the strain  $rh_+/\eta$ , including the  $\ell = 2$  and  $\ell = 3$  modes, for an observer located at distance  $r$  on the system's orbital axis. The waveforms are aligned

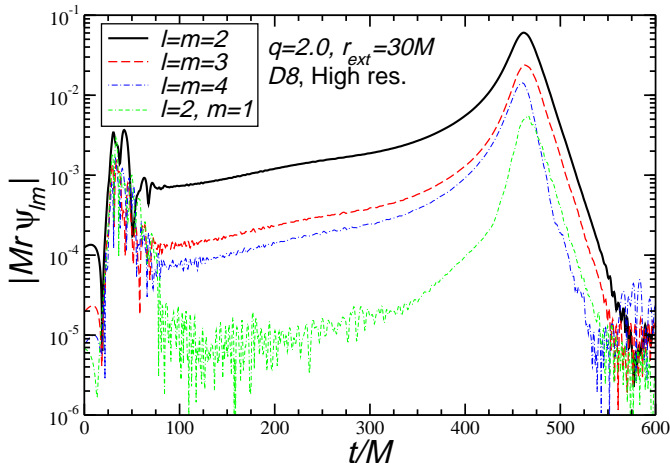


FIG. 18 The amplitudes of several  $(\ell, m)$  modes of  $Mr\Psi_4$  for mass ratio  $q = 2$  from simulations by Berti *et al.* (2007b). The initial burst of radiation is an artifact of the initial data, and the wiggles at late times result from numerical noise.

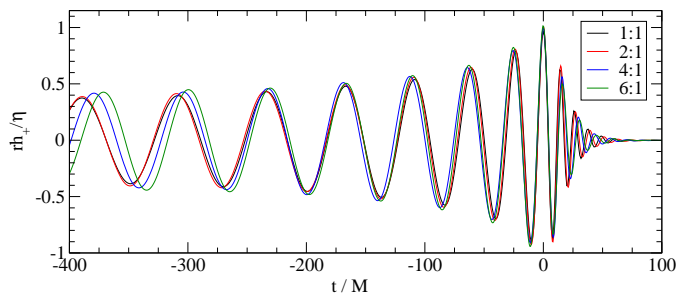


FIG. 19 Strain waveforms scaled by  $\eta$  for different mass ratios, from Baker *et al.* (2008b).  $h_+$  is calculated for different mass ratios using the  $\ell = 2$  and  $\ell = 3$  modes. The observer is located at distance  $r$  along the axis of the system.

so that the maximum amplitude of the  $\ell = 2, m = 2$  mode occurs at  $t = 0$ . The differences in phase during the final ringdown portion of the waveforms are consistent with the differing spins of the final black holes; for example, with nonspinning black holes, a larger mass ratio  $q$  results in a smaller final spin for the remnant black hole. When viewed off-axis, the waveforms show modest amplitude and phase modulations, while still preserving the overall simplicity in shape.

Baker *et al.* (2008b) also found that each of the individual spherical harmonic components is circularly polarized during the inspiral, merger, and ringdown, as seen by distant observers on the system's rotational axis. During the inspiral, the phase and frequency of the different  $(\ell, m)$  components are the same for each mass ratio; this is expected since the waveform phase is directly related to the orbital phase. More interestingly, for the  $\ell = m$  modes, this relationship continues to hold during merger

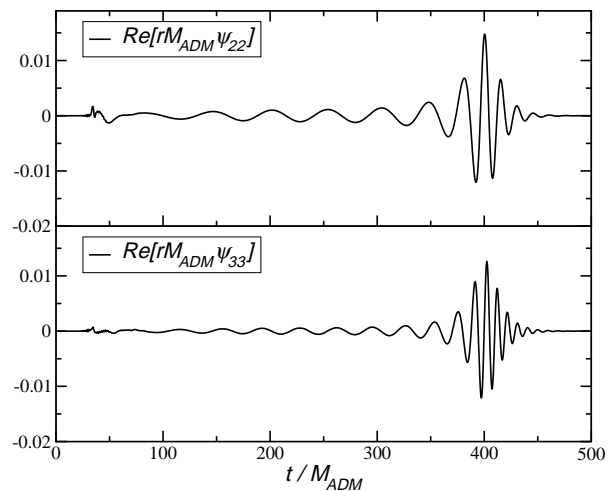


FIG. 20 The  $\ell = m = 2$  and  $\ell = m = 3$  component of  $\text{Re}(rM\Psi_4)$  from the 10:1 mass ratio simulation by González *et al.* (2009)

and ringdown.

Based on these observations, they developed a simple conceptual picture in which each  $(\ell, m)$  mode of the gravitational radiation is produced separately by the  $(\ell, m)$  mode of some *implicit rotating source*. The fixed relationship between the phase and frequency of the  $\ell = m$  modes shows that these components of the implicit source rotate rigidly during the entire coalescence from inspiral through ringdown. In comparison, the  $\ell \neq m$  source components peel away from the main trend of the  $\ell = m$  parts during merger, indicating less rigid rotation.

González *et al.* (2009) have carried out the highest mass ratio merger simulation to date, with  $q = 10$ . This binary radiates  $\sim 0.42\%$  of its mass as gravitational radiation as it undergoes  $\sim 3$  orbits before merging to form a black hole with  $(a/M)_f \sim 0.26$ ; these values fit the scaling relations found by Berti *et al.* (2007b) and Pan *et al.* (2008). Figure 20, from González *et al.* (2009) shows that the  $\ell = m = 2$  and  $\ell = m = 3$  modes of  $\text{Re}(rM\Psi_4)$  exhibit the simple waveform shape individually; this trend continues through  $\ell = m = 5$ , the highest mode they studied.

## 2. A Qualitatively New Feature: Kicks

Unequal-mass black-hole binaries can form as a result of galaxy mergers, dynamical processes in star clusters, and the final stages of binary stellar evolution. Mergers of unequal-mass binaries bring a qualitatively new phenomenon of great importance to astrophysical scenarios of black-hole growth and retention: recoils or kicks.

As discussed in Sec. II.A, the gravitational waves emitted by a merging black-hole binary carry away linear momentum. If the pattern of gravitational-wave emission is not symmetrical (*i.e.*, if there is more radiation emitted in some direction than in others), then global conserva-

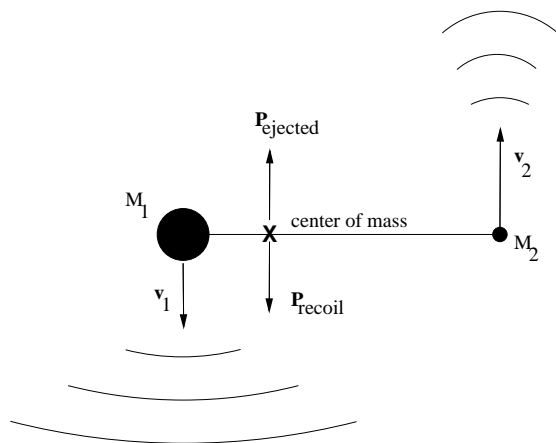


FIG. 21 Schematic drawing of the physical basis of the recoil or kick produced by a merging black-hole binary with unequal masses. A net flux of momentum  $P_{\text{ejected}}$  is emitted parallel to the smaller hole’s velocity. Momentum conservation requires that the system center of mass recoil in the opposite direction,  $P_{\text{recoil}}$ . Reproduced with kind permission from Springer Science+Business Media: Fig. 1 of Hughes *et al.* (2005).

tion of momentum requires the center of mass, and thus the remnant black hole that forms, to recoil in the opposite direction.

The situation for an unequal-mass, nonspinning binary is shown schematically in Fig. 21, from Hughes *et al.* (2005), who attributed this argument to Alan Wiseman; we summarize their discussion here. The two holes are orbiting in a plane about their center of mass. Since the smaller black hole moves faster, its wave emission undergoes more “forward beaming” than that of the larger hole. Instantaneously this gives a net flux of momentum parallel to the smaller hole’s velocity, and an opposing recoil or kick at the center of mass. The direction of this kick changes continually as the black holes orbit. If the orbit was circular, the center of mass would move in a circle and suffer no net recoil. However, since the black holes are spiralling together (due to the energy and angular momentum carried away by the gravitational waves), the instantaneous kicks do not cancel exactly but rather accumulate. This causes the final merged black hole to have a non-zero net recoil in the orbital plane.

This recoil has been studied by several authors, including Bekenstein (1973); Fitchett (1983); Fitchett and Detweiler (1984); Peres (1962); Redmount and Rees (1989). More recent analytic treatments using PN approximations were carried out by Blanchet *et al.* (2005); Damour and Gopakumar (2006); Favata *et al.* (2004); Le Tiec *et al.* (2010); Wiseman (1992), while some comparable-mass estimates were also made with the Lazarus approach (Campanelli, 2005). However, since the dominant part of the kick depends sensitively on the strong-field regime close to merger, where the orbits are less circular, an accurate calculation of the kick requires full numerical relativity simulations of the final stages of binary inspiral, merger

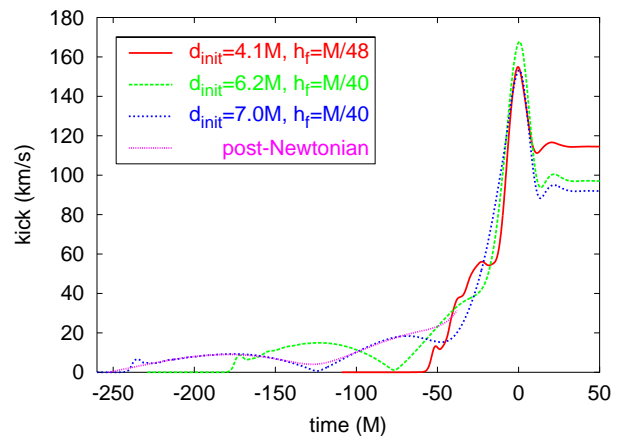


FIG. 22 The magnitude of the kick velocity for a nonspinning, unequal mass merger with  $q = 1.5$  from Baker *et al.* (2006c). Results are shown from three simulations, with increasingly wider initial black-hole coordinate separations  $d_{\text{init}}$ . The small-dotted (purple) curve shows a 2 PN calculation starting with initial conditions commensurate with the  $d_{\text{init}} = 7.0M$  case (blue dotted line). Reproduced by permission of the AAS.

and ringdown (Schnittman *et al.*, 2008).

The Goddard group (Baker *et al.*, 2006c) carried out the first accurate calculation of black-hole recoil for the merger of a nonspinning binary with  $q = 1.5$ . Figure 22 shows the kick velocity as a function of time for three simulations in which the black holes start out on orbits with increasingly larger initial separations  $d_{\text{init}}$ . The kick velocity grows rapidly during merger, reaching a peak value  $\sim 10M$  after the time of peak radiation amplitude in  $\Psi_4$ , and then dropping to a lower, final value. It is clear from this figure that the black holes must start far enough apart in order to get a consistent and reliable value for the final recoil velocity. For this  $q = 1.5$  case, their results spanned the range  $v_{\text{kick}} = 101 \pm 15 \text{ km s}^{-1}$ , with a best estimate of  $v_{\text{kick}} = 92 \pm 6 \text{ km s}^{-1}$ .

Following on from this, and other unequal-mass simulations by Herrmann *et al.* (2007b), González *et al.* (2007b) performed the first systematic parameter study of nonspinning black-hole binary mergers with mass ratios in the range  $0.253 \leq 1/q \leq 1$ . They found that the maximum recoil velocity  $v_{\text{kick}} = 175.2 \pm 11 \text{ km s}^{-1}$  occurs for the mass ratio  $1/q = 0.36 \pm 0.03$ . For the case  $q = 10$ , González *et al.* (2009) found a recoil velocity  $v_{\text{kick}} = 66.7 \pm 3.3 \text{ km s}^{-1}$ .

#### D. Mergers of Spinning Black Holes

Astrophysical black holes are generally expected to be spinning. Including the spin vector of both black holes in the binary adds six more dimensions to the parameter space, giving seven in all when the mass ratio  $q$  is included. Exploration of this large parameter space began in 2006, with the simplest cases of equal masses



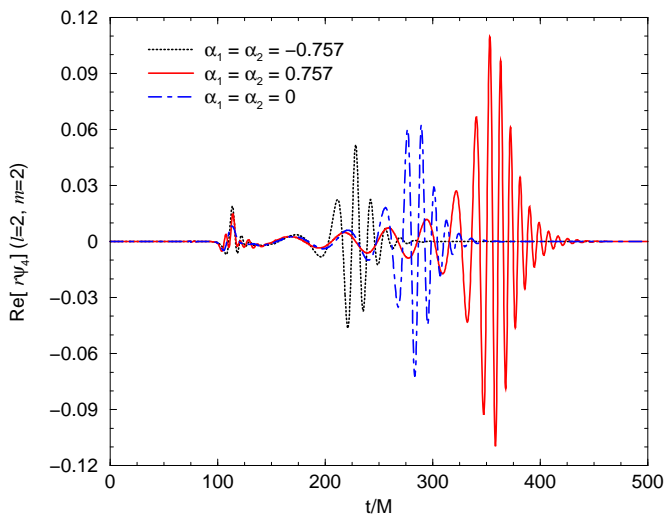


FIG. 23 Gravitational waveforms for mergers of equal-mass spinning binaries as in Campanelli *et al.* (2006d). The dominant  $\ell = 2, m = 2$  mode is shown for three cases: aligned spins (solid/red), anti-aligned spins (dotted/black), and no spins (dashed/blue). All three simulations start with the same initial orbital period at  $t = 0$ . Figure kindly provided by M. Campanelli.

and spins, and is gradually growing to incorporate more generic binaries.

## 1. Gravitational Waveforms

The UTB group carried out the first black-hole binary mergers with spin (Campanelli *et al.*, 2006d). They simulated three binaries, each having equal masses and starting on quasicircular orbits with initial orbital frequency  $M\Omega = 0.5$ , giving an initial orbital period  $\sim 125M$ . In the aligned case, both holes have spin parameters  $(a/M)_{1,2} = 0.757$  and vectors parallel to the orbital angular momentum  $\vec{L}$ ; in the anti-aligned case, the black holes have the same spin parameters but the vectors are anti-parallel to  $\vec{L}$ . A nonspinning equal-mass binary was run for comparison.

The  $\ell = 2, m = 2$  components of the waveforms are plotted in Fig. 23, which shows all three cases starting out at the same time  $t = 0$  at the same orbital period and gravitational-wave frequency  $f_{\text{GW}} \sim 2f_{\text{orb}}$ . Notice that the aligned system takes longer to merge, completing more orbits and producing a longer wavetrain. This behavior is caused by a spin-orbit interaction that produces an effective repulsive force between the black holes. In the anti-aligned case, this interaction yields an effective attraction, causing the binary to merge more quickly and with fewer orbits. The nonspinning case is intermediate between the other two. All three cases produce similar waveforms with a clean, simple shape.

It is also interesting to compare the total energy radiated as gravitational waves  $E_{\text{rad}}$  and the spin parameter

of the final black hole  $(a/M)_f$  for these three cases. The aligned case yields  $E_{\text{rad}} \sim 0.07M$  and  $(a/M)_f \sim 0.89$  while the anti-aligned case gives  $E_{\text{rad}} \sim 0.02M$  and  $(a/M)_f \sim 0.44$ . The nonspinning case is again between these two cases, with  $E_{\text{rad}} \sim 0.04M$  and  $(a/M)_f \sim 0.69$  (Campanelli *et al.*, 2006d).

The black-hole mergers discussed so far have resulted from simple binary dynamics with no precession and have produced simple waveforms with a similar shape, at least when examined mode-by-mode in a spin-weighted spherical harmonic decomposition. Might more “generic” precessing binaries generate waveforms with more complex patterns? This important question pertains not only to basic orbital dynamics in general relativity, but also to strategies for developing templates to search for signals in data from gravitational-wave detectors (see Sec. VII).

The parameter space for such binaries is very large, and explorations of this space have only recently started. The UTB group, now at the Rochester Institute of Technology (RIT), pioneered the study of precessing black-hole binary mergers. They evolved a generic black-hole binary with unequal masses and unequal, non-aligned precessing spins that undergoes  $\sim 9$  orbits before merger and produces a relatively long wavetrain (Campanelli *et al.*, 2009). This system has a mass ratio  $q = 1.25$  and arbitrarily oriented spins with magnitudes  $(a/M)_1 \sim 0.6$  and  $(a/M)_2 \sim 0.4$ . The initial conditions were determined from point-mass evolutions using 2.5 PN and 3.5 PN parameters.

Figure 24 shows the difference in the black-hole trajectories  $\vec{x}_1 - \vec{x}_2$ . For a non-precessing binary,  $\vec{x}_1 - \vec{x}_2$  would have no component in the  $z$  direction. In this generic case, the precession of the total system spin drives a precession of the orbital plane, producing evolution of the trajectory in the  $z$  direction. The resulting waveforms demonstrate the effects of precession on the amplitudes of the sub-dominant modes. Figure 25 shows the  $\ell = 2, m = 1$  mode of the strain  $h_+$ . The numerical-relativity evolution is shown by the solid curve; note the amplitude modulations induced by the precession. The dotted curve shows a solution of the PN equations of motion at 3.5 PN order.

## 2. Spinning Binary Mergers and Spin Flips

The merger of a binary consisting of nonspinning black holes produces a single spinning black hole with spin direction aligned with the orbital angular momentum  $\vec{L}$  of the binary. In this case, the spin of the final hole arises purely from  $\vec{L}$ . When the individual black holes have spins that are not aligned with  $\vec{L}$ , the spin of the final hole will, in general, not be aligned with the initial spin but rather will have a different direction. This phenomenon, in which the spin direction of the final black hole differs significantly from the spin directions of the individual holes prior to merger, is known as a “spin flip.” The simplest situation in which a spin flip can occur is a

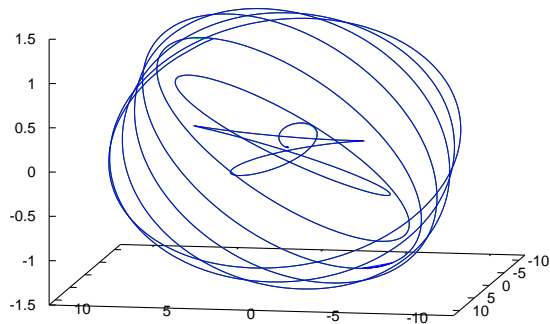


FIG. 24 The difference in the black-hole trajectories  $\vec{x}_1 - \vec{x}_2$  for the generic binary evolution from Campanelli *et al.* (2009). The precession of the system spin induces precession of the orbital plane.

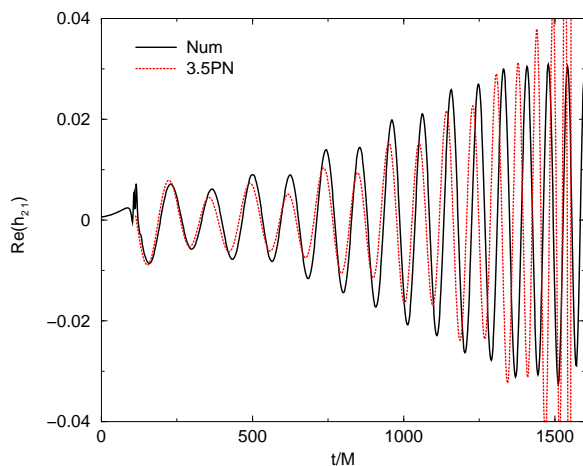


FIG. 25 Precession-induced amplitude modulations in the waveforms from the generic black-hole binary merger from Campanelli *et al.* (2009). The  $\ell = 2, m = 1$  mode of the strain ( $h_+$ ) is shown for the numerical-relativity simulation (solid) and a 3.5 PN calculation (dotted). The amplitude oscillations are induced by precession.

binary with both spins anti-aligned with  $\vec{L}$ .

The case of generic binaries, with unequal masses and arbitrarily-oriented spins has a much larger parameter space. The RIT group (Campanelli *et al.*, 2007a,b) has examined spin flips for several such cases. Figure 26 shows the puncture trajectories for an equal-mass binary with equal spins having magnitude  $(a/M)_{1,2} = 0.5007$  and initially pointing  $45^\circ$  above the initial orbital plane. The black holes execute  $\sim 2.25$  orbits before merger, during which time the spins, shown as arrows along each trajectory, precess by  $\sim 151^\circ$ . The evolution of the spin

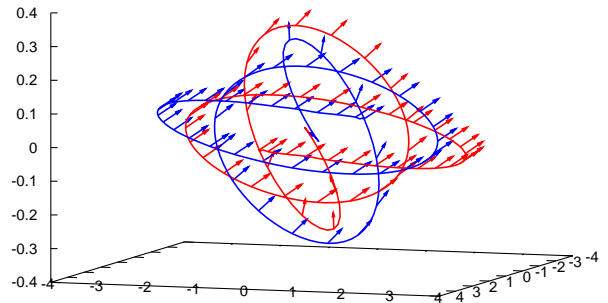


FIG. 26 Black hole trajectories for the spin flip case studied by Campanelli *et al.* (2007a). The black holes have equal masses, and equal spins initially pointing  $45^\circ$  above the initial orbital plane. The spin directions are shown as arrows along each trajectory every  $4M$  until merger.

direction for this case is shown in Fig. 27. The final black hole has  $(a/M)_f \sim 0.8$  with a spin direction flipped by  $\sim 35^\circ$  with respect to the component spins just before merger.

In a related phenomenon, the direction of the *total* angular momentum ( $\vec{L} + \vec{S}_1 + \vec{S}_2$ ) may change. This case was studied using general principles and extrapolations from point-particle results by Buonanno *et al.* (2008), who predicted that binaries with  $q > 6.78$  will experience a flip in total angular momentum direction provided that the initial spins are equal and anti-aligned with  $\vec{L}$ , and that the individual black hole spins obey  $(a/M)_{1,2} \geq 0.5$ . In particular, they predicted that, for  $q = 4$ , a Schwarzschild black hole should form if  $(a/M)_1 = (a/M)_2 = 0.8$ .

Motivated by this work, Berti *et al.* (2008) simulated a series of binaries with  $q = 4$  and having equal anti-aligned spins in the range  $(a/M)_{1,2} \in [-0.75, -0.87]$ . They found that a Schwarzschild hole is formed when the initial spin is  $(a/M)_{1,2} \simeq -0.842 \pm 0.003$ .

### 3. Kicks from Mergers of Spinning Black Holes

The mergers of asymmetrical spinning binaries will produce recoiling remnant black holes. In the simplest case, the binary components have equal masses and spin magnitudes, and the asymmetry arises from the spin vectors pointing in opposite directions. In early 2007, several new results appeared in quick succession, generating considerable excitement among numerical relativists as well as astrophysicists eager to apply these results. In this section we discuss the basic results and defer to Sec. VIII their impact on astrophysics.

Herrmann *et al.* (2007a) simulated the merger of equal-mass black holes with equal spin magnitudes  $(a/M)_{1,2} \in (0.2, 0.4, 0.6, 0.8)$  and having one spin vector aligned and the other anti-aligned with the orbital angular momentum. These mergers produced kicks directed purely in the orbital plane with magnitudes  $\sim$

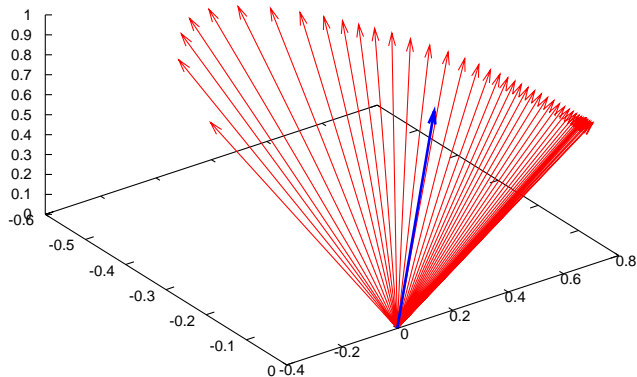


FIG. 27 The spin flip produced by the evolution in Fig. 26, from Campanelli *et al.* (2007a). The spin direction of the component holes, shown by the red arrows plotted every  $4M$  until merger, varies continuously due to precession. The blue arrow shows the final black-hole spin, with direction flipped discontinuously from that of the component holes just prior to merger.

$475(a/M)_{1,2} \text{ km s}^{-1}$ . Shortly thereafter Koppitz *et al.* (2007) showed that, for the specific case  $(a/M)_{1,2} = 0.584$ ,  $v_{\text{kick}} = 257 \pm 15 \text{ km s}^{-1}$ ; linear extrapolation of results to the maximally spinning case  $(a/M)_{1,2} = 1$  yields  $v_{\text{kick}} \simeq 440 \text{ km s}^{-1}$ . Pollney *et al.* (2007) carried out a systematic study of equal-mass mergers with spin magnitude  $(a/M)_2 = 0.584$  and direction aligned with the orbital angular momentum. The other black hole has spin magnitude  $(a/M)_1 \in (0, 0.25, 0.50, 0.75, 1.0)(a/M)_2$ , and direction both aligned and anti-aligned. They found a maximum kick velocity  $v_{\text{kick}} = 448 \pm 5 \text{ km s}^{-1}$ .

These results all demonstrated that mergers of spinning black holes can produce significantly larger kick velocities than nonspinning mergers. However, new results would soon show that kicks from the mergers of spinning black holes could get much larger indeed.

The idea of “superkicks” was first discussed by the RIT group (Campanelli *et al.*, 2007b). They observed that a PN treatment (Kidder, 1995) predicts that the recoil due to spin is maximized when  $M_1 = M_2$ ,  $(a/M)_1 = (a/M)_2$ , and the spin directions are anti-aligned with each other and lying in the orbital plane.

The Jena group first simulated binaries in this configuration and demonstrated the phenomenon of superkicks. Using  $(a/M)_{1,2} \sim 0.8$ , they found a resulting kick velocity  $v_{\text{kick}} \sim 2500 \text{ km s}^{-1}$  (González *et al.*, 2007a). Figure 28 shows the coordinate positions of the black-hole punctures from one of their simulations. Notice that the trajectories move out of the initial orbital plane and that the final black hole is kicked in the  $-z$  direction. The RIT group (Campanelli *et al.*, 2007c) carried

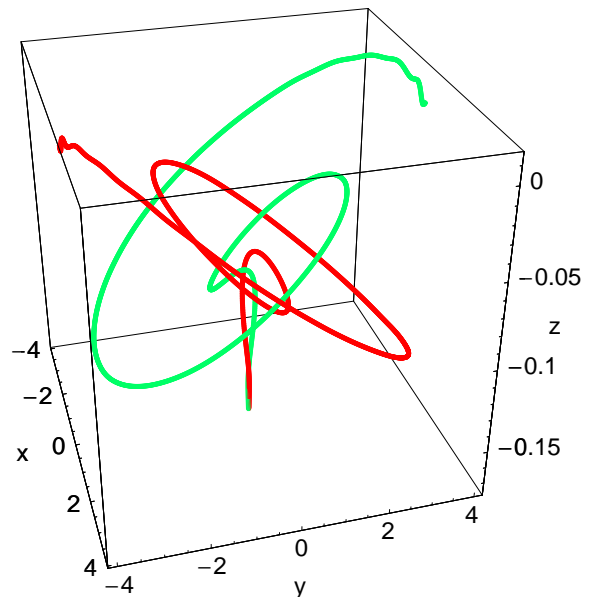


FIG. 28 Puncture trajectories from a superkick simulation carried out by González *et al.* (2007a). The black holes have equal masses and spins  $(a/M)_{1,2} \sim 0.8$ , initially oppositely directed in the orbital plane. During the evolution, the black holes move out of the original plane, and the final black hole recoils with velocity  $v_{\text{kick}} \sim 2500 \text{ km s}^{-1}$  in the negative  $z$ -direction.

out similar simulations with  $(a/M)_{1,2} = 0.5$ . Their results show kicks perpendicular to the orbital plane with magnitudes up to  $v_{\text{kick}} \sim 1800 \text{ km s}^{-1}$ ; using the expression from Kidder (1995) they predict a maximum recoil  $v_{\text{kick}} \sim 4000 \text{ km s}^{-1}$  for the case of maximally spinning black holes,  $(a/M)_{1,2} = 1$ .

Schnittman *et al.* (2008) performed a multipolar analysis of recoil from black-hole mergers, for both unequal masses and non-zero, non-precessing spins. They found that multipole moments up to and including  $\ell = 4$  are sufficient to accurately reproduce the final recoil velocity (within  $\simeq 2\%$ ), and that only a few dominant modes contribute significantly to it (within  $\simeq 5\%$ ). Brüggmann *et al.* (2008a) studied the role of spin in producing superkicks. They showed that the recoil velocity is almost entirely due to the asymmetry between the  $(\ell = 2, m = +2)$  and  $(\ell = 2, m = -2)$  modes of  $\Psi_4$ . In addition, the major contribution to the recoil occurs within a period  $\sim 30M$  before and after merger, after the time at which a standard PN treatment of the evolution breaks down.

## VI. INTERACTION OF NUMERICAL RELATIVITY WITH POST-NEWTONIAN THEORY

Einstein’s theory of general relativity implies predictions for the dynamics and gravitational-wave genera-

tion for generic black-hole binaries at all stages of the merger process. As we have seen, numerical relativity now provides an excellent tool for concretely deriving these predictions beginning in the last orbits and continuing through the conclusion of the coalescence in the ringdown of the remnant black hole. There is no hard limit to how early numerical relativity can be applied in these simulations, but the considerable costs of these simulations tends to limit the duration to tens of orbital periods. Though the PN expansion provides only an approximation to general relativity, it succeeds in making accurate and efficient predictions over very long time-scales, while the black holes remain well separated. Late in the merger, however, as the black-hole velocities increase, these errors grow, and PN theory is no longer reliable

A full understanding of general relativity’s predictions for the merger process must draw on both approaches. The maturation of numerical relativity has fueled efforts toward synthesizing a complete understanding of black-hole mergers built from the results and techniques of both these fields. Even a coarse general review of the PN formalism and results is outside the scope of this presentation. Decades of work in this area have already been covered (Blanchet, 2006, 2010; Blanchet *et al.*, 2008; Damour and Nagar, 2010; Schäfer, 2010). Here we focus exclusively on key synergistic areas where fruitful research interactions drawing from both numerical relativity and PN results and formalisms are yielding a more complete general-relativistic understanding of black-hole binary systems. The broad range of research that interfaces these two approaches can be grouped into four categories, based on the different ways that PN theory impacts numerical-relativity research. PN theory: 1) provides independent results for cross-checking and comparing with NR; 2) provides models for the initial values needed to begin astrophysically realistic NR simulations; 3) provides insight for interpreting NR results; and 4) may provide the basis for empirical models representing the combined knowledge drawn from PN and NR investigations.

### A. Independent Post-Newtonian Dynamics and Waveforms

As mentioned, PN theory is based on an approximate expansion of Einstein’s equations in powers of velocity  $\epsilon^n \sim (v/c)^{2n}$  providing general relativistic corrections to the Newtonian, small-velocity limit. This approach has a long history of success as the primary framework for deriving explicit predictions from general relativity for physical and astrophysical observations. The relatively small velocities involved in most observations have made low-order PN theory an ideal tool for testing general relativity as the standard model for gravitational physics in many contexts including Earth-orbit experiments, solar-system dynamical observations, and in even precision pulsar timing observations of binary neutron

star systems (Will, 2006).

Gravitational-wave researchers have applied PN theory to represent general relativity-based signal expectations for the vast majority of gravitational-wave searches for anticipated observations of black-hole and neutron-star binary inspirals, and likewise in the development and planning for current and future gravitational-wave instruments. The early epoch of black-hole binary inspiral is also well-described by low-order PN theory. For near-circular inspirals,  $\epsilon \sim (v/c)^2 \sim M/R$ , where the binary separation  $R$  is scaled by the total system mass  $M$ . At large  $R$ , the PN expansion provides excellent predictions, even at low order. As the black holes lose energy and sink closer together, the velocity grows, requiring higher-order PN terms for sufficiently accurate predictions. Currently, PN predictions are available up to 3.5 PN order (2.5 PN for spin-terms). These higher-order expansions seem to provide PN predictions sufficiently accurate for the analysis of data from current instruments for all but the last several orbits. Once the separation approaches, say,  $R/M \sim 10$ , the accuracy of the PN expansion diminishes. Even at (hypothetical) arbitrarily high orders, the expansion may fail, if the expansion parameter  $v/c$  exceeds the series’ radius of convergence. Precisely when the PN approximation effectively fails depends on the details of the system being studied and the requisite accuracy, but generally, for the last orbits and merger PN theory is no longer reliable.

The strongest gravitational radiation is generated in the late stages of inspiral or merger where the internal consistency of the PN approach has been, at best, difficult to assess (Simone *et al.*, 1997). Numerical simulation can treat the late portions of the mergers, with practical resource limitations on the duration of the simulations, and consequently how far apart the black holes can be at the start of the simulation. Would it be practical, however, to run numerical simulations long enough to “overlap” with the part of the problem treated successfully by PN methods, or would there be an intermediate region requiring yet another approach (Brady *et al.*, 1998)?

The first numerical inspiral results were quickly compared against PN calculations (Baker *et al.*, 2006a; Buonanno *et al.*, 2007a). These first comparisons yielded promising indications that the gap between NR and PN could be bridged, but also made clear that PN results were not uniquely determined for the final part of the inspiral. Numerical results can be verified by internal consistency studies, examining, for instance, the convergence of the results toward consistency with Einstein’s equations as the resolution is increased. External verification, however, would strengthen the case that these new results are indeed correct. Even more importantly, these comparisons would allow an independent check of the late inspiral PN predictions which are not easily confirmed by self-consistency studies.

Roughly one year after the first robust numerical-relativity results, simulations lasting  $\sim 1000M$  were con-

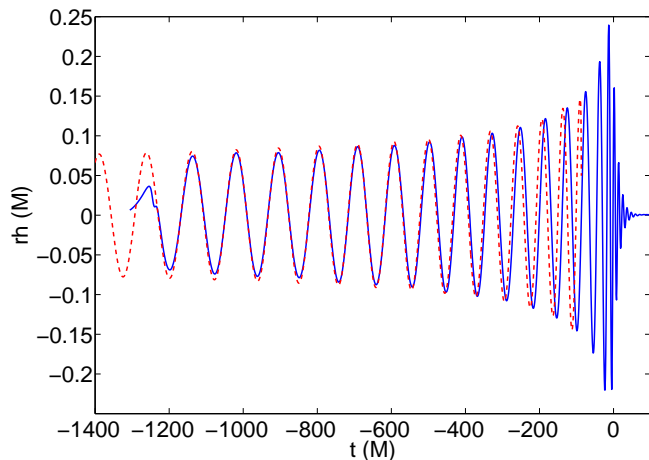


FIG. 29 Comparison of NR and PN waveforms from Baker *et al.* (2007d) provided mutual affirmation of the results from each approach and showed that in combination NR and PN results could treat the complete signal.

ducted, and quantitatively compared with various PN approximations. Quantitatively cross-checking waveform comparisons requires some care. How do the differences between PN and numerical results compare with intrinsic numerical error estimate? How do different variants of PN predictions compare with the numerical results? Because each waveform comes with no meaningful absolute reference in time and phase, how can the freedom to offset these parameters be controlled for the comparison? Effective comparisons also require longer waveforms than those produced in the earliest simulations. The first comparison addressing these issues came at the end of 2006 (Baker *et al.*, 2007d). The study considered the case of equal-mass non-spinning black-hole mergers, comparing a 3.5 PN waveform with numerical results covering the last seven orbits. The compared waveforms are shown in Fig. 29. In the comparison the waveform phases agreed within 1 rad of phase drift, for a little over ten gravitational-wave cycles preceding the last orbit before merger, comparable to numerical error estimates. This result gave clear indication that PN waveforms could be accurate in the last orbits approaching merger, and that PN and NR, combined, could treat the complete waveform signal.

Not all equally valid variants (approximants) of the approximate PN waveforms agree this well with numerical results. To understand this, it is worthwhile to consider PN results in a little more detail. The PN approximation is formally understood as an expansion in powers of the speed of the merging black holes,  $v/c$ . A concrete result of the theory will typically be a Taylor expansion for a specific dependent variable, in terms of a chosen independent variable. The obvious choice, to express the waveform itself (gravitational-wave strain) as a function of time, would give a poor result since the sinu-

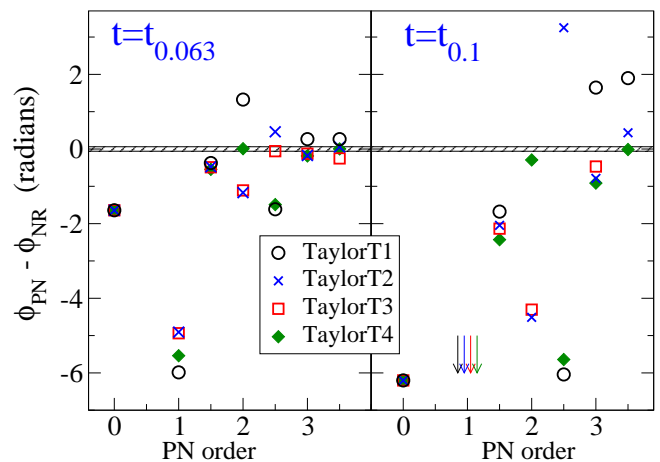


FIG. 30 Phase differences between a numerical simulation and various PN models from Boyle *et al.* (2007a). The left panel shows phase differences from an initial (waveform) angular frequency of  $M\omega = 0.04$  up to  $M\omega = 0.063$ , while the comparison in right panel extends this range to  $M\omega = 0.10$ .

soidal shape of the waveform is difficult to approximate by a polynomial. PN waveform results are typically expressed as separate expansions for the orbital phase, and polarization component amplitudes. These are given as expansions in the time to merger  $v/c \propto t^{-1/8}$  or orbital frequency  $v/c \propto \Omega^{1/3}$ . The orbital phase information may also be expressed by an expansion for  $\dot{\Omega}$ , referred to as the chirp-rate; see Blanchet (2006) for a review of the approach and a particular explicit waveform expansion. The PN information may also be encoded in an Hamiltonian formulation description of the dynamics, which may be integrated numerically. Researchers also choose between Taylor series and other “resummed” expressions of the results based, for instance, on Padé approximants (Damour *et al.*, 1998).

In the comparisons described above, the PN waveform phasing was found to agree with numerical results derived from a Taylor series expansion for chirp-rate  $\dot{\Omega}(\Omega)$  expanded in powers of frequency. This is known as the TaylorT4 approximant in the language of the ground-based gravitational-wave community. Later studies with longer and more accurate numerical simulations provided more precise tests of phases and amplitudes for a variety of PN approximants (Boyle *et al.*, 2007a; Hannam *et al.*, 2008c). Boyle *et al.* (2007a) found even closer agreement (than found in (Baker *et al.*, 2007d)) with the TaylorT4 approximant, to within 0.05 rad over nearly 30 cycles before the orbital frequency reaches  $M\Omega = 0.1$  at roughly an orbit before merger.

Figure 30 shows the results of four PN approximants with terms kept to various PN orders. The excellent agreement of the TaylorT4 approximant with numerical results is not matched by other equally consistent PN waveform approximants in the late portions of the waveforms. However, all four approximants agree to within about a radian if the comparison is cut off at waveform

frequency  $M\omega = 0.1$ , about five orbits before merger [note that this is the frequency of the dominant  $(2, 2)$  mode, twice the orbital frequency  $M\Omega$ ].

While most attention has so far been given to the non-spinning cases, some results exist for other regions of parameter space. For equal-mass configurations of black holes with spins aligned with the orbital angular momentum, the phase agreement of the TaylorT4 approximant is not generally best, and phase differences (over ten cycles preceding  $M\omega = 0.1$ ) are much larger than those seen in the nonspinning case, with differences near 1 rad or more for spins  $(a/M)_{1,2} \geq 0.5$  (Hannam *et al.*, 2008a). PN spin effects are not yet derived beyond 2.5 PN order, possibly limiting the accuracy of the PN waveforms in these comparisons. Some PN comparisons have also been examined for other configurations, including a precessing system (Campanelli *et al.*, 2009) and for eccentric configurations of equal-mass, non-spinning mergers (Hinder *et al.*, 2010).

In comparing Fourier-domain PN approximants with numerical results for a set of non-spinning mergers with various mass ratios, Pan *et al.* (2008) discovered that the abrupt truncation of the Fourier-domain waveforms, inducing Gibbs oscillations in the time-domain, can approximately emulate the physical quasinormal ringdown that terminates the numerical-simulation waveforms. Even better agreement is possible if  $\eta$ , the symmetric mass ratio (1), is allowed to extend beyond its physical range (to  $\eta > 0.25$ ) or if an extra pseudo-4PN order term is added. More recent studies have confirmed that these simple models are directly useful in some gravitational-wave observation applications (Boyle *et al.*, 2009). These results have motivated further development of phenomenological full-waveform models.

## B. Analytic Full-Waveform Models

For the early part of the waveforms various PN approximants agree at 3.5 PN order, the best currently available, providing excellent approximations. At late times, the results of different approximants diverge, and the numerical-simulation results are the only way to accurately derive the predictions of general relativity. Can an analytic waveform description be developed that simultaneously encodes the results of both complementary theoretical approaches? The generally simple features of the numerically simulated merger waveforms raise hopes that fairly accurate approximate analytic waveform descriptions may be produced with simple dependence on the binary system parameters, providing an efficient means also of interpolating from a sparse sampling of the full parameter space for which numerical-simulation studies are completed. These waveform models would be computationally efficient (compared to numerical simulations) and may have applications in a broad class of observational data analysis applications.

Ajith and collaborators have developed a Fourier-

domain full-waveform model phenomenological approach resembling the treatment of Pan *et al.* (2008), but with greater emphasis on matching the numerical waveforms (Ajith, 2008; Ajith *et al.*, 2008, 2007). They begin combining information from the PN and NR-based waveforms by first stitching together time-series data for the dominant ( $\ell = 2, m = 2$ ) component waveforms, including a long PN precursor joined to a numerical merger waveform. Fourier transforms of waveforms are then fit to a parametrized model of the waveform similar to waveform families previously applied in phenomenological treatments of purely PN waveforms (Arun *et al.*, 2006; Buonanno *et al.*, 2003). Their waveform model for mergers of non-spinning binaries has the form

$$h(f) \equiv \frac{C(M, \eta)}{d} \mathcal{A}_{\text{eff}}(f) e^{i\Psi_{\text{eff}}(f)}, \quad (36)$$

where  $C$  is a constant related to the masses, and  $d$  is the distance to the source. The effective Fourier amplitude  $\mathcal{A}_{\text{eff}}$  is modeled piecewise,

$$\mathcal{A}_{\text{eff}}(f) \equiv f_m^{-7/6} \begin{cases} (f/f_m)^{-7/6} & , f < f_m \\ (f/f_m)^{-2/3} & , f_m \leq f < f_r \\ \frac{\pi\sigma}{2} \left(\frac{f}{f_m}\right)^{-2/3} \mathcal{L}(f, f_r, \sigma) & , f_r \leq f \end{cases}, \quad (37)$$

with distinct power-law segments before and after a merger frequency  $f_m$ , and a Lorentzian  $\mathcal{L}(f, f_r, \sigma)$  decay beyond the transition frequency  $f_r$  demarking the ringdown of the final black hole. The Fourier phase is represented by a single power-law expansion

$$\Psi_{\text{eff}}(f) = 2\pi f t_0 + \phi_0 + \sum_{k=0}^7 \psi_k f^{(k-5)/3}. \quad (38)$$

For each waveform, the free amplitude and phase coefficients are determined by a fit to the stitched NR-PN hybrid waveforms. It was found that the mass-ratio parameter dependence could be modeled by simple fits to quadratic functions of the symmetric mass ratio (1). These waveforms have been applied in gravitational-wave data analysis studies (see Sec. VII.A; (Ajith and Bose, 2009)). Recently Ajith *et al.* (2009) have developed a generalization of this model for non-precessing system of spinning black holes.

Stitching together PN and NR waveforms can be avoided, and closer contact with the basic physics maintained, by requiring direct PN consistency in the full waveform model. Some PN approximants can resemble the numerical late-merger results. If such approximants can be tuned to agree with numerical results right up to merger by careful choice of adjustable parameters which only affect PN consistency beyond known PN order, the result would simultaneously encode PN and numerical-relativity results. The effective-one-body (EOB) family of PN Hamiltonian models has promise

as a tunable model for encoding both PN and NR results (Buonanno and Damour, 1999, 2000; Damour, 2008; Damour and Nagar, 2010). In the time domain, techniques have also been developed for extending these waveforms into the ringdown of the final black hole. Analysis of the early numerical results in comparison with an untuned EOB model gave promising indications that the waveforms could be closely approximated this way (Buonanno *et al.*, 2007a). With tuning, it appears that this construction can provide an analytic but potentially very accurate, approximation to the complete

coalescence waveform.

In the EOB model, the binary motion is recast as the motion of a single *effective* body of mass  $\mu = M_1 M_2 / (M_1 + M_2)$  moving about a central potential, as is familiar from Newtonian mechanics. In the general relativistic version of this framework, the effective body's motion follows a geodesic (to 2 PN order) around a modified version of a Schwarzschild metric. The motion of the effective body is described by an effective Hamiltonian, which, for systems of nonspinning black holes, may take the form

$$H_{\text{eff}}(\mathbf{r}, \mathbf{p}) = \mu \sqrt{A(r) \left[ 1 + \mathbf{p}^2 + \left( \frac{A(r)}{D(r)} - 1 \right) (\mathbf{n} \cdot \mathbf{p})^2 + Q(r) (\mathbf{n} \cdot \mathbf{p})^4 \right]}. \quad (39)$$

The expressions for  $A(r)$ ,  $D(r)$  and  $Q(r)$  are chosen so that the PN-expansion of the Hamiltonian is consistent with the results from PN theory to known order (3 PN for nonspinning black holes) (Buonanno and Damour, 1999, 2000; Damour *et al.*, 2000). The nonconservative contribution to the motion, arising from the loss of angular momentum to gravitational radiation, is encoded in an additional flux term entering as an external force in Hamilton's equations, which is also constrained to be consistent with PN theory (typically to 3.5PN order). Hamilton's equations are integrated to derive the effective body's motion, and hence the black-hole trajectories. Waveforms are constructed using PN extension of the quadrupole formula relating the motion of the black holes to the amplitude and phase of the multipolar radiation components. The last part of the radiation, arising after merger, is completed by continuously matching a sum of quasinormal ringdown modes to the waveforms truncated near the point of merger.

While consistent with PN theory, the formalism can be adjusted to also match the wave forms derived from numerical-relativity simulations. The flux function, as well as  $A(r)$  and  $D(r)$ , can be adjusted by the addition of higher-order PN terms to modify the strong-field dynamics to agree with NR without violating PN consistency. An early implementation of this approach, encoding the combined results PN and NR for nonspinning black-hole mergers was presented by Buonanno *et al.* (2007b). Figure 31 shows their result comparing numerical and adjusted EOB-model waveforms for a 4:1 mass-ratio merger. Subsequent work involving more accurate numerical simulations, and more careful tuning of the EOB model has improved EOB model waveforms (Boyle *et al.*, 2008b; Damour and Nagar, 2008; Damour *et al.*, 2008). Recent comparisons of improved EOB models with high-accuracy numerical results from Scheel *et al.* (2009) yield differences comparable to numerical errors showing phase agreement within about 0.01 rad through

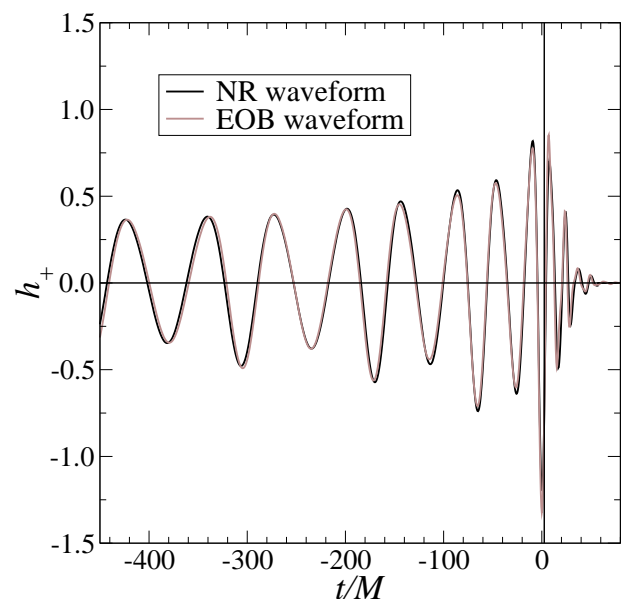


FIG. 31 Comparison of EOB-model and numerical-relativity waveforms from Buonanno *et al.* (2007b) for the  $h_+$  component of the gravitational-wave strain from the merger of binary with mass ratio 4:1. The waveform is for an observer located at an inclination angle  $\theta = \pi/3$  from the axis of rotation.

$\sim 30$  gravitational-wave cycles (Buonanno *et al.*, 2009b; Damour and Nagar, 2009).

Recently the EOB approach has been extended to match cases of non-precessing spinning black-hole mergers (Pan *et al.*, 2010). There remain open questions in extending these waveform models to generic spin configurations, more extreme mass ratios, and full multipolar content.

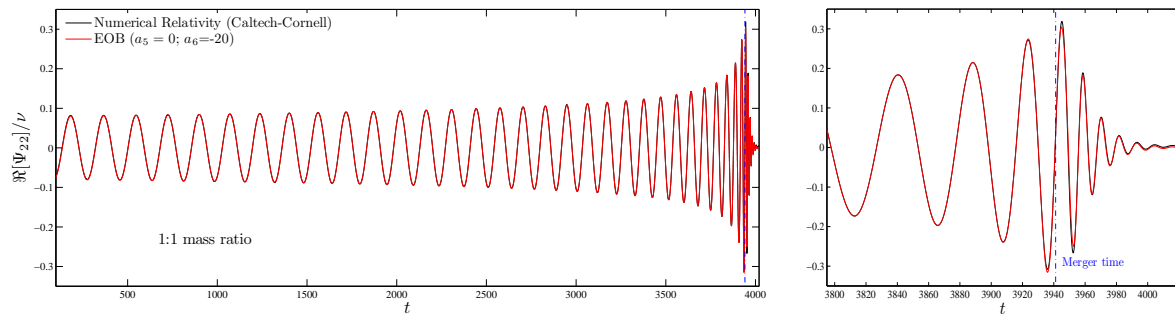


FIG. 32 Agreement of refined EOB-model  $\ell = m = 2$  waveform (Damour and Nagar, 2009) (red) with numerical result from Ref. (Scheel *et al.*, 2009) for equal-mass non-spinning merger (black). Slight differences near the merger time are difficult to perceive without color.

### C. Post-Newtonian Models for Numerical Initial Data.

Before a numerical simulation can commence, a numerical relativist requires a model for the initial configuration of the two black holes and the geometric fields which represent them. As discussed in Sec. IV.D this involves not only solving the general relativistic constraint equations, but also providing some ansatz for the free data. In some cases, some information from PN theory may be applied to produce an initial data model that more precisely represents the desired physical configuration.

To understand how PN information can be applied, it will be useful to revisit the discussion of numerical initial data. Typical simulations begin with a modeling ansatz, the Brandt-Brügmann model, for instance, which produces initial *field* data from a given set of particle-like parameters related to the black holes' masses, spins, initial positions, and momenta. Usually, the initial data models make no attempt to represent the gravitational radiation fields which would have been previously generated by the motion of the black holes, and do not utilize PN information in this reduction of the field degrees of freedom to particle parameters. Information from PN theory is frequently applied in choosing the specific particle parameters which correspond to the sought-after simulation, particularly for circular inspiral configurations. Work has also begun toward making richer use of PN information for improving the field ansatz.

Most of the simulations discussed have been designed to represent black holes in circularized orbits. Before long-lasting numerical-simulation results were available, comparative studies of numerical initial data sets with PN-derived information provided a gauge of the results [see for instance Baker *et al.* (2002b); Caudill *et al.* (2006); Cook and Pfeiffer (2004)]. Without evolutions, these studies focused on theoretical properties of the black-hole configuration space such as the ISCO (see Sec. II.A.1).

Still subtle imbalances in the initial data, such as excess angular momentum for the chosen separation,

can lead to eccentricity in the simulation which impacts the simulated radiation waveforms (Boyle *et al.*, 2008b; Pfeiffer *et al.*, 2007). The residual eccentricity can be reduced via a straightforward iterative procedure (Pfeiffer *et al.*, 2007), but this requires repeated simulations lasting several orbits; expensive in both time and computational resources. To minimize this eccentricity without resorting to iteration, several groups use trajectory information from PN theory in setting up the parameters for the numerical initial data. This approach enables simulations with eccentricities  $e < 0.002$  for equal-mass non-spinning mergers with initial separations  $d_{\text{init}} > 10M$  (Husa *et al.*, 2008b). The technique is helpful in simulations with unequal masses and nonvanishing spins as well, though the residual eccentricity is generally larger (Walther *et al.*, 2009).

Work is underway on techniques allowing the richer application of PN information from numerical initial data modeling. The common assumption of a conformally flat spatial metric in numerical initial data, disagrees with PN results at the 2 PN order (Damour *et al.*, 2000), making this a likely leading source of modeling error which produces spurious initial transients in the simulations. Though not yet as well-developed as the widely applied models, an alternative approach applies metric information from PN theory for a non-trivial initial conformal metric (Jaranowski and Schäfer, 1998; Ohta *et al.*, 1974; Schäfer, 1985). With these techniques it is also possible to encode in the initial data information about the prior radiation generated by the system before the “initial” time of the simulation (Kelly *et al.*, 2007; Tichy *et al.*, 2003).

### D. Post-Newtonian Theory for Interpretation of Numerical Results.

We have noted several specific areas where research in numerical simulations makes contact with PN theory. These alone do not provide a full picture of the interplay



between the two theoretical approaches. Most broadly, PN theory provides a foundation for interpreting numerical results.

Numerical relativists draw widely from PN-based background knowledge of the black-hole binary. Many important phenomena, such as the ISCO, spin-orbit coupling, spin precession, and ‘gravitational rocket’ kicks were first studied in the PN approximation, providing a foundation for subsequent numerical studies. Small examples can be noted throughout this review. In particular we point to the value of PN results in interpreting mergers of spinning black holes (Sec. V.D) and kicks (Sec. V.C). Analytic formulas for approximately expressing the final state of the black hole, mass, spin, and momentum have also drawn heavily from insights based on the PN treatment (see Sec. VIII.A.1.)

## VII. APPLICATIONS TO GRAVITATIONAL WAVE DATA ANALYSIS

Several detectors are active or in their planning stages to detect the gravitational-wave signals from astrophysical processes. Prominent among these are the ground-based interferometric detectors – LIGO (U.S.A.) (Abbott *et al.*, 2009a), GEO (Germany), Virgo (Italy), TAMA (Japan), and AIGO (Australia) – sensitive to frequencies in the range  $10^1 - 10^3$  Hz, as well as next-generation instruments such as the Einstein Telescope (Freise *et al.*, 2009). Also planned to launch at the end of the next decade is the Laser Interferometer Space Antenna (LISA), with complementary frequency sensitivities between  $10^{-4} - 10^{-1}$  Hz. All of these instruments are subject to a variety of noise sources; in the ground-based detectors, these sources will completely overwhelm the signal, unless filtered intelligently. Figure 33 shows the design sensitivity curve resulting from these disparate noise sources, for the LIGO and Virgo detectors.

Burst analysis can extract many signals, but optimal results in gravitational-wave data analysis require *matched filtering* of the noisy input signal (Flanagan and Hughes, 1998; Wainstein and Zubakov, 1962). Fundamental to this approach is some measure of overlap between a physical signal  $h_1(t)$  and filtering template waveform  $h_2(t)$ . For this it is convenient to use a frequency-space inner product  $\langle \cdot | \cdot \rangle$  between signals, defined as (Cutler and Flanagan, 1994)

$$\begin{aligned} \langle h_1 | h_2 \rangle &\equiv 2 \int_0^\infty \frac{\tilde{h}_1(f) \tilde{h}_2(f)^* + \tilde{h}_1(f)^* \tilde{h}_2(f)}{S_n(f)} df \\ &= 4 \text{Re} \left[ \int_0^\infty \frac{\tilde{h}_1(f) \tilde{h}_2(f)^*}{S_n(f)} df \right], \end{aligned} \quad (40)$$

where  $\tilde{h}_1(f)$  and  $\tilde{h}_2(f)$  are the Fourier transforms of the signals, and  $S_n(f)$  is the (one-sided) noise power spectral density of the detector we are interested in. This can be normalized to produce the *match* (or *overlap*) (Owen, 1996) between two waveforms.

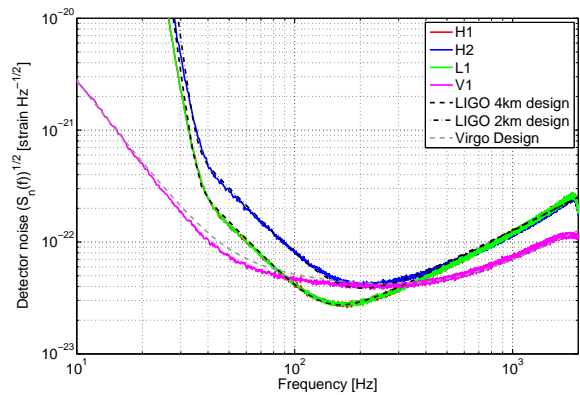


FIG. 33 Design sensitivity curves for the LIGO & Virgo detectors (dashed lines), as well as the approximate curves used for the NINJA project (solid lines). LIGO sensitivity is effectively zero below  $\sim 30$  Hz, while Virgo does a little better (note that achieved sensitivities may not perfectly mirror the design curves). Taken from Aylott *et al.* (2009). Reproduced by permission of the Institute of Physics.

To use (40) requires the availability of a set of waveform *templates* – simple, few-parameter analytic model waveforms to filter against. Even for a relatively simple system such as a black-hole binary, the combination of possible source and detector configurations leads to a 17-dimensional parameter space<sup>5</sup>. Some of these parameters are intrinsic to the source: total binary mass  $M = M_1 + M_2$ , symmetric mass ratio  $\eta$  (1), spins  $\vec{S}_{1,2}$ , time to coalescence  $t_c$ , eccentricity  $e$ , and eccentric phase  $\phi_e$ . The remaining parameters have to do with the relation between source and detector: (luminosity) distance to source  $D_L$ , inclination  $\iota$ , orbital phase  $\phi$ , waveform polarization  $\psi$ , and position of the binary on the detector’s sky  $\{\Theta, \Phi\}$ . Restricting consideration to binaries that have circularized by the time they enter the detector’s window (Peters, 1964) allows us to neglect the eccentricity parameters  $\{e, \phi_e\}$ . Crucially also all observables have a simple dependence on the total (redshifted) mass,  $(1+z)M$ . Similarly, the observed waveforms have a trivial dependence on the time to coalescence  $t_c$ . As this means only one theoretical waveform has to be generated to cover all astrophysical masses and coalescence times,

<sup>5</sup> It is easy to see that there are a total of 17 dimensions. Generally, the instantaneous state of each black hole has ten degrees of freedom for its mass, position, momentum and spin. Of the 20 degrees of freedom for two black holes, the three related to the center-of-mass momentum are unmeasurable by distant gravitational-wave observations. The peculiar motion has negligible effect, and the proper motion results in a Doppler shift indistinguishable from a change in the total mass. Also note that changes in eight more degrees of freedom, corresponding to the center-of-mass position in spacetime, spatial orientation and total mass have trivial effects which can be treated analytically, leaving, in full generality, a space of nine parameters that must be covered by simulations.

$(1+z)M$  and  $t_c$  are sometimes treated as extrinsic parameters instead. Nevertheless, numerical relativists are left with a seven-dimensional parameter space to cover  $(\eta, \vec{S}_1, \vec{S}_2)$ , with no obvious shortcuts to lighten the workload further. Moreover, numerical methods will always struggle with finite accuracy.

Equipped with a parametrized set of template waveforms  $h_m(t; \vec{\lambda})$ , we can test an incoming detector data stream  $s(t) = h_e(t) + n(t)$ , consisting of a (possible) “exact” gravitational wave  $h_e(t)$  and detector noise  $n(t)$  by calculating the *signal-to-noise ratio* (SNR) (Cutler and Flanagan, 1994):

$$\rho(\lambda_i) \equiv \frac{\langle h_m(\lambda_i) | s \rangle}{\sqrt{\langle h_m(\lambda_i) | h_m(\lambda_i) \rangle}}. \quad (41)$$

In the case where the signal  $h_e(t)$  in the data stream corresponds perfectly (up to overall scaling) with the model waveform  $h_m(t; \lambda_i)$  for some value of the model parameters  $\lambda_i = \lambda'_i$ , we obtain the optimal SNR:  $\rho_{\text{opt}} = \sqrt{\langle h_e | h_e \rangle}$ . We refer to this simply as the “SNR”  $\rho$  for the remainder of this section.

Expected SNRs depend strongly on the detector in question. Generally speaking, the ground-based detectors in operation (LIGO, GEO, VIRGO, etc) are expected to observe with only modest optimal SNRs, while LISA is expected to observe MBH mergers with SNRs of hundreds (Danzmann *et al.*, 1998).

Of course, real model waveforms will be inaccurate, due to incomplete knowledge of the underlying physics, or perhaps a desire for simplicity. In this case, the achieved SNR cannot be optimal. Apostolatos (1995) defined the *fitting factor* (FF) as the reduction in signal from such imperfect templates:

$$\text{FF} \equiv \max_{\lambda_i} \frac{\langle h_m(\lambda_i) | h_e \rangle}{\sqrt{\langle h_m(\lambda_i) | h_m(\lambda_i) \rangle \langle h_e | h_e \rangle}} \quad (42)$$

A fitting factor of 1 means that the exact signal lies somewhere in the model space. However, for a particular detector, it is impossible to generate templates arbitrarily close together in any one parameter dimension. We can develop a sense of how closely spaced a set of templates must be so that any physical signal will be detected by at least one of them with high likelihood. Owen (1996) developed a geometric picture of a template-space metric defining the distance between neighboring closely-spaced templates. With these tools, he was able to link the number of templates  $\mathcal{N}$  to the desired *minimal match* (MM) – the worst value of the match between the signal and any template. The connection between these concepts is nicely laid out by Lindblom *et al.* (2008). Figure 34, from Lindblom *et al.* (2008), demonstrates how  $\varepsilon_{\text{MM}} \equiv 1 - \text{MM}$  and  $\varepsilon_{\text{FF}} \equiv 1 - \text{FF}$  combine to produce an effective mismatch  $\varepsilon_{\text{EFF}}$ .

The percentage of detected signals scales as the cube of the fitting factor. For this reason, detector analysts require rather stringent fitting factors from their

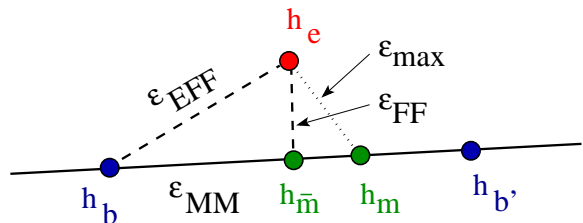


FIG. 34 Relationship between exact waveform  $h_e$ , model waveform with the same physical parameters  $h_m$ , actual “best fit” model waveform  $h_{\bar{m}}$ , and template bank waveforms  $h_b$ ,  $h_{b'}$ . [Figure taken from Lindblom *et al.* (2008)]

template banks, e.g., 97% (implying detection of 90% of all signals present). For initial LIGO, for instance, Baumgarte *et al.* (2008) estimate that  $\sim 100$  zero-spin templates (produced from  $\sim 10$  different numerical simulations) would suffice to detect all nonspinning merging binaries. Obviously we expect that the addition of spins of significant magnitude and arbitrary direction will greatly increase this number.

Detection is only a first step, although an important one. When signal strengths are high, as is expected with LISA for massive binaries, we might expect to be able to read off some of the system’s intrinsic and extrinsic parameters. Achieving this requires templates that accurately cover the parameter space of the binary, with a one-to-one relationship with the parameters of the binary – that is, that the best-fit model waveform  $h_{\bar{m}}$  and closest-parameters model waveform  $h_m$  in Fig. 34 coincide closely (within statistical errors). It also requires that we have an understanding of the probabilistic correlations between parameters.

For high- $\rho$  signals, the simplest way to estimate parameter uncertainties is using the *Fisher information matrix* (Cutler and Flanagan, 1994; Finn, 1992), which uses simple derivatives of the template waveform shape with respect to the physical parameters:

$$F_{ij} \equiv \left\langle \frac{\partial h}{\partial \theta^i} \middle| \frac{\partial h}{\partial \theta^j} \right\rangle. \quad (43)$$

In the high-SNR limit, the parameters are assumed to have a multivariate Gaussian distribution, and the Fisher matrix is the inverse of the covariance matrix between parameters. More sophisticated approaches that do not assume high SNR include Markov-chain Monte Carlo methods (Gilks *et al.*, 1996).

Different requirements can be made on the quality of the developed templates, as described by Damour *et al.* (1998). The first is that they be *effectual*. Roughly speaking, this means that the templates must be capable in the bulk of detecting gravitational-wave signals. In the language of matched filtering above, we demand that the fitting factor  $FF$  be extremely close to unity for any signal.

More stringently, we might demand that the templates be *faithful*: that is, that the template waveform cor-

responds to underlying source parameters that correspond closely to the parameters of the detected waveform source. In the language of Lindblom *et al.* (2008), the model waveforms  $h_m$  and  $h_{\bar{m}}$  coincide closely (see Fig. 34). This requirement will be crucial for identifying the astrophysical source of the radiation.

Traditionally, templates used in the search for comparable-mass black-hole binaries have depended wholly on PN theory. As detection strategies are most sensitive to phase discrepancies between template and observed signal (see below), the determination of waveform phase to high accuracy has been crucial. Modern PN templates include phase terms up to 3.5PN order for nonspinning binaries, with 2.5 PN order spin corrections. Many templates use this high-accuracy phase with the leading-order quadrupole amplitude to produce *restricted* templates; however, amplitude corrections are known to 2.5 PN order (higher for certain low- $\ell$  modes) (Kidder, 2008).

While such PN-driven templates offer excellent phase accuracy during the long, slow inspiral of the binary, their usefulness becomes questionable as we approach the last pre-merger orbits of the binary. We may ask, then, what does our new numerical insight into the final moments of merger bring us?

### A. The Direct Impact of Merger Waveforms in Data Analysis

Once full numerical waveforms became available, several groups used the results to test older predictions of the effect of the merger segment on observability. For the equal-mass nonspinning case, the numerical merger gave results consistent with Flanagan and Hughes (1998) for initial LIGO, though with a smaller merger SNR (Baker *et al.*, 2007c; Buonanno *et al.*, 2007a). The boost in SNR from merger is significantly greater for Advanced LIGO and LISA, as shown in Fig. 35, from Baker *et al.* (2007c).

The relevance of the final plunge and merger to the overall SNR of the binary depends on the total mass of the binary and where it falls in the window of the detector. Figure 36, adapted from Baker *et al.* (2007c), shows this for LISA, plotting the “characteristic signal strain”  $h_{\text{char}}(f) \equiv 2f|h(f)|$  (for the dominant quadrupole radiation). Lower-mass binaries have higher-frequency waveforms at all dynamical stages: for an equal-mass binary with  $M \lesssim 10^4 M_\odot$ , the late-merger and ringdown signal will fall outside LISA’s sensitivity band. For such low masses, inspiral-only waveforms should be adequate for data-analysis purposes.

The LIGO and Virgo detectors are sensitive to frequencies above  $\sim 30\text{Hz}$  (see Fig. 33). The merger of binary systems is marked by a chirp gravitational-wave signal, whose monotonically increasing frequency saturates at the dominant quasinormal mode, which depends on the post-merger hole’s mass and spin. For

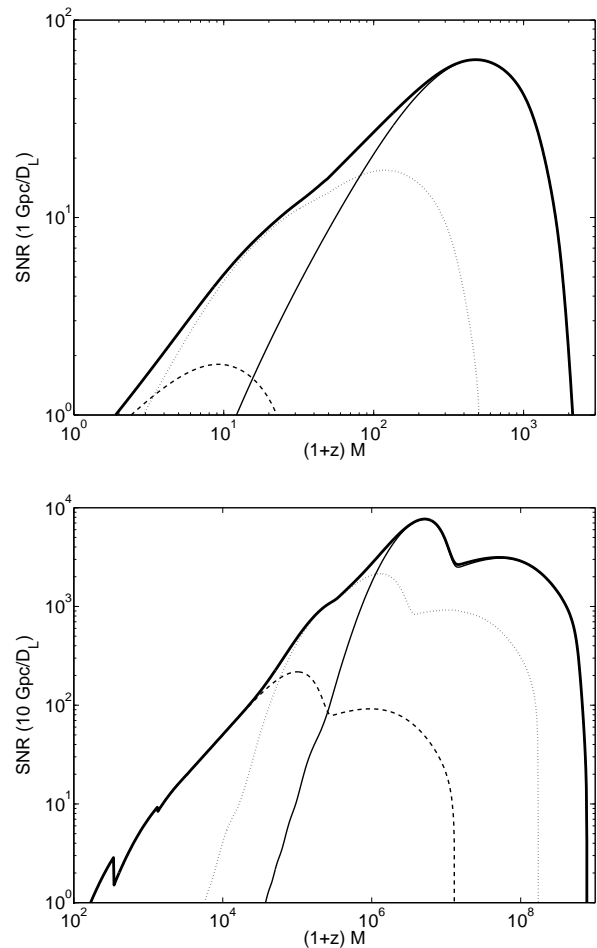


FIG. 35 The importance of including NR merger waveforms in data analysis can be seen here for Advanced LIGO (top) and LISA (bottom), taken from Baker *et al.* (2007c). In both panels, the dashed curve is the achieved SNR (for a given redshifted source mass) when only the early inspiral signal (up to  $\sim 1000M$  before merger) is used; the dotted curve uses the signal between this time and when final plunge commences ( $1000M$  to  $50M$  before merger; the thin solid curve uses just the merger waveform (starting  $50M$  before merger). The thick solid curve is the combined result of using the entire waveform. The SNR, and hence distance reach, of the detector is clearly greatly enhanced by the final merger portion.

a nonspinning binary of total mass  $M$ , this  $f_{\text{QNM}} \approx 1.75 \times 10^4 (M/M_\odot)^{-1} \text{Hz}$ . This means that a merging binary of mass greater than  $\sim 600 M_\odot$  will never be seen by LIGO. In contrast, most post-Newtonian templates stop at  $f_{\text{ISCO}}$ , the frequency at the innermost stable circular orbit (well defined only for test particles; see Sec. II.A.1). This is

$$f_{\text{ISCO}} = \frac{1}{6\sqrt{6}M} \approx 1.36 \times 10^4 (M/M_\odot)^{-1} \text{Hz}. \quad (44)$$

For an incomplete PN waveform to be useful, we want the missing merger-ringdown section (i.e. the part of the signal with  $f > f_{\text{ISCO}}$ ) to contribute as little as possi-

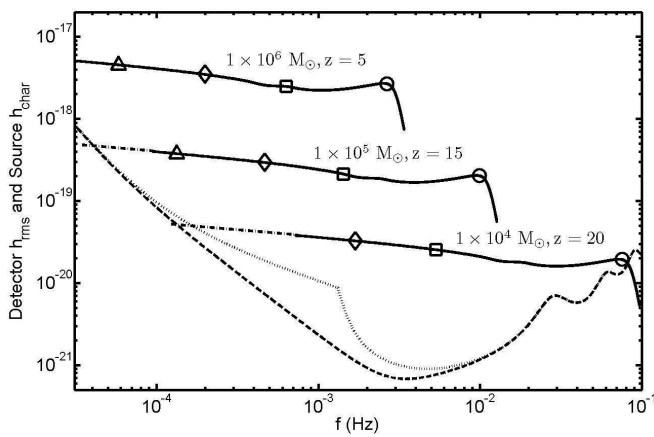


FIG. 36 The importance of binary mass for the LISA observation window, demonstrated by the characteristic amplitudes (Baker *et al.*, 2007c) of three different sources, relative to the rms noise amplitude of the LISA detector. On each  $h_{\text{char}}$  curve, we mark times before the peak amplitude (circle) – one hour (square), one day (diamond) and one month (triangle).

ble to the total SNR. For instance, if we take the high end of LIGO’s sensitivity window to be  $\sim 800\text{Hz}$ , this is  $f_{\text{ISCO}}$  for a binary of total mass  $M \approx 17M_{\odot}$ . Then, for binaries with  $M \gtrsim 17M_{\odot}$ ,  $f > f_{\text{ISCO}}$  will fall within the visible window; that is, LIGO will see the final stages of the binary merger, where no acceptable PN waveform is available. Recent work by Buonanno *et al.* (2009a) supplied a more precise answer: inspiral-only PN templates can be trusted for all LIGO configurations for systems with  $M \lesssim 12M_{\odot}$ . Above this critical mass, there is a gap in reliable information, which must be filled by numerical results.

Figure 37, adapted from Pan *et al.* (2008), shows the importance of the last stages of merger in initial LIGO as a function of mass range. The thin blue curves are hybrid NR/EOB waveforms, while the thick red waveforms are generated from these by “whitening”: that is, they have been Fourier-transformed to the frequency domain, then rescaled by  $1/\sqrt{S_n(f)}$ , and finally re-transformed to the time domain. The whitened amplitude in a segment is proportional to the contribution of that segment to the total SNR; each marked segment accounts for 10% of the total. As the total system mass  $M$  increases, the whitened amplitude becomes more bulked toward the merger time. For the largest total mass shown,  $M = 100M_{\odot}$ , more than 90% of the signal power comes from the last cycle + merger + ringdown.

In Sec. V.B.3, we referenced the recent “Samurai” project (Hannam *et al.*, 2009a), which establishes the consistency of all of the “long” (pre-merger duration  $\gtrsim 1000M$ ) equal-mass nonspinning waveforms within their stated numerical accuracy. As well as direct comparisons of phase and amplitude errors over time, they conducted mismatch tests in the regime of the LIGO and Virgo ground-based detectors. They demonstrated that

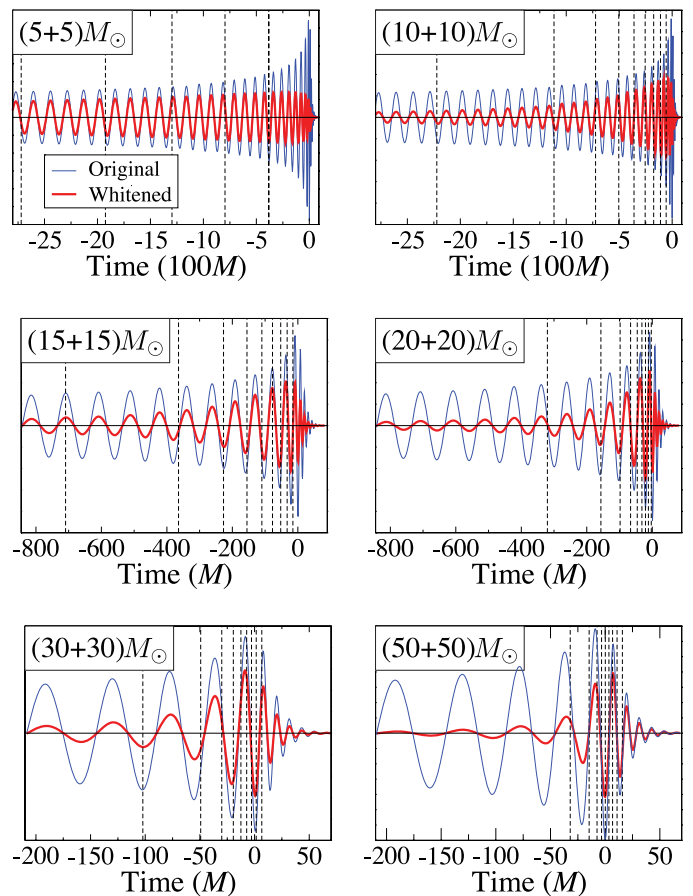


FIG. 37 The power distribution in 10% segments of the waveform before merger, for a range of LIGO-appropriate equal-mass binaries. Note that as the total mass  $M$  increases, the final merger and ringdown account for a greater fraction of the total power. Adapted from Pan *et al.* (2008).

quadrupole waveforms ( $\ell = 2, m = \pm 2$ ) from the five numerical codes have tiny mismatches ( $\sim 10^{-3}$ ) for binary masses above  $60M_{\odot}$  with “enhanced” LIGO, and masses above  $180M_{\odot}$  with Advanced LIGO, Virgo and Advanced Virgo. All waveforms would be indistinguishable for SNRs below 14, entirely reasonable for the current generation of ground-based detectors; this is shown for the Advanced LIGO detector in Fig. 38.

Studies using incomplete (non-merger) PN waveforms have shown that introducing fuller harmonics of spinning and precessing binary systems greatly enhances parameter estimation, removing some parameter correlations and hence reducing certain errors by several orders of magnitude (though other parameters are significantly less improved) (Lang and Hughes, 2006, 2008, 2009; Sintes and Vecchio, 2000; Trias and Sintes, 2008). It is expected that the introduction of full numerical waveforms for the merger portion will lead to further improvements, at least in regions of the detector’s window where the binary merger is visible. A recent study by Ajith and Bose (2009) used phenomenological merger-inspiral-ringdown templates (discussed in Sec. VII.B) to

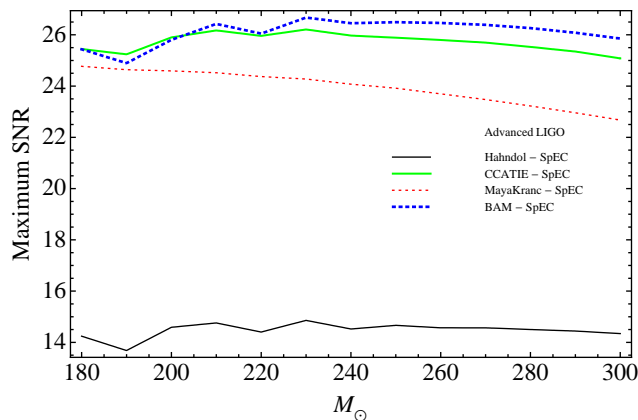


FIG. 38 Maximum signal-to-noise ratio (SNR)  $\rho$  below which different “long” numerical waveforms are indistinguishable for the Advanced LIGO detector. Even the earliest, lowest-accuracy published long waveforms are indistinguishable for SNR levels below 14, as demonstrated in this figure from the Samurai paper (Hannam *et al.*, 2009a).

assess these improvements for Advanced LIGO and Advanced Virgo. They showed that parameter-estimate accuracy is improved substantially compared to inspiral-only waveforms for system masses  $\gtrsim 20M_{\odot}$ ; in particular, the average sky-position error for an  $M = 100M_{\odot}$  equal-mass, nonspinning binary at a luminosity distance of 1 Gpc drops to about one-tenth of a square degree. Since they only use the dominant mode for this investigation, there will be systematic errors as well.

Numerical verification of the extent of parameter estimation improvements for LISA has led to differing estimates (Babak *et al.*, 2008; McWilliams *et al.*, 2010; Thorpe *et al.*, 2009). In particular, Babak *et al.* (2008) find that 50% of injected signals could be located on the detector sky within an error box of 3 arc min, while  $t_c$  could be measured to less than a second and  $D_L$  within 1.5% (ignoring issues of weak lensing). They attributed these impressive results to a combination of very high SNR (between 900 and 9000) and the use of higher multipoles of the radiation. In contrast, McWilliams *et al.* (2010) found smaller (by about one order of magnitude) improvements over inspiral-only waveforms. This may in part be attributable to the use of different mass ratios and different-length waveforms by the two groups, but has not been fully resolved.

## B. Developing Analytic Inspiral-Merger-Ringdown Gravitational Waveform Templates

One of the eventual aims of numerical-relativity simulations of binary mergers is the production of a set of gravitational-wave “templates” that will cover the many-dimensional space of astrophysical parameters. Numerical merger simulations are still orders of magnitude too slow to run on the fly to filter incoming detector data

streams; thus there is a need to develop analytic waveform expressions that encode the numerics.

It has been demonstrated in the physical regime of nonspinning binary mergers (Buonanno *et al.*, 2009a) that inspiral-only PN-based templates become inconsistent with each other (and with full waveforms) at total binary masses  $M \gtrsim 12M_{\odot}$  for initial and advanced LIGO configurations; above this mass, full templates including the numerical-simulation-based understanding of merger/ringdown become necessary.

One such set of templates incorporating numerical-relativity data is due to Pan *et al.* (2008). These were extensions of the Stationary-Phase Approximation (SPA) templates used in LIGO/Virgo data analysis, with input from equal-mass numerical waveforms supplied by Frans Pretorius (Buonanno *et al.*, 2007a), as well as equal- and unequal-mass numerical waveforms from the Goddard group. These templates are effectual – they achieved fitting factors of  $\gtrsim 0.96$  – but they did this by extending source parameters into unphysical space.

To date a handful of useful faithful full-waveform template banks has been produced, aimed at covering all mass ratios for nonspinning binaries. The “phenomenological” templates of Ajith *et al.* (2008, 2007) are simple three-segment curves in frequency space, with matching parameters tuned by numerical data generated by the BAM (Brügmann *et al.*, 2008b) and CCATIE (Pollney *et al.*, 2007) codes. The templates of Boyle *et al.* (2008b); Buonanno *et al.* (2007b), coded in the LSC Algorithm Library as “EOBNR”, are an extension of effective-one-body waveforms, with a single “pseudo-4PN” parameter tuned by numerical data (initially from the Goddard Hahndol code, and later using waveforms from the Caltech-Cornell group. Both the phenomenological and EOBNR template banks are discussed in Sec. VI.B.

Both template banks are faithful in the sense described above, in the restricted  $(M, \eta)$  parameter space, and both have been used in data-analysis injection tests (Aylott *et al.*, 2009; Santamaría *et al.*, 2009). Currently, EOBNR templates are being used both for injection and filtering in the high-mass region of LIGO test analysis, and also for injection for the ringdown band. They were also both used in the matched-filter analyses of the NINJA project (see Sec. VII.C), performing as well as the inspiral-only templates in detection, and considerably better in the limited parameter estimation attempted. Figure 39, from Aylott *et al.* (2009), shows the accuracy with which the total mass  $M$  and time of merger were extracted from all detected injections in NINJA, when the EOBNR templates were used. Results for the phenomenological templates were similar for  $M$ , but performed slightly less well for time of merger, as it is not an explicit part of this model (given the relatively small number of samples in the NINJA tests, such minor differences may not be significant).

As significant spin is expected in astrophysical black holes at all scales, it is important to develop templates

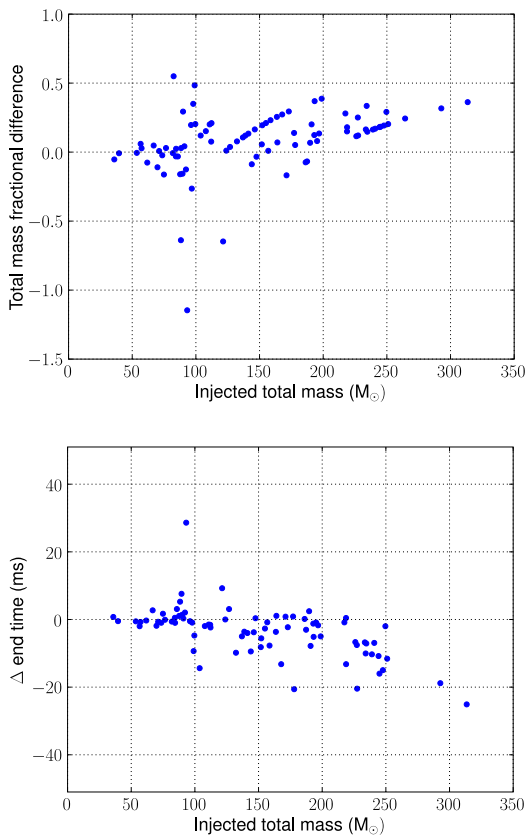


FIG. 39 Accuracy in parameter estimation for EOBNR templates in the NINJA project. The top panel shows the fractional error in estimated total mass,  $(M_{\text{injected}} - M_{\text{detected}})/M_{\text{injected}}$ , for all detected signals, while the lower shows the error in merger time. Adapted from Aylott *et al.* (2009). Reproduced by permission of the Institute of Physics.

that encode spin also. Vaishnav *et al.* (2007) demonstrated that matched filtering with nonspinning merger waveforms does a good job in detecting waveforms from binaries with significant spins. As their spinning waveforms come from aligned-spin mergers where the total spin is zero (one hole’s spin is aligned with the orbital angular momentum, while the other’s is anti-aligned), their configurations will lack some prominent spin-related effects, including spin-orbit effects (pulling in or pushing out the ISCO of the orbit) and precession of the orbital plane. Their conclusions, then, are likely to be optimistic, and more generic configurations can be expected to do much worse with nonspinning templates. The phenomenological templates of Ajith *et al.* have recently been extended to include non-precessing spinning systems (Ajith, 2009). These have been shown to be both effectual and faithful in searches over non-precessing binary hybrid waveforms with LIGO, where earlier zero-spin templates failed badly. For maximum simplicity, these new phenomenological template families are ultimately parametrized by three numbers: the total mass  $M$ , the symmetric mass ratio  $\eta$  (1), and a single effective

spin

$$(a/M)_{\text{eff}} \equiv \frac{(1 + \delta)}{2}(a/M)_1 + \frac{(1 - \delta)}{2}(a/M)_2, \quad (45)$$

where  $\delta = (M_1 - M_2)/M = \sqrt{1 - 4\eta^2}$ .

### C. Using Numerical Waveforms in Data Analysis Applications

An obvious application of numerical waveforms for data analysis is in directly testing analysis algorithms. As current templates are overwhelmingly based on PN information – either extended heuristically to include merger and ringdown, or terminating before merger – so current detection and parameter estimation algorithms are also based on incomplete information.

Recently, a multi-group collaboration (the NINJA project) has performed the first direct insertion of explicit numerical waveforms into a simulated LIGO datastream, and investigated detection efficiency and systematic errors (Aylott *et al.*, 2009). Essentially all active numerical-relativity groups contributed waveforms; these were scaled randomly to represent different-mass sources, resulting in 126 different injections. Nine data-analysis groups analyzed the post-injection data stream, with a variety of methods. These fell into three main groups: matched filtering, burst analysis, and Bayesian techniques.

For the matched filtering, some groups used standard “TaylorF2” inspiral-only templates generated by PN theory, some used ringdown-only templates, and some used full inspiral-merger-ringdown templates, such as the EOBNR and phenomenological waveforms discussed below and in Sec. VI.B. Both the TaylorF2 and the full template waveforms yielded quite high detection rates – around 80 of the 126 injected signals in triple coincidence between the LIGO detectors – while the ringdown templates performed more poorly, detecting only 45 signals in triple coincidence. However for parameter estimation of the total mass  $M$ , most of the TaylorF2 estimates have an error of 40% or more, significantly more than for the EOBNR and phenomenological estimates. Figure 39 shows errors in detected mass (upper panel) and coalescence time (lower panel) when using the EOBNR templates. While mass errors are still quite large, between  $\sim -30\%$  and  $+50\%$  for the bulk of detected signals, they are significantly less biased than those from the TaylorF2 templates (compare with Fig. 8 of Aylott *et al.* (2009)). Estimation of the coalescence time  $t_c$  was better for the EOBNR and phenomenological template banks as well, as might be expected (since TaylorF2 templates must necessarily cut off before coalescence). However, the EOBNR and phenomenological templates typically covered a larger mass range as well (up to  $200M_\odot$  compared to  $90M_\odot$  for TaylorF2), which will bias the results when the injected signals had a large mass.

Burst analysis is a more abstract approach to the problem, using partial information about signals, such as dominant frequency and approximate duration. In NINJA, two burst techniques were used – the “Q pipeline” and the Hilbert-Huang transform (HHT). The Q pipeline fits signals to a sine-Gaussian model parametrized by a central frequency and a  $Q$  factor ( $\sim f\tau$ , the number of oscillations under the Gaussian). At the single-detector level, the detection rate is comparable to that of the EOBNR and phenomenological matched-filter searches. Parameter estimation is limited to estimates of the peak power time (close to  $t_c$ ) and peak frequency; for these parameters, performance was comparable to the ringdown matched-filter search. The Hilbert-Huang transform decomposes input data into “intrinsic mode functions”, each characterized by a single frequency scale. Applied to the signal, the HHT generates a high-resolution time-frequency map of the data (Camp *et al.*, 2007; Stroer *et al.*, 2009). The HHT applied to the NINJA data found  $\sim 80$  coincident events, competitive with the best matched-filter results; however, no parameter estimation is currently possible with this method.

Bayesian analysis attempts to reconstruct the posterior probability density function of a parametrized signal based on the observed signal. Two variant Bayesian approaches were taken in NINJA analysis, involving different Monte Carlo methods – Markov Chain Monte Carlo (MCMC) and Nested Sampling. In both cases, a parametrized waveform model is needed. For the MCMC study, a restricted PN waveform was used, only 1.5 PN in phase, but including leading spin effects. Detection of injected signals performed well, but the high mass of the injections meant that the bulk of the SNR occurred in the merger-ringdown phase; as a result the inspiral-only model masses merger time was significantly biased. The Nested Sampling effort instead uses the TaylorF2 templates (restricted amplitude, 2.0 PN in phase) as well as phenomenological templates. In detection, the phenomenological templates significantly out-perform the TaylorF2 model; in parameter estimation, it achieves results consistent with those of the matched-filter analysis.

Overall, current results are encouraging, with high detection rates of injected waveforms, and good, if limited, accuracy in estimated parameters when attempted with faithful template banks. However, the project was hampered by the limited length of the contributed waveforms and unrealistically stationary LIGO and Virgo noise profiles. Follow-on work in this area will demand longer numerical waveforms that span the LIGO sensitivity window, or more likely, a systematic blending of long PN inspiral waveforms to late-inspiral/merger numerical waveforms, but also may be extended to other gravitational-wave sources.

## VIII. IMPACT ON ASTROPHYSICS

The recent successes in modeling of binary black-hole mergers have captured the attention of astronomers and astrophysicists. While black-hole binaries have been studied both observationally and theoretically for many years, most efforts have been primarily within the framework of Newtonian gravity. The new developments in numerical relativity now supply the missing piece: the effects of the final merger in the strong-field general relativistic regime. In this section we highlight three key areas of current interest: recoiling black holes, the spin of the merged black hole, and electromagnetic signatures from the final merger.

### A. Recoiling Black Holes

One of the more dramatic implications of gravitational-wave computations for astrophysical observations is the possibility that gravitational radiation-induced recoil will eject black holes from their host galaxies. The largest recoil velocities predicted by numerical relativity exceed the escape velocities of many galaxies ( $\sim 1000 \text{ km s}^{-1}$ ). Calculating the probability of this kind of event requires a detailed understanding of the recoil on mass ratios, spin magnitudes, and spin orientations, together with some expectations about the distributions of these parameters.

#### 1. Predicting the Recoil

It would be useful to have in hand a simple, analytic formula expressing the relevant dependencies of the recoil velocity. The highly nonlinear, strong-field interactions of merger dynamics determine the final recoil velocity of the merged remnant. Numerical simulations are required to accurately compute such results. However, in attempting to construct an ansatz for a phenomenological formula, one might initially assume a form consistent with PN predictions. This will suggest the functional dependence on mass and spin, and their leading powers. For example, PN analysis (Fitchett, 1983) suggests that the recoil due to unequal masses may be proportional to  $v = A\eta^2\sqrt{1-4\eta}(1+B\eta)$  (the “Fitchett formula”), where  $\eta$  is the symmetric mass ratio (1). Meanwhile, to leading PN orders, the spins should contribute through components of  $\vec{\Delta} \equiv \vec{S}_2/M_2 - \vec{S}_1/M_1$  and  $\vec{S} \equiv \vec{S}_1 + \vec{S}_2$  (Campanelli *et al.*, 2007b; Kidder, 1995; Racine *et al.*, 2009).

Such an ansatz can be further supported and constrained by symmetry arguments. An economical approach is to consider the recoil velocity as a Taylor expansion in all six spin components (three for each black hole), where the coefficients are functions of mass and initial separation. Rotation, parity, and exchange symmetries of the binary system then impose relationships between these coefficients (Boyle and Kesden, 2008; Boyle *et al.*,

2008a). By such arguments, for example, the component of the recoil velocity parallel to the orbital angular momentum can be shown to be proportional, to leading order in spin, to the dot product of the coordinate separation vector between the black holes and some linear combination of the spins (Baker *et al.*, 2008a; Boyle *et al.*, 2008a).

Unknown coefficients in the ansatz can then be fit to numerical results, and correction terms can be added as needed for numerical agreement. With these considerations, a tentative formula has been taking shape through the combined efforts of the numerical-relativity community, of the following form (Baker *et al.*, 2007a, 2008a; Brüggmann *et al.*, 2008a; Campanelli *et al.*, 2007c; González *et al.*, 2007b; Lousto *et al.*, 2010; Lousto and Zlochower, 2009; van Meter *et al.*, 2010a):

$$\vec{V}_{\text{recoil}} = v_m \hat{e}_1 + v_{\perp} (\cos \xi \hat{e}_1 + \sin \xi \hat{e}_2) + v_{\parallel} \hat{e}_2, \quad (46)$$

$$v_m = A\eta^2 \sqrt{1 - 4\eta(1 + B\eta)}, \quad (47)$$

$$v_{\perp} = H \frac{\eta^2}{(1+q)} (\alpha_2^{\parallel} - q\alpha_1^{\parallel}), \quad (48)$$

$$\begin{aligned} v_{\parallel} &= \frac{K_2\eta^2 + K_3\eta^3}{q+1} \\ &\times [q\alpha_1^{\perp} \cos(\phi_1 - \Phi_1) - \alpha_2^{\perp} \cos(\phi_2 - \Phi_2)] \\ &+ \frac{K_S(q-1)\eta^2}{(q+1)^3} \\ &\times [q^2\alpha_1^{\perp} \cos(\phi_1 - \Phi_1) + \alpha_2^{\perp} \cos(\phi_2 - \Phi_2)] \end{aligned} \quad (49)$$

where  $v_m$  is the contribution due to mass asymmetry,  $v_{\perp}$  is the contribution due to spin that yields a kick perpendicular to the orbital angular momentum,  $v_{\parallel}$  is the contribution due to spin that yields a kick parallel to the orbital angular momentum,  $\alpha_i^{\parallel}$  is the projection of the dimensionless spin vector  $\vec{\alpha}_i = \vec{S}_i/M_i^2$  of black hole  $i$  along the orbital angular momentum,  $\alpha_i^{\perp}$  is the magnitude of its projection  $\vec{\alpha}_i^{\perp}$  into the orbital plane,  $\phi_i$  refers to the angle made by  $\vec{\alpha}_i^{\perp}$  with respect to some reference angle in the orbital plane, and  $\Phi_1$  and  $\Phi_2$  are constants for a given mass ratio and initial separation. Here the spins are considered to have been measured at some point before merger or ideally, arbitrarily close to merger.  $\Phi_1$  and  $\Phi_2$  encode the amount of precession of each spin before merger.

One can then evaluate the formula over ranges of expected mass ratios and spin magnitudes, and for all spin orientations, to compute the probability of a given recoil speed. For example, for mass ratios between 1 and 10, and spin magnitudes of 0.9, the probability of exceeding  $1000 \text{ km s}^{-1}$  is predicted to be  $\sim 10\%$ . Studies of various model-dependent speed probabilities are given by Schnittman (2007) and Baker *et al.* (2008a).

## 2. Consequences of Black Hole Recoil

Among the significant astrophysical consequences of gravitational-radiation recoil, growth rates of black holes can be affected. For example, the recoil of massive black holes imparting less than the escape velocity of their host galaxies tends to have regulatory effects on the amount of mass accreted (Blecha and Loeb, 2008). Recoil velocities that exceed galactic escape velocities can impact massive black-hole growth in a different way, by reducing the chances of subsequent mergers (Sesana *et al.*, 2007; Volonteri, 2007). This in turn may modestly reduce the rate of coalescence events observable by LISA (Sesana *et al.*, 2007).

The recoil might also have more directly observable consequences. Some quasars are thought to originate from the coalescence of massive black holes during galactic mergers. Quasars ejected from their host galaxies might therefore be expected. A study by Bonning *et al.* (2007) found no evidence for such events, indicating that they are rare. However, recent observations of two rapidly moving extragalactic quasars (Shields *et al.*, 2009) are strong candidates for such recoiled black holes (Komossa *et al.*, 2008).

### B. The Spin of the Final Black Hole

The final spin of the merged remnant of a binary is also of astrophysical interest. It would be useful to know the probability of various spin magnitudes in constructing matched filtering templates and estimating gravitational signal detectability for LIGO and LISA (Berti *et al.*, 2007a). The ability to predict a final spin given initial binary parameters also implies that observation of the spin of a black hole may help understand its origin. In particular, an understanding of the relationship between the final spin of a black hole and the orbital angular momentum of its binary precursor may help explain the formation of X-shaped jets (Barausse and Rezzolla, 2009).

As with the kick, it would be advantageous to construct a simple analytic formula with which to estimate the spin. Observations from numerical simulations suggest this might be possible. For example, in the case of nonspinning, equal-mass binaries undergoing circular inspiral, the final spin is insensitive to the initial separation, being determined by the terminal dynamics of the merger. Such evolution results in a universal final spin of  $\sim 0.7$  (Baker *et al.*, 2006a; Campanelli *et al.*, 2006a,b,d; Pretorius, 2005a). Additionally, for unequal-mass, nonspinning binaries, the final spin scales roughly linearly with symmetric mass ratio (1) (González *et al.*, 2007b).

Various approaches to constructing an ansatz for the final spin have been proposed. For aligned-spin, equal-mass mergers, Campanelli *et al.* (2006d) produced a simple formula quadratic in the (common) initial spin; this satisfied the ‘‘cosmic censorship’’ hypothesis:  $a_f/M_f < 1$ . For nonspinning mergers, Berti *et al.* (2007b) sim-



ply assumed  $a_f/M_f = a\eta + b\eta^2$ , for fitting parameters  $a$  and  $b$ , which agreed with data from nonspinning binaries reasonably well. Lousto *et al.* (2010) arrived at a more generic ansatz, for initial black holes of arbitrary spins, using the PN approximation. Barausse and Rezzolla (2009) proposed a different expression for generic binaries, using a set of assumptions about the approximate conservation of the magnitudes and relative angles of certain angular momentum vectors. Several other formulas have been suggested (Buonanno *et al.*, 2008; Rezzolla, 2009; Rezzolla *et al.*, 2008a,b; Tichy and Marronetti, 2008), each in good agreement with some subset of available numerical data. However, broad agreement on an analytic formula for the final spin from generically precessing binaries has yet to be achieved.

### C. Electromagnetic Counterparts of Black Hole Mergers

We have seen above that black-hole mergers are expected to be “loud,” since they produce strong gravitational-wave signals. But will they also be “bright?” That is, will there be an accompanying display of photons, detectable by telescopes in any frequency range of the full electromagnetic spectrum?

#### 1. Astrophysical Considerations

The answer to this question depends critically on the amount and distribution of gas and magnetic fields surrounding the merging binary. For stellar black-hole binaries, and intermediate-mass black-hole binaries in stellar clusters, any matter in an accretion disk would be consumed by one or both black holes and disappear relatively quickly, making an electromagnetic counterpart highly unlikely.

Massive black-hole binaries formed from galaxy mergers, however, present a very different situation. In a gas-rich or “wet” merger, there is likely enough gas available to feed accretion disks around each black hole that eventually evolve into a circumbinary disk; this provides a source of gas and magnetic fields that could generate detectable electromagnetic emission. Even in the case of gas-poor or “dry” mergers, the thin hot gas present is such (elliptical) galaxies might be sufficient to produce an electromagnetic signature.

Such electromagnetic signatures would be valuable to astrophysics. Identification of the source on the sky would help confirm and characterize the merger, and probe accretion physics. A measurement of its redshift using electromagnetic radiation, taken together with the determination of luminosity distance using gravitational waves observed by LISA (Lang and Hughes, 2009), would provide an independent calibration of the distance scale and a precise probe of cosmology including the nature of the mysterious dark energy (Arun *et al.*, 2009b;

Dalal *et al.*, 2006; Holz and Hughes, 2005; Jonsson *et al.*, 2007; Kocsis *et al.*, 2006, 2008, 2007). Differences in arrival times of the electromagnetic and gravitational-wave signatures could also test fundamental principles such as the relative propagation speed of photons and gravitational waves.

With the recent successes in numerical-relativity modeling of black-hole mergers, we find considerable interest in understanding possible electromagnetic signals from these events. Most work to date has focused on mechanisms that could produce emission from a surrounding accretion disk, including signals induced by a recoiling merged black hole encountering the disk (Armitage and Natarajan, 2002; Bode and Phinney, 2007; Chang *et al.*, 2009; Dotti *et al.*, 2006; Haiman *et al.*, 2009a,b; Kocsis *et al.*, 2006, 2008; Kocsis and Loeb, 2008; Lippai *et al.*, 2008; Megevand *et al.*, 2009; Milosavljević and Phinney, 2005; O’Neill *et al.*, 2009; Phinney, 2007; Schnittman and Krolik, 2008; Shields and Bonning, 2008). Moreover, explorations of possible electromagnetic signals that could arise in the dynamic spacetime near the binary during its last few orbits and merger are just now beginning.

#### 2. Simulations with Magnetic Fields or Gas near the Merging Holes

Palenzuela *et al.* (2009) recently studied the effects of a merging black-hole binary on a surrounding magnetic field. The equal-mass, nonspinning holes start out with separation  $\approx 6M$  on quasicircular orbits somewhat outside the ISCO. The magnetic field is initially poloidal and assumed to be generated by currents in a distant circumbinary disk located at  $\approx 10^3M$ . The electric field around the binary is initially zero. There is no matter near the black holes, as predicted when the circumbinary disk is thin (Milosavljević and Phinney, 2005). They solved the coupled Einstein-Maxwell equations for a binary evolving in presence of externally sourced electromagnetic fields. As the system evolves, the inspiralling black holes stir up the fields. Figures 40 and 41 show the electric and magnetic field lines at  $\approx 40M$  and  $\approx 20M$  before the merger, respectively. The magnetic fields are mostly aligned with the  $z$  axis, while the electric fields are twisted around the black holes. The binary dynamics induce oscillations in the electromagnetic energy flux, with a period approximately half of the dominant (quadrupole) gravitational-wave signal. The energy in the electromagnetic field is also enhanced gradually.

Palenzuela *et al.* (2009) have certainly made an interesting start on this important problem. Can this scenario generate detectable electromagnetic emission? The answer awaits more realistic simulations, including spinning black holes.

Other astrophysical scenarios allow both matter and magnetic fields in the vicinity of the binary close to

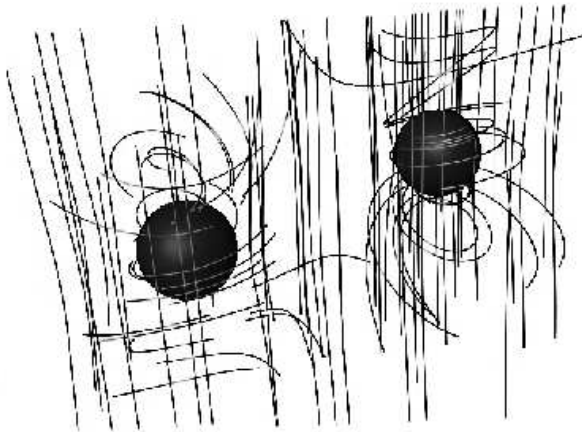


FIG. 40 Magnetic and electric fields lines around inspiralling equal-mass, nonspinning black holes at  $\approx 40M$  before the merger, from Palenzuela *et al.* (2009). The electric field lines are twisted around the black holes, while the magnetic field lines are mainly aligned with the  $z$  axis.

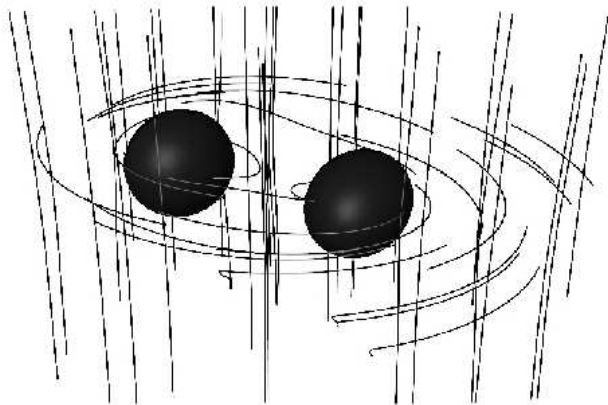


FIG. 41 Same as Fig. 40, except at a later time,  $\approx 20M$  before merger.

merger. In this case, calculation of possible electromagnetic signatures requires solving the equations of general relativistic magnetohydrodynamics in a dynamically evolving spacetime governed by the Einstein equations.

van Meter *et al.* (2010b) took a step towards solving this problem by mapping the flow of pressureless matter, modeled as non-interacting point particles, in the dynamical spacetime around the merging black holes. They started with a distribution of particles around the black-hole binary, and then evolved the binary using numerical relativity while tracing the motion of the particles along geodesics as the binary evolves. To estimate the energetics of the flow, they detected “collisions” by looking for particles within a small distance (typically,  $\lesssim 0.1M$ ) of each other and then calculating the Lorentz factors  $\gamma_{\text{coll}}$  in the center-of-mass frame of each collision.

They began with equal-mass inspiralling black-hole binaries  $\sim 5$  orbits before merger, and considered both black holes to have either zero spin, or  $(a/M)_{1,2} = 0.8$  with spin vectors aligned with the binary orbital angular momentum. A single black hole of mass  $M$  is also evolved as a control case. Approximately 75,000 geodesic particles are then initially distributed uniformly throughout a solid annulus centered on the binary and having inner radius  $8M$ , outer radius  $25M$ , and vertical full thickness  $10M$ . Particles within the inner radius are excluded, to avoid transient signatures from particles initially near the horizons. Note that these circumbinary disks are geometrically thick, and thus potentially have high enough inward radial speeds to keep up with the shrinking separation of the inspiralling binary, providing a source of gas near the black holes during their merger (Milosavljević and Phinney, 2005).

van Meter *et al.* (2010b) studied two initial velocity configurations for the particles. In the “orbital” configuration, the initial velocities are randomly distributed around a tangential velocity  $V_c$  that would give a circular orbit in a Schwarzschild spacetime of mass  $M$ , resulting in a scale height of  $5M$ . In contrast, the “isotropic” configuration is an extreme (that is, very hot) case in which the particles only have random velocities, with each component sampled from a Gaussian distribution of standard deviation  $V_c/\sqrt{3}$ .

For the orbital initial velocities, the particles remain mostly in a rotational configuration; some particles do enter the region around the black holes, but are soon ejected by a gravitational slingshot. The collisions typically occur at relatively low velocities with Lorentz factors  $\gamma_{\text{coll}} \lesssim 1.8$ . By the time of merger, there are essentially no particles near the black holes, and thus there is no energetic signature of the merger. The situation is quite different with the isotropic initial conditions, which provide a continual influx of particles throughout the evolution. Moreover, there is a clear signature of the merger visible in the maximum Lorentz factor, which takes on values  $\gamma_{\text{coll,max}} \sim 2$  during the inspiral and spikes up to  $\gamma_{\text{coll,max}} \sim 3.5$  just before merger for the nonspinning case. For rotating black holes,  $\gamma_{\text{coll,max}} \sim 3$  during the inspiral, spiking to  $\gamma_{\text{coll,max}} \sim 6$  just before merger. In addition, gravitational torques from the merging binary effectively stir the particle distribution, leading to high-velocity outflows with particles reaching  $\gamma_{\text{coll}} \sim 4$  or more.

van Meter *et al.* (2010b) point out that, in realistic astrophysical disks, viscosity would cause angular momentum transport, bringing material inward towards the merging black holes. This could produce a scenario between the two extremes they studied, with a clear merger signal. More recent work by Bode *et al.* (2010), using hydrodynamical simulations of gas around black-hole binaries, provided strong support in this regard. Further confirmation of this interesting possibility, along with other mechanisms involving general relativistic magnetohydrodynamics, awaits more detailed simulations with gas and

magnetic fields, currently in development.

## IX. FRONTIERS AND FUTURE DIRECTIONS

Five years ago, we did not know what obstacles might conspire to prevent the effective application of numerical-relativity simulations in deriving predictions of general relativity to address questions of astrophysical black-hole binaries. Up to that time, the numerical relativity researchers addressed their research primarily to questions of theoretical and computational physics.

Then, quite suddenly, the last obstacles vanished. As reported, numerical relativity can now be applied to understand general relativity’s predictions of strong-field gravitational physics and to begin addressing questions of astrophysics and gravitational-wave data analysis. We expect future work in this field to be guided not by internal problems in gravitational theory, but by questions of astrophysics, and other areas where strong-field gravitational theory applies. These questions will motivate both continued, more detailed, investigation of some of the phenomena which have already been revealed, and the development of new capabilities to bring simulation results to bear on new questions.

### A. Gravitational-Wave Astronomy

Though the work has begun in applying numerical-relativity results to gravitational-wave observations, much more work is still needed. It is now clear that the signal-to-noise (SNR) ratio from the last moments of the merger will dominate over the inspiral signal in many potential observations. Though numerical-relativity simulations have shed considerable light on the basic features of the burst of gravitational radiation that completes the predicted signals, applications in data analysis will require *comprehensive* quantitative knowledge of the merger signals generated over the full parameter space of mergers.

While we discussed examples of mergers that sample the binary black-hole parameter space along what may be its principal axes, a full quantification of the signal space will require a long systematic program of investigation. Even with the aid of empirical models for encoding numerical results, many simulations must be conducted to qualify possible models. Initial models suitable for detection and (perhaps) parameter estimation of low-SNR signals, will require much further development for application to the high-SNR observations expected with future instrument upgrades, such as Advanced LIGO, and future instruments such as LISA. Considerably more simulations of high quality will be required to achieve these goals.

In addition to understanding the signals generated by mergers through the bulk of parameter space in greater depth, relativists must also extend the region of pa-

rameter space covered by simulations. Typical current simulations are limited in the range of parameters that can be practically covered. Currently popular initial data models, particularly those assuming conformal flatness, are limited to  $(a/M)_{1,2} \lesssim 0.93$  (Dain *et al.*, 2002; Lovelace *et al.*, 2008). Alternatives more suited to rapidly spinning Kerr black holes are less well developed in other ways. While astrophysical limits on spin magnitudes remain unclear, it is likely that larger spins will have to be treated with possibly novel initial data models. Other, related challenges in the simulations may also exist.

Current simulations are also restricted to comparable mass ratios. Simulations beyond  $q \sim 5$  require somewhat heroic investments of computational resources with present techniques. Astrophysical mergers may occur, however, over a broad range of mass ratios. In the limit of extremely large mass ratios, approximation techniques are possible that treat the motion of the smaller object as a perturbed geodesic in the spacetime of the larger black hole. Such analytic methods look promising in this limit, where numerical simulations are less practical. However, there is a rather large middle ground, say  $10 < q < 100$ , where new techniques may be required. One problem is that the small spatial scale of the smaller black hole requires extremely small timesteps for stable explicit time integrations, even though there is nothing interesting happening on these timescales. Alternatives such as implicit schemes (Lau *et al.*, 2009) may open the door to a broader range of applications.

Most of the simulations discussed also focus on circular, or nearly circular orbits. While this is clearly an important portion of the black-hole-binary population, scenarios have been proposed in which one black hole captures another from nearly parabolic initial encounters. Understanding the potential signals from such systems may require new techniques appropriate for long periods of slow, effectively Newtonian evolution, punctuated by brief periods of strong gravitational interaction.

### B. Other Astrophysics

As discussed, the numerical discovery of strong gravitational-wave recoils in asymmetric mergers of spinning black holes has had significant impact in areas of astrophysics beyond direct gravitational-wave observations. These results have spurred excitement in the black-hole astronomy community about other possible applications of numerical relativity. Since other areas of astronomy are based on (primarily) electromagnetic observations, these interactions naturally lead to applications involving the interactions of black holes and electromagnetically visible matter. There are many relevant phenomena of interest: accretion disks around black holes, possibly disturbed by gravitational recoil, black-hole–neutron-star binaries, neutron-star–neutron-star binaries, jets from active galactic nuclei, quasars, and the mysterious ori-

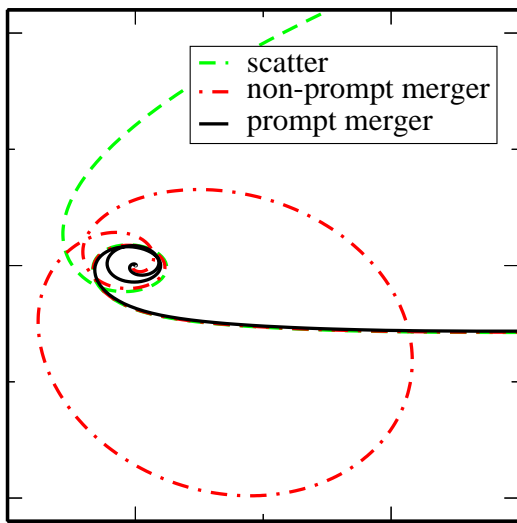


FIG. 42 Numerical simulations are applied to study the critical transition separating mergers from scattering events in high-velocity black-hole encounters (Sperhake *et al.*, 2009). The curves show the path of one black hole in each of three simulations begun with different initial conditions near the critical impact parameter. The trajectories track closely together coming in from the right until the black holes encounter each other near the origin. Figure kindly provided by U. Sperhake.

gins of gamma ray bursts.

A key direction for future work has been adding physics beyond the purely gravitational simulations we have reviewed here. As discussed, efforts are currently underway to use and develop magnetohydrodynamics in a dynamical spacetime. As such simulations are applied with increasing realism to more astrophysical scenarios, refinement of the techniques will be required. Adequately resolving shocks and turbulence interacting with magnetic fields, achieving robust accuracy in the presence of very strong magnetic fields, and enforcing the vanishing divergence of the magnetic fields, all in curved spacetime, are among the challenges that need to be met.

### C. Other Physics

Astrophysical mergers typically involve nearly circular orbits, or in extreme scenarios, initially parabolic encounters. Numerical simulations can be applied to other sorts of black-hole interactions as well.

For high-velocity black-hole encounters, one expects a phase transition dividing the spacetimes in which the black holes merge from those in which they pass each other hyperbolically, never to approach each other again: see Fig. 42. Numerical simulation studies are beginning to elucidate critical behavior near this phase transition (Pretorius, 2006; Pretorius and Khurana, 2007; Sperhake *et al.*, 2009).

These fascinating phenomena at the extreme limit of strong gravitational dynamics have been discussed in

the context of upcoming experimental measurements. In the trans-Planckian energy limit, some particle collisions may be describable by classical black-hole dynamics (Banks and Fischler, 1999; Eardley and Giddings, 2002). In highly speculative theories involving large extra spatial dimensions, it is conceivable that TeV scale physics may be sufficient to produce such black-hole-like collisions (Giddings, 2001; Giddings and Thomas, 2002). These possibilities motivate the first numerical-simulation studies of ultra-relativistic black-hole collisions (Shibata *et al.*, 2008; Sperhake *et al.*, 2008b, 2009).

### D. Strong Gravity as Observational Science

Einstein gave us general relativity nearly 100 years ago. Over the past century this theory, our standard model of gravitational physics, has passed experimental and observational tests over ranging from laboratory-scale physics experiments and solar-system tests to observations of compact astronomical objects and cosmology (Will, 2006). These measurements have, so far, provided no need for a refinement of Einstein’s theory of gravity [though some models to explain cosmic acceleration do involve alternative gravity (Silvestri and Trodden, 2009)].

Numerical simulations are now revealing the detailed predictions of Einstein’s theory for the final merger dynamics of a black-hole binary, and its record in the emitted gravitational radiation. Gravitational-wave observations of these events will expose such gravitational phenomena to measurements in a strong-gravity regime far beyond anything which has previously been tested. These include the first tests of higher-order terms in the PN expansion and, indeed, of the physical predictions which numerical relativity is just now revealing.

The possibility that general relativity will find its limits in these observations motivates a better understanding of what waveforms might be predicted by alternative theories of gravity (Yunes and Pretorius, 2009). Alternative-gravity models of black-hole mergers would also likely require numerical simulation to derive waveform predictions, but little work has been done in this direction so far [see one related example from Salgado *et al.* (2008)].

If Einstein’s theory proves correct in predicting the detailed physics revealed by numerical relativity, it would stand as a truly incredible achievement of scientific induction, divining the details of phenomena vastly removed from physical observations on which the theory was founded. If not, then these observations, together with a confident understanding of Einstein’s predictions founded in numerical relativity simulations, may indeed lay the foundation for the next theory of gravity.

## Acknowledgments

This review draws on the work of a broad research community and would not have been possible without the many contributions and support of our colleagues. We especially want to thank a few individuals who have made particularly valuable contributions. William D. Boggs, Bernd Brügmann, Alessandra Buonanno, Mark Hannam, Richard Matzner, Cole Miller, and Harald Pfeiffer gave insightful and helpful comments on our article. Manuela Campanelli and Harald Pfeiffer supplied us with figures from their simulations that were not in the published literature. We also benefited from many useful discussions with Sean McWilliams. We acknowledge support from NASA Grant No. 06-BEFS06-19. B.J.K. was supported in part by an appointment to the NASA Postdoctoral Program at the Goddard Space Flight Center, administered by Oak Ridge Associated Universities through a contract with NASA.

## References

- Abbott, B. P., *et al.* (LIGO Scientific), 2009a, “LIGO: The Laser Interferometer Gravitational-Wave Observatory,” *Rep. Prog. Phys.* **72**, 076901.
- Abbott, B. P., *et al.* (LIGO Scientific), 2009b, “Search for Gravitational Waves from Low Mass Compact Binary Coalescence in 186 Days of LIGO’s fifth Science run,” *Phys. Rev. D* **80**, 047101.
- Abrahams, A. M., A. Anderson, Y. Choquet-Bruhat, and J. W. York Jr., 1997, “Geometrical hyperbolic systems for general relativity and gauge theories,” *Class. Quantum Grav.* **14**, A9–A22.
- Abramovici, A. A., W. E. Althouse, R. W. P. Drever, Y. Gürsel, S. Kawamura, F. J. Raab, D. Shoemaker, L. Sievers, R. E. Spero, K. S. Thorne, R. E. Vogt, R. Weiss, *et al.*, 1992, “LIGO: The Laser Interferometer Gravitational-Wave Observatory,” *Science* **256**, 325–333.
- Ajith, P., 2008, “Gravitational-wave data analysis using binary black-hole waveforms,” *Class. Quantum Grav.* **25**, 114033 proceedings of GR18: 18th International Conference on General Relativity and Gravitation 7th Edoardo Amaldi Conference on Gravitational Waves Amaldi7), Sydney, Australia, 8-13 Jul 2007.
- Ajith, P., 2009, ““Complete” gravitational-waveform templates for black-hole binaries,” presentation at Numerical Relativity and Data Analysis meeting 2009, Golm bei Potsdam, Germany.
- Ajith, P., S. Babak, Y. Chen, M. Hewitson, B. Krishnan, A. M. Sintes, J. T. Whelan, B. Brügmann, P. Diener, E. N. Dorband, J. A. González, M. D. Hannam, *et al.*, 2008, “Template bank for gravitational waveforms from coalescing binary black holes: Nonspinning binaries,” *Phys. Rev. D* **77**, 104017 Erratum: *ibid.* **79**, 129901(E) (2009).
- Ajith, P., S. Babak, Y. Chen, M. Hewitson, B. Krishnan, J. T. Whelan, B. Brügmann, P. Diener, J. A. González, M. D. Hannam, S. Husa, M. Koppitz, *et al.*, 2007, “A phenomenological template family for black-hole coalescence waveforms,” *Class. Quantum Grav.* **24**, S689–S699.
- Ajith, P., and S. Bose, 2009, “Estimating the parameters of nonspinning binary black holes using ground-based gravitational-wave detectors: Statistical errors,” *Phys. Rev. D* **79**, 084032.
- Ajith, P., M. D. Hannam, S. Husa, Y. Chen, B. Brügmann, E. N. Dorband, D. Müller, F. Ohme, D. Pollney, C. Reisswig, L. Santamaría, and J. Seiler, 2009, “Inspiraling-merger-ringdown waveforms for black-hole binaries with nonprecessing spins,” arXiv:0909.2867 [gr-qc].
- Alcubierre, M., 2008, *Introduction to 3+1 Numerical Relativity* (Oxford University Press, Oxford, U.K.).
- Alcubierre, M., G. D. Allen, B. Brügmann, E. Seidel, and W.-M. Suen, 2000, “Towards an understanding of the stability properties of the 3+1 evolution equations in general relativity,” *Phys. Rev. D* **62**, 124011.
- Alcubierre, M., W. Bengert, B. Brügmann, G. Lanfermann, L. Neger, E. Seidel, and R. Takahashi, 2001a, “3D Grazing Collision of Two Black Holes,” *Phys. Rev. Lett.* **87**, 271103.
- Alcubierre, M., and B. Brügmann, 2001, “Simple excision of a black hole in 3+1 numerical relativity,” *Phys. Rev. D* **63**, 104006.
- Alcubierre, M., B. Brügmann, P. Diener, M. Koppitz, D. Pollney, E. Seidel, and R. Takahashi, 2003, “Gauge conditions for long-term numerical black hole evolutions without excision,” *Phys. Rev. D* **67**, 084023.
- Alcubierre, M., B. Brügmann, D. Pollney, E. Seidel, and R. Takahashi, 2001b, “Black hole excision for dynamic black holes,” *Phys. Rev. D* **64**, 061501 (R).
- Anderson, A., Y. Choquet-Bruhat, and J. W. York Jr., 1997, “Einstein-Bianchi Hyperbolic System for General Relativity,” *Topol. Meth. Nonlinear Anal.* **10**, 353–373.
- Anninos, P., K. Camarda, J. Massó, E. Seidel, W.-M. Suen, and J. Towns, 1995a, “Three-dimensional numerical relativity: The evolution of black holes,” *Phys. Rev. D* **52**(4), 2059–2082.
- Anninos, P., G. E. Daues, J. Massó, E. Seidel, and W.-M. Suen, 1995b, “Horizon Boundary Conditions for Black Hole Spacetimes,” *Phys. Rev. D* **51**(10), 5562–5578.
- Anninos, P., D. W. Hobill, E. Seidel, L. L. Smarr, and W.-M. Suen, 1993, “Collision of Two Black Holes,” *Phys. Rev. Lett.* **71**(18), 2851–2854.
- Apostolatos, T. A., 1995, “Search templates for gravitational waves from precessing, inspiraling binaries,” *Phys. Rev. D* **52**, 605–620.
- Armitage, P. J., and P. Natarajan, 2002, “Accretion during the Merger of Supermassive Black Holes,” *Astrophys. J.* **567**, L9–L12.
- Arnowitt, R., S. Deser, and C. W. Misner, 1962, “The dynamics of general relativity,” in *Gravitation: An Introduction to Current Research*, edited by L. Witten (Wiley, New York), 227–265, eprint arXiv:gr-qc/0405109.
- Arun, K. G., S. Babak, E. Berti, N. Cornish, C. Cutler, J. Gair, S. A. Hughes, B. R. Iyer, R. N. Lang, I. Mandel, E. K. Porter, B. S. Sathyaprakash, *et al.*, 2009a, “Massive Black Hole Binary Inspirals: Results from the LISA Parameter Estimation Taskforce,” *Class. Quantum Grav.* **26**, 094027 in Proceedings of the 7th International LISA Symposium, Barcelona, Spain, 16-20 June 2008.
- Arun, K. G., B. R. Iyer, M. S. S. Qusailah, and B. S. Sathyaprakash, 2006, “Testing post-Newtonian theory with gravitational wave observations,” *Class. Quantum Grav.* **23**, L37–L43.
- Arun, K. G., C. K. Mishra, C. van den Broeck, B. R. Iyer, B. S. Sathyaprakash, and S. Sinha, 2009b, “LISA as a dark energy probe,” *Class. Quantum Grav.* **26**, 094021.
- Aylott, B., *et al.*, 2009, “Testing gravitational-wave searches

- with numerical relativity waveforms: results from the first Numerical INjection Analysis (NINJA) project,” *Class. Quantum Grav.* **26**, 165008.
- Babak, S., M. D. Hannam, S. Husa, and B. F. Schutz, 2008, “Resolving Super Massive Black Holes with LISA,” arXiv:0806.1591 [gr-qc].
- Baker, J. G., W. D. Boggs, J. M. Centrella, B. J. Kelly, S. T. McWilliams, M. C. Miller, and J. R. van Meter, 2007a, “Modeling kicks from the merger of non-precessing black-hole binaries,” *Astrophys. J.* **668**, 1140–1144.
- Baker, J. G., W. D. Boggs, J. M. Centrella, B. J. Kelly, S. T. McWilliams, M. C. Miller, and J. R. van Meter, 2008a, “Modeling kicks from the merger of generic black-hole binaries,” *Astrophys. J.* **682**, L29–L32.
- Baker, J. G., W. D. Boggs, J. M. Centrella, B. J. Kelly, S. T. McWilliams, and J. R. van Meter, 2008b, “Mergers of non-spinning black-hole binaries: Gravitational radiation characteristics,” *Phys. Rev. D* **78**, 044046.
- Baker, J. G., B. Brüggmann, M. Campanelli, and C. O. Lousto, 2000, “Gravitational waves from black hole collisions via an eclectic approach,” *Class. Quantum Grav.* **17**, L149–L156.
- Baker, J. G., B. Brüggmann, M. Campanelli, C. O. Lousto, and R. Takahashi, 2001, “Plunge waveforms from inspiralling binary black holes,” *Phys. Rev. Lett.* **87**, 121103.
- Baker, J. G., M. Campanelli, and C. O. Lousto, 2002a, “The Lazarus project: A pragmatic approach to binary black hole evolutions,” *Phys. Rev. D* **65**, 044001.
- Baker, J. G., M. Campanelli, C. O. Lousto, and R. Takahashi, 2002b, “Modeling gravitational radiation from coalescing binary black holes,” *Phys. Rev. D* **65**, 124012.
- Baker, J. G., M. Campanelli, C. O. Lousto, and R. Takahashi, 2004, “Coalescence remnant of spinning binary black holes,” *Phys. Rev. D* **69**, 027505.
- Baker, J. G., M. Campanelli, F. Pretorius, and Y. Zlochower, 2007b, “Comparisons of binary black hole merger waveforms,” *Class. Quantum Grav.* **24**, S25–S31.
- Baker, J. G., J. M. Centrella, D.-I. Choi, M. Koppitz, and J. R. van Meter, 2006a, “Binary black hole merger dynamics and waveforms,” *Phys. Rev. D* **73**, 104002.
- Baker, J. G., J. M. Centrella, D.-I. Choi, M. Koppitz, and J. R. van Meter, 2006b, “Gravitational wave extraction from an inspiraling configuration of merging black holes,” *Phys. Rev. Lett.* **96**, 111102.
- Baker, J. G., J. M. Centrella, D.-I. Choi, M. Koppitz, J. R. van Meter, and M. C. Miller, 2006c, “Getting a kick out of numerical relativity,” *Astrophys. J.* **653**, L93–L96.
- Baker, J. G., S. T. McWilliams, J. R. van Meter, J. M. Centrella, D.-I. Choi, B. J. Kelly, and M. Koppitz, 2007c, “Binary black hole late inspiral: Simulations for gravitational wave observations,” *Phys. Rev. D* **75**, 124024.
- Baker, J. G., J. R. van Meter, S. T. McWilliams, J. M. Centrella, and B. J. Kelly, 2007d, “Consistency of post-Newtonian waveforms with numerical relativity,” *Phys. Rev. Lett.* **99**, 181101.
- Banks, T., and W. Fischler, 1999, “A model for high energy scattering in quantum gravity,” arXiv:hep-th/9906038.
- Barausse, E., and L. Rezzolla, 2009, “Predicting the direction of the final spin from the coalescence of two black holes,” *Astrophys. J.* **704**, L40–L44.
- Baumgarte, T. W., 2000, “Innermost stable circular orbit of binary black holes,” *Phys. Rev. D* **62**, 024018.
- Baumgarte, T. W., P. R. Brady, J. D. E. Creighton, L. Lehner, F. Pretorius, and R. DeVoe, 2008, “Learning about compact binary merger: The interplay between numerical relativity and gravitational-wave astronomy,” *Phys. Rev. D* **77**, 084009.
- Baumgarte, T. W., and S. G. Naculich, 2007, “Analytic representation of a black hole puncture solution,” *Phys. Rev. D* **75**, 067502.
- Baumgarte, T. W., and S. L. Shapiro, 1998, “Numerical integration of Einstein’s field equations,” *Phys. Rev. D* **59**, 024007.
- Baumgarte, T. W., and S. L. Shapiro, 2003, “Numerical Relativity and Compact Binaries,” *Phys. Rept.* **376**, 41–131.
- Begelman, M. C., R. D. Blandford, and M. J. Rees, 1980, “Massive black hole binaries in active galactic nuclei,” *Nature* **287**, 307–309.
- Bekenstein, J. D., 1973, “Gravitational radiation recoil and runaway black holes,” *Astrophys. J.* **183**, 657–664.
- Berentzen, I., M. Preto, P. Berczik, D. Merritt, and R. Spurzem, 2009, “Binary Black Hole Merger in Galactic Nuclei: Post-Newtonian Simulations,” *Astrophys. J.* **695**, 455–468.
- Bernstein, D. H., 1993, *A Numerical Study of the Black Hole Plus Brill Wave Spacetime*, Ph.D. thesis, University of Illinois Urbana-Champaign.
- Bernstein, D. H., D. W. Hobill, E. Seidel, L. L. Smarr, and J. Towns, 1994, “Numerically Generated Axisymmetric Black Hole Spacetimes: Numerical Methods and Code Tests,” *Phys. Rev. D* **50**(8), 5000–5024.
- Berti, E., J. Cardoso, V. Cardoso, and M. Cavagliá, 2007a, “Matched filtering and parameter estimation of ringdown waveforms,” *Phys. Rev. D* **76**, 104044.
- Berti, E., V. Cardoso, J. A. González, U. Sperhake, and B. Brüggmann, 2008, “Multipolar analysis of spinning binaries,” *Class. Quantum Grav.* **25**, 114035.
- Berti, E., V. Cardoso, J. A. González, U. Sperhake, M. D. Hannam, S. Husa, and B. Brüggmann, 2007b, “Inspiraling merger, and ringdown of unequal mass black hole binaries: A multipolar analysis,” *Phys. Rev. D* **76**, 064034.
- Berti, E., V. Cardoso, and A. O. Starinets, 2009, “Quasinormal modes of black holes and black branes,” *Class. Quantum Grav.* **26**, 163001.
- Blanchet, L., 2006, “Gravitational Radiation from Post-Newtonian Sources and Inspiralling Compact Binaries,” *Living Rev. Relativity* **9**(4) <http://www.livingreviews.org/lrr-2006-4>.
- Blanchet, L., 2010, in *Mass and Motion in General Relativity*, edited by L. Blanchet, A. Spallicci, and B. F. Whiting (Springer, New York), Fundamental Theories of Physics, proceedings of the C.N.R.S. “School on Mass” in Orléans, France, June 2008, eprint arXiv:0907.3596 [gr-qc].
- Blanchet, L., G. Faye, B. R. Iyer, and S. Sinha, 2008, “The third post-Newtonian gravitational wave polarisations and associated spherical harmonic modes for inspiralling compact binaries in quasi-circular orbits,” *Class. Quantum Grav.* **25**, 165003.
- Blanchet, L., M. S. S. Qusailah, and C. M. Will, 2005, “Gravitational recoil of inspiralling black-hole binaries to second post-Newtonian order,” *Astrophys. J.* **635**, 508–515.
- Blecha, L., and A. Loeb, 2008, “Effects of gravitational-wave recoil on the dynamics and growth of supermassive black holes,” *Mon. Not. R. Astron. Soc.* **390**, 1311–1325.
- Bode, N., and E. S. Phinney, 2007, “Variability in Circumbinary Disks Following Massive Black Hole Mergers,” bulletin of the 2007 APS April Meeting, abstract S1.00010.
- Bode, T., R. Haas, T. Bogdanovic, P. Laguna, and D. M. Shoemaker, 2010, “Relativistic Mergers of Supermassive

- Black Holes and their Electromagnetic Signatures,” *Astrophys. J.* **715**, 1117–1131.
- Bode, T., D. M. Shoemaker, F. Herrmann, and I. Hinder, 2008, “Robustness of Binary Black Hole Mergers in the Presence of Spurious Radiation,” *Phys. Rev. D* **77**, 044027.
- Bona, C., and J. Massó, 1992, “Hyperbolic Evolution System for Numerical Relativity,” *Phys. Rev. Lett.* **68**, 1097–1099.
- Bona, C., J. Massó, E. Seidel, and J. Stela, 1995, “New Formalism for Numerical Relativity,” *Phys. Rev. Lett.* **75**, 600–603.
- Bona, C., and C. Palenzuela (eds.), 2005, *Elements of Numerical Relativity*, volume 673 of *Lecture Notes in Physics* (Springer, Berlin/Heidelberg).
- Bonning, E. W., G. A. Shields, and S. Salivander, 2007, “Recoiling Black Holes in Quasars,” *Astrophys. J.* **666**, L13–L16.
- Bowen, J. M., and J. W. York Jr., 1980, “Time-asymmetric initial data for black holes and black-hole collisions,” *Phys. Rev. D* **21**, 2047–2056.
- Boyle, L., and M. Kesden, 2008, “Spin expansion for binary black hole mergers: New predictions and future directions,” *Phys. Rev. D* **78**, 024017.
- Boyle, L., M. Kesden, and S. Nissanke, 2008a, “Binary black hole merger: Symmetry and the spin expansion,” *Phys. Rev. Lett.* **100**, 151101.
- Boyle, M., D. A. Brown, L. E. Kidder, A. H. Mroué, H. P. Pfeiffer, M. A. Scheel, G. B. Cook, and S. A. Teukolsky, 2007a, “High-accuracy comparison of numerical relativity simulations with post-Newtonian expansions,” *Phys. Rev. D* **76**, 124038.
- Boyle, M., D. A. Brown, and L. Pekowsky, 2009, “Comparison of high-accuracy numerical simulations of black-hole binaries with stationary phase post-Newtonian template waveforms for Initial and Advanced LIGO,” *Class. Quantum Grav.* **26**, 114006.
- Boyle, M., A. Buonanno, L. E. Kidder, A. H. Mroué, Y. Pan, H. P. Pfeiffer, and M. A. Scheel, 2008b, “High-accuracy numerical simulation of black-hole binaries: Computation of the gravitational-wave energy flux and comparisons with post-Newtonian approximants,” *Phys. Rev. D* **78**, 104020.
- Boyle, M., L. Lindblom, H. P. Pfeiffer, M. Scheel, and L. E. Kidder, 2007b, “Testing the accuracy and stability of spectral methods in numerical relativity,” *Phys. Rev. D* **75**, 024006.
- Brady, P. R., J. D. E. Creighton, and K. S. Thorne, 1998, “Computing the merger of black-hole binaries: The IBBH problem,” *Phys. Rev. D* **58**, 061501.
- Brandt, S. R., and B. Brüggmann, 1997, “A Simple Construction of Initial Data for Multiple Black Holes,” *Phys. Rev. Lett.* **78**(19), 3606–3609.
- Brandt, S. R., K. Camarda, E. Seidel, and R. Takahashi, 2003, “Three Dimensional Distorted Black Holes,” *Class. Quantum Grav.* **20**, 1–20.
- Brandt, S. R., R. Correll, R. Gómez, M. F. Huq, P. Laguna, L. Lehner, P. Marronetti, R. A. Matzner, D. Neilsen, J. A. Pullin, E. Schnetter, D. Shoemaker, *et al.*, 2000, “Grazing Collisions of Black Holes via the Excision of Singularities,” *Phys. Rev. Lett.* **85**, 5496–5499.
- Brill, D. R., and R. W. Lindquist, 1963, “Interaction energy in geometrostatics,” *Phys. Rev.* **131**, 471–476.
- Brown, J. D., 2008, “Puncture evolution of Schwarzschild black holes,” *Phys. Rev. D* **77**, 044018.
- Brüggmann, B., 1999, “Binary black hole mergers in 3D numerical relativity,” *Int. J. Mod. Phys. D* **8**, 85–100.
- Brüggmann, B., J. A. González, M. D. Hannam, S. Husa, and U. Sperhake, 2008a, “Exploring black hole superkicks,” *Phys. Rev. D* **77**, 124047.
- Brüggmann, B., J. A. González, M. D. Hannam, S. Husa, U. Sperhake, and W. Tichy, 2008b, “Calibration of moving puncture simulations,” *Phys. Rev. D* **77**, 024027.
- Brüggmann, B., W. Tichy, and N. Jansen, 2004, “Numerical simulation of orbiting black holes,” *Phys. Rev. Lett.* **92**, 211101.
- Bulik, T., and K. Belczynski, 2009, “Observational evidence for stellar mass binary black holes and their coalescence rate,” arXiv:0907.5515 [astro-ph.CO].
- Buonanno, A., Y. Chen, and M. Vallisneri, 2003, “Detection template families for gravitational waves from the final stages of binary-black-hole inspirals: Nonspinning case,” *Phys. Rev. D* **67**, 024016.
- Buonanno, A., G. B. Cook, and F. Pretorius, 2007a, “Inspirational merger and ring-down of equal-mass black-hole binaries,” *Phys. Rev. D* **75**, 124018.
- Buonanno, A., and T. Damour, 1999, “Effective one-body approach to general relativistic two-body dynamics,” *Phys. Rev. D* **59**, 084006.
- Buonanno, A., and T. Damour, 2000, “Transition from inspiral to plunge in binary black hole coalescences,” *Phys. Rev. D* **62**, 064015.
- Buonanno, A., B. R. Iyer, E. Ochsner, Y. Pan, and B. Sathyaprakash, 2009a, “Comparison of post-Newtonian templates for compact binary inspiral signals in gravitational-wave detectors,” *Phys. Rev. D* **80**, 084043.
- Buonanno, A., L. E. Kidder, and L. Lehner, 2008, “Estimating the final spin of a binary black hole coalescence,” *Phys. Rev. D* **77**, 026004.
- Buonanno, A., Y. Pan, J. G. Baker, J. M. Centrella, B. J. Kelly, S. T. McWilliams, and J. R. van Meter, 2007b, “Approaching faithful templates for nonspinning binary black holes using the effective-one-body approach,” *Phys. Rev. D* **76**, 104049.
- Buonanno, A., Y. Pan, H. P. Pfeiffer, M. A. Scheel, L. T. Buchman, and L. E. Kidder, 2009b, “Effective-one-body waveforms calibrated to numerical relativity simulations: Coalescence of nonspinning, equal-mass black holes,” *Phys. Rev. D* **79**, 124028.
- Calabrese, G., J. A. Pullin, O. Sarbach, and M. Tiglio, 2002a, “Convergence and stability in numerical relativity,” *Phys. Rev. D* **66**, 041501.
- Calabrese, G., J. A. Pullin, O. Sarbach, and M. Tiglio, 2002b, “Stability properties of a formulation of Einstein’s equations,” *Phys. Rev. D* **66**, 064011.
- Camarda, K., and E. Seidel, 1999, “Three-dimensional simulations of distorted black holes: Comparison with axisymmetric results,” *Phys. Rev. D* **59**, 064019.
- Camp, J. B., J. K. Cannizzo, and K. Numata, 2007, “Application of the Hilbert-Huang transform to the search for gravitational waves,” *Phys. Rev. D* **75**, 061101(R).
- Camp, J. B., and N. J. Cornish, 2004, “Gravitational wave astronomy,” *Annu. Rev. Nucl. Part. Sci.* **54**, 525–577.
- Campanelli, M., 2005, “Understanding the fate of merging supermassive black holes,” *Class. Quantum Grav.* **22**, S387–S394.
- Campanelli, M., C. O. Lousto, P. Marronetti, and Y. Zlochower, 2006a, “Accurate evolutions of orbiting black-hole binaries without excision,” *Phys. Rev. Lett.* **96**, 111101.
- Campanelli, M., C. O. Lousto, H. Nakano, and Y. Zlochower, 2009, “Comparison of numerical and post-Newtonian wave-

- forms for generic precessing black-hole binaries,” *Phys. Rev. D* **79**, 084010.
- Campanelli, M., C. O. Lousto, and Y. Zlochower, 2006b, “Last orbit of binary black holes,” *Phys. Rev. D* **73**, 061501(R).
- Campanelli, M., C. O. Lousto, and Y. Zlochower, 2006c, “Spin-orbit interactions in black-hole binaries,” *Phys. Rev. D* **74**, 084023.
- Campanelli, M., C. O. Lousto, and Y. Zlochower, 2006d, “Spinning-black-hole binaries: The orbital hang up,” *Phys. Rev. D* **74**, 041501(R).
- Campanelli, M., C. O. Lousto, Y. Zlochower, B. Krishnan, and D. Merritt, 2007a, “Spin flips and precession in black-hole-binary mergers,” *Phys. Rev. D* **75**, 064030.
- Campanelli, M., C. O. Lousto, Y. Zlochower, and D. Merritt, 2007b, “Large Merger Recoils and Spin Flips From Generic Black-Hole Binaries,” *Astrophys. J.* **659**, L5–L8.
- Campanelli, M., C. O. Lousto, Y. Zlochower, and D. Merritt, 2007c, “Maximum Gravitational Recoil,” *Phys. Rev. Lett.* **98**, 231102.
- Caudill, M., G. B. Cook, J. D. Grigsby, and H. P. Pfeiffer, 2006, “Circular orbits and spin in black-hole initial data,” *Phys. Rev. D* **74**, 064011.
- Chang, P., L. E. Strubbe, K. Menou, and E. Quataert, 2009, “Fossil Gas and the Electromagnetic Precursor of Supermassive Binary Black Hole Mergers,” arXiv:0906.0825 [astro-ph.HE].
- Choquet-Bruhat, Y., 1962, “The Cauchy Problem,” in *Gravitation: An Introduction to Current Research*, edited by L. Witten (John Wiley, New York), 130–168.
- Chu, T., H. P. Pfeiffer, and M. A. Scheel, 2009, “High accuracy simulations of black hole binaries: Spins anti-aligned with the orbital angular momentum,” *Phys. Rev. D* **80**, 124051.
- Colbert, E. J. M., and M. C. Miller, 2005, in *Proceedings of the Tenth Marcel Grossmann Meeting on General Relativity, Rio de Janeiro 2003, Brazil, 20-26 July 2004*, edited by M. Novello, S. Perez-Bergliaffa, and R. Ruffini (World Scientific, Singapore), 530–549, eprint arXiv:astro-ph/0402677.
- Colpi, M., S. Callegari, M. Dotti, and L. Mayer, 2009, “Massive black hole binary evolution in gas-rich mergers,” *Class. Quantum Grav.* **26**, 094029.
- Cook, G. B., 1994, “Three-dimensional initial data for the collision of two black holes. II. Quasi-circular orbits for equal-mass black holes,” *Phys. Rev. D* **50**(8), 5025–5032.
- Cook, G. B., 2000, “Initial Data for Numerical Relativity,” *Living Rev. Relativity* **3**(5) <http://www.livingreviews.org/lrr-2000-5>.
- Cook, G. B., 2002, “Corotating and irrotational binary black holes in quasi-circular orbits,” *Phys. Rev. D* **65**, 084003.
- Cook, G. B., M. F. Huq, S. A. Klasky, M. A. Scheel, A. M. Abrahams, A. Anderson, P. Anninos, T. W. Baumgarte, N. T. Bishop, S. R. Brandt, J. C. Browne, K. Camarda, et al., 1998, “Boosted three-dimensional black-hole evolutions with singularity excision,” *Phys. Rev. Lett.* **80**, 2512–2516.
- Cook, G. B., and H. P. Pfeiffer, 2004, “Excision boundary conditions for black hole initial data,” *Phys. Rev. D* **70**, 104016.
- Cutler, C., and E. E. Flanagan, 1994, “Gravitational waves from merging compact binaries: How accurately can one extract the binary’s parameters from the inspiral waveform?” *Phys. Rev. D* **49**, 2658–2697.
- Dain, S., C. O. Lousto, and R. Takahashi, 2002, “New conformally flat initial data for spinning black holes,” *Phys. Rev. D* **65**, 104038.
- Dalal, N., D. E. Holz, S. A. Hughes, and B. Jain, 2006, “Short GRB and binary black hole standard sirens as a probe of dark energy,” *Phys. Rev. D* **74**, 063006.
- Damour, T., 2008, “Introductory lectures on the Effective One Body formalism,” *Int. J. Mod. Phys. C* **23**, 1130–1148 lectures given at 2nd Stueckelberg Workshop on Relativistic Field Theories, Pescara, Italy, 3-7 Sep 2007.
- Damour, T., and A. Gopakumar, 2006, “Gravitational recoil during binary black hole coalescence using the effective one body approach,” *Phys. Rev. D* **73**, 124006.
- Damour, T., B. R. Iyer, and B. S. Sathyaprakash, 1998, “Improved filters for gravitational waves from inspiralling compact binaries,” *Phys. Rev. D* **57**, 885–907.
- Damour, T., P. Jaranowski, and G. Schäfer, 2000, “Determination of the last stable orbit for circular general relativistic binaries at the third post-Newtonian approximation,” *Phys. Rev. D* **62**, 084011.
- Damour, T., and A. Nagar, 2008, “Comparing effective-one-body gravitational waveforms to accurate numerical data,” *Phys. Rev. D* **77**, 024043.
- Damour, T., and A. Nagar, 2009, “Improved analytical description of inspiralling and coalescing black-hole binaries,” *Phys. Rev. D* **79**, 081503(R).
- Damour, T., and A. Nagar, 2010, “The Effective One Body description of the Two-Body problem,” in *Mass and Motion in General Relativity*, edited by L. Blanchet, A. Spallicci, and B. F. Whiting (Springer, New York), Fundamental Theories of Physics, proceedings of the C.N.R.S. “School on Mass” in Orléans, France, June 2008, eprint arXiv:0906.1769 [gr-qc].
- Damour, T., A. Nagar, E. N. Dorband, D. Pollney, and L. Rezzolla, 2008, “Faithful effective-one-body waveforms of equal-mass coalescing black-hole binaries,” *Phys. Rev. D* **77**, 084017.
- Danzmann, K., P. L. Bender, A. Brillet, I. Ciufolini, A. Cruise, C. Cutler, F. Fidecaro, W. Folkner, J. Hough, P. McNamara, M. Peterseim, D. Robertson, et al., 1998, *LISA Pre-Phase A Report, 2nd ed.*, Technical Report 233, Max-Planck-Institut für Quantenoptik.
- Desroches, L.-B., J. E. Greene, and L. C. Ho, 2009, “X-ray Properties of Intermediate-Mass Black Holes in Active Galaxies. II. X-ray-Bright Accretion and Possible Evidence for Slim Disks,” *Astrophys. J.* **698**, 1515–1522.
- Djorgovski, S. G., M. Volonteri, V. Springel, V. Bromm, and G. Meylan, 2008, in *Proceedings of the Eleventh Marcel Grossmann Meeting on General Relativity, Berlin, Germany, 2006*, edited by R. T. J. H. Kleinert and R. Ruffini (World Scientific, Singapore), 340–367, eprint arXiv:0803.2862 [astro-ph].
- Dotti, M., R. Salvaterra, A. Sesana, M. Colpi, and F. Haardt, 2006, “On the search of electromagnetic cosmological counterparts to coalescences of massive black hole binaries,” *Mon. Not. R. Astron. Soc.* **372**, 869–875.
- Dreyer, O., B. Krishnan, D. M. Shoemaker, and E. Schnetter, 2003, “Introduction to Isolated Horizons in Numerical Relativity,” *Phys. Rev. D* **67**, 024018.
- Duez, M. D., S. L. Shapiro, and H.-J. Yo, 2004, “Relativistic Hydrodynamic Evolutions with Black Hole Excision,” *Phys. Rev. D* **69**, 104016.
- Eardley, D. M., and S. B. Giddings, 2002, “Classical black hole production in high-energy collisions,” *Phys. Rev. D*



- 66**, 044011.
- Einstein, A., and N. Rosen, 1935, “The Particle Problem in the General Theory of Relativity,” *Phys. Rev.* **48**, 73–77.
- Eppley, K., 1975, *The Numerical Evolution of the Collision of Two Black Holes*, Ph.D. thesis, Princeton University, Princeton, New Jersey.
- Estabrook, F. B., H. Wahlquist, S. Christensen, B. S. DeWitt, L. L. Smarr, and E. Tsiang, 1973, “Maximally Slicing a Black Hole,” *Phys. Rev. D* **7**(10), 2814–2817.
- Favata, M., S. A. Hughes, and D. E. Holz, 2004, “How black holes get their kicks: Gravitational radiation recoil revisited,” *Astrophys. J.* **607**, L5–L8.
- Ferrarese, L., and H. Ford, 2005, “Supermassive black holes in galactic nuclei: past, present, and future research,” *Space Science Reviews* **116**, 523–624.
- Finn, L. S., 1992, “Detection, measurement, and gravitational radiation,” *Phys. Rev. D* **46**, 5236–5249.
- Fitchett, M. J., 1983, “The influence of gravitational wave momentum losses on the centre of mass motion of a Newtonian binary system,” *Mon. Not. R. Astron. Soc.* **203**, 1049–1062.
- Fitchett, M. J., and S. L. Detweiler, 1984, “Linear momentum and gravitational waves - Circular orbits around a Schwarzschild black hole,” *Mon. Not. R. Astron. Soc.* **211**, 933–942.
- Flanagan, E. E., and S. A. Hughes, 1998, “Measuring gravitational waves from binary black hole coalescences. I. Signal to noise for inspiral, merger, and ringdown,” *Phys. Rev. D* **57**, 4535–4565.
- Flanagan, E. E., and S. A. Hughes, 2005, “The basics of gravitational wave theory,” *New J. Phys.* **7**, 204.
- Freise, A., S. Chelkowski, S. Hild, W. D. Pozzo, A. Perreca, and A. Vecchio, 2009, “Triple Michelson interferometer for a third-generation gravitational wave detector,” *Class. Quantum Grav.* **26**, 085012.
- Friedrich, H., 1985, “On the hyperbolicity of Einstein’s and other gauge field equations,” *Commun. Math. Phys.* **100**, 525–543.
- Friedrich, H., and A. D. Rendall, 2000, “The Cauchy Problem for the Einstein Equations,” *Lect. Notes Phys.* **540**, 127–224.
- Garfinkle, D., 2002, “Harmonic coordinate method for simulating generic singularities,” *Phys. Rev. D* **65**, 044029.
- Giddings, S. B., 2001, in *Proceedings of Snowmass 2001, Snowmass Village, Colorado, June 30–July 21, 2001*, edited by N. Graf, P328, on-line only, <http://www.slac.stanford.edu/econf/C010630/proceedings.shtml>, eprint arXiv:hep-ph/0110127.
- Giddings, S. B., and S. D. Thomas, 2002, “High energy colliders as black hole factories: The end of short distance physics,” *Phys. Rev. D* **65**, 056010.
- Gilks, W. R., S. Richardson, and D. J. Spiegelhalter (eds.), 1996, *Markov Chain Monte Carlo in Practice: Interdisciplinary Statistics* (Chapman & Hall/CRC, Boca Raton).
- Glebbeek, E., E. Gaburov, S. E. de Mink, O. R. Pols, and S. F. Portegies Zwart, 2009, “The evolution of runaway stellar collision products,” *Astron. Astrophys.* **497**, 255–264.
- González, J. A., M. D. Hannam, U. Sperhake, B. Brügmann, and S. Husa, 2007a, “Supermassive Recoil Velocities for Binary Black-Hole Mergers with Antialigned Spins,” *Phys. Rev. Lett.* **98**, 231101.
- González, J. A., U. Sperhake, and B. Brügmann, 2009, “Black-hole binary simulations: the mass ratio 10:1,” *Phys. Rev. D* **79**, 124006.
- González, J. A., U. Sperhake, B. Brügmann, M. D. Hannam, and S. Husa, 2007b, “Maximum kick from nonspinning black-hole binary inspiral,” *Phys. Rev. Lett.* **98**, 091101.
- Gould, A., and H.-W. Rix, 2000, “Binary Black Hole Mergers from Planet-like Migrations,” *Astrophys. J.* **532**, L29–L32.
- Gourgoulhon, E., 2007, “3+1 Formalism and Bases of Numerical Relativity,” lectures given at the General Relativity Trimester held in the Institut Henri Poincaré (Paris, Sept.-Dec. 2006) and at the VII Mexican School on Gravitation and Mathematical Physics (Playa del Carmen, Mexico, 26. Nov. - 2 Dec. 2006), eprint arXiv:gr-qc/0703035.
- Gourgoulhon, E., P. Grandclement, and S. Bonazzola, 2002, “Binary black holes in circular orbits. I. A global spacetime approach,” *Phys. Rev. D* **65**, 044020.
- Gundlach, C., and J. M. Martín-García, 2006, “Well-posedness of formulations of the Einstein equations with dynamical lapse and shift conditions,” *Phys. Rev. D* **74**, 024016.
- Gundlach, C., J. M. Martín-García, G. Calabrese, and I. Hinder, 2005, “Constraint damping in the Z4 formulation and harmonic gauge,” *Class. Quantum Grav.* **22**, 3767–3774.
- Gürkan, M. A., J. M. Fregeau, and F. A. Rasio, 2006, “Massive Black Hole Binaries from Collisional Runaways,” *Astrophys. J.* **640**, L39–L42.
- Hahn, S. G., and R. W. Lindquist, 1964, “The two body problem in geometrodynamics,” *Ann. Phys.* **29**, 304–331.
- Haiman, Z., B. Kocsis, and K. Menou, 2009a, “The Population of Viscosity- and Gravitational Wave-Driven Supermassive Black Hole Binaries Among Luminous AGN,” *Astrophys. J.* **700**, 1952–1969.
- Haiman, Z., B. Kocsis, K. Menou, Z. Lippai, and Z. Frei, 2009b, “Identifying decaying supermassive black hole binaries from their variable electromagnetic emission,” *Class. Quantum Grav.* **26**, 094032.
- Hannam, M. D., 2009, “Status of black-hole binary simulations for gravitational-wave detection,” *Class. Quantum Grav.* **26**, 114001.
- Hannam, M. D., S. Husa, J. G. Baker, M. Boyle, B. Brügmann, T. Chu, E. N. Dorband, F. Herrmann, I. Hinder, B. J. Kelly, L. E. Kidder, P. Laguna, *et al.*, 2009a, “Samurai Project: Verifying the consistency of black-hole-binary waveforms for gravitational-wave detection,” *Phys. Rev. D* **79**, 084025.
- Hannam, M. D., S. Husa, B. Brügmann, J. A. González, U. Sperhake, and N. Ó Murchadha, 2007a, “Where do moving punctures go?,” *J. Phys. Conf. Ser.* **66**, 012047 in the proceedings of 29th Spanish Relativity Meeting (ERE 2006): Einstein’s Legacy: From the Theoretical Paradise to Astrophysicsl Observation, Palma de Mallorca, Spain, 4-8 Sep 2006.
- Hannam, M. D., S. Husa, B. Brügmann, and A. Gopakumar, 2008a, “Comparison between numerical-relativity and post-Newtonian waveforms from spinning binaries: The orbital hang-up case,” *Phys. Rev. D* **78**, 104007.
- Hannam, M. D., S. Husa, and N. Ó Murchadha, 2009b, “Bowen-York trumpet data and black-hole simulations,” *Phys. Rev. D* **80**, 124007.
- Hannam, M. D., S. Husa, F. Ohme, B. Brügmann, and N. Ó Murchadha, 2008b, “Wormholes and trumpets: Schwarzschild spacetime for the moving-puncture generation,” *Phys. Rev. D* **78**, 064020.
- Hannam, M. D., S. Husa, D. Pollney, B. Brügmann, and N. Ó Murchadha, 2007b, “Geometry and Regularity of

- Moving Punctures,” *Phys. Rev. Lett.* **99**, 241102.
- Hannam, M. D., S. Husa, U. Sperhake, B. Brügmann, and J. A. González, 2008c, “Where post-Newtonian and numerical-relativity waveforms meet,” *Phys. Rev. D* **77**, 044020.
- Harrison, B. K., K. S. Thorne, M. Wakano, and J. A. Wheeler, 1965, *Gravitation Theory and Gravitational Collapse* (University of Chicago Press, Chicago).
- Herrmann, F., I. Hinder, D. M. Shoemaker, P. Laguna, and R. A. Matzner, 2007a, “Gravitational recoil from spinning binary black hole mergers,” *Astrophys. J.* **661**, 430–436.
- Herrmann, F., D. M. Shoemaker, and P. Laguna, 2007b, “Unequal mass binary black hole plunges and gravitational recoil,” *Class. Quantum Grav.* **24**, S33–S42.
- Hinder, I., F. Herrmann, P. Laguna, and D. Shoemaker, 2010, “Comparisons of eccentric binary black hole simulations with post-Newtonian models,” *Phys. Rev. D* **82**, 024033.
- Hinder, I., B. Vaishnav, F. Herrmann, D. M. Shoemaker, and P. Laguna, 2008, “Circularization and final spin in eccentric binary-black-hole inspirals,” *Phys. Rev. D* **77**, 081502(R).
- Holz, D. E., and S. A. Hughes, 2005, “Using gravitational-wave standard sirens,” *Astrophys. J.* **629**, 15–22.
- Hughes, S. A., 2009, “Gravitational waves from merging compact binaries,” *Annu. Rev. Astron. Astrophys.* **47**, 107–157.
- Hughes, S. A., M. Favata, and D. E. Holz, 2005, in *Growing Black Holes: Accretion in a Cosmological Context; Proceedings of the MPA/ESO/MPE/USM Joint Astronomy Conference Held at Garching, Germany, 21–25 June 2004*, edited by A. Merloni, S. Nayakshin, and R. A. Sunyaev (Springer, Berlin/Heidelberg), ESO Astrophysics Symposia, 333–339, eprint arXiv:astro-ph/0408492.
- Hulse, R. A., and J. H. Taylor, 1975, “Discovery of a pulsar in a binary system,” *Astrophys. J.* **195**, L51–L53.
- Husa, S., J. A. González, M. D. Hannam, B. Brügmann, and U. Sperhake, 2008a, “Reducing phase error in long numerical binary black hole evolutions with sixth-order finite differencing,” *Class. Quantum Grav.* **25**, 105006.
- Husa, S., M. D. Hannam, J. A. González, U. Sperhake, and B. Brügmann, 2008b, “Reducing eccentricity in black-hole binary evolutions with initial parameters from post-Newtonian inspiral,” *Phys. Rev. D* **77**, 044037.
- Jaranowski, P., and G. Schäfer, 1998, “Third post-Newtonian higher order ADM Hamilton dynamics for two-body point-mass systems,” *Phys. Rev. D* **57**, 7274–7291 Erratum: *ibid.* **63**, 029902(E) (2001).
- Jennrich, O., 2009, “LISA technology and instrumentation,” *Class. Quantum Grav.* **26**, 153001.
- Jonsson, J., A. Goobar, and E. Mortsell, 2007, “Tuning Gravitationally Lensed Standard Sirens,” *Astrophys. J.* **658**, 52–59.
- Kelly, B. J., W. Tichy, M. Campanelli, and B. F. Whiting, 2007, “Black-hole puncture initial data with realistic gravitational wave content,” *Phys. Rev. D* **76**, 024008.
- Kidder, L. E., 1995, “Coalescing binary systems of compact objects to (post)<sup>5/2</sup>-Newtonian order. V. Spin effects,” *Phys. Rev. D* **52**, 821–847.
- Kidder, L. E., 2008, “Using full information when computing modes of post-Newtonian waveforms from inspiralling compact binaries in circular orbit,” *Phys. Rev. D* **77**, 044016.
- Kidder, L. E., M. A. Scheel, and S. A. Teukolsky, 2001, “Extending the lifetime of 3D black hole computations with a new hyperbolic system of evolution equations,” *Phys. Rev. D* **64**, 064017.
- Kocsis, B., Z. Frei, Z. Haiman, and K. Menou, 2006, “Finding the Electromagnetic Counterparts of Cosmological Standard Sirens,” *Astrophys. J.* **637**, 27–37.
- Kocsis, B., Z. Haiman, and K. Menou, 2008, “Premerger Localization of Gravitational Wave Standard Sirens With LISA: Triggered Search for an Electromagnetic Counterpart,” *Astrophys. J.* **684**, 870–887.
- Kocsis, B., Z. Haiman, K. Menou, and Z. Frei, 2007, “Premerger localization of gravitational-wave standard sirens with LISA: Harmonic mode decomposition,” *Phys. Rev. D* **76**, 022003.
- Kocsis, B., and A. Loeb, 2008, “Brightening of an Accretion Disk due to Viscous Dissipation of Gravitational Waves during the Coalescence of Supermassive Black Holes,” *Phys. Rev. Lett.* **101**(4), 041101.
- Komossa, S., 2003, “Observational evidence for supermassive black hole binaries,” AIP Conf. Proc. **686**, 161–174 in Proceedings of THE ASTROPHYSICS OF GRAVITATIONAL WAVE SOURCES, College Park, Maryland, 24–26 Apr 2003; ed. Joan M. Centrella.
- Komossa, S., V. Burwitz, G. Hasinger, P. Predehl, J. S. Kaastra, and Y. Ikebe, 2003, “Discovery of a Binary Active Galactic Nucleus in the Ultraluminous Infrared Galaxy NGC 6240 Using Chandra,” *Astrophys. J.* **582**, L15–L20.
- Komossa, S., H. Zhou, and H. Lu, 2008, “A recoiling supermassive black hole in the quasar SDSS J092712.65+294344.0,” *Astrophys. J.* **678**, L81–L84.
- Koppitz, M., D. Pollney, C. Reisswig, L. Rezzolla, J. Thornburg, P. Diener, and E. Schnetter, 2007, “Recoil Velocities from Equal-Mass Binary-Black-Hole Mergers,” *Phys. Rev. Lett.* **99**, 041102.
- Kormendy, J., and D. Richstone, 1995, “Inward bound: The Search for supermassive black holes in galactic nuclei,” *Annu. Rev. Astron. Astrophys.* **33**, 581–624.
- Kreiss, H.-O., and J. Oliger, 1973, “Methods for the approximate solution of time dependent problems,” Global Atmospheric Research Programme publications series **10**.
- Krishnan, B., C. O. Lousto, and Y. Zlochower, 2007, “Quasilocal linear momentum in black-hole binaries,” *Phys. Rev. D* **76**, 081501.
- Lang, R. N., and S. A. Hughes, 2006, “Measuring coalescing massive binary black holes with gravitational waves: The impact of spin-induced precession,” *Phys. Rev. D* **74**, 122001 Errata: *ibid.* **75**, 089902 (2007); **77**, 109901 (2008).
- Lang, R. N., and S. A. Hughes, 2008, “Localizing coalescing massive black hole binaries with gravitational waves,” *Astrophys. J.* **677**, 1184–1200.
- Lang, R. N., and S. A. Hughes, 2009, “Advanced localization of massive black hole coalescences with LISA,” *Class. Quantum Grav.* **26**, 094035.
- Laplace, P.-S., 1796, *Exposition du Système du Monde* (Cercle Social, Paris), second edition.
- Lau, S. R., H. P. Pfeiffer, and J. S. Hesthaven, 2009, “IMEX evolution of scalar fields on curved backgrounds,” *Commun. Comput. Phys.* **6**, 1063–1094.
- Le Tiec, A., L. Blanchet, and C. M. Will, 2010, “The gravitational-wave recoil from the ringdown phase of coalescing black hole binaries,” *Class. Quantum Grav.* **27**, 012001.
- Leaver, E. W., 1986, “An Analytic Representation for the Quasi-Normal Modes of Kerr Black Holes,” *Proc. R. Soc. London Ser. A* **402**(1823), 285–298.
- Lehner, L., 2001, “Numerical Relativity: A Review,” *Class. Quantum Grav.* **18**, R25–R86.
- Lichnerowicz, A., 1944, “L’intégration des équations de la

- gravitation relativiste et la problème des  $n$  corps,” *J. Math Pures et Appl.* **23**, 37–63.
- Lindblom, L., B. J. Owen, and D. A. Brown, 2008, “Model waveform accuracy standards for gravitational wave data analysis,” *Phys. Rev. D* **78**, 124020.
- Lindblom, L., M. A. Scheel, L. E. Kidder, R. Owen, and O. Rinne, 2006, “A new generalized harmonic evolution system,” *Class. Quantum Grav.* **23**, S447–S462.
- Lippai, Z., Z. Frei, and Z. Haiman, 2008, “Prompt Shocks in the Gas Disk Around a Recoiling Supermassive Black Hole Binary,” *Astrophys. J.* **676**, L5–L8.
- Lousto, C. O., M. Campanelli, and Y. Zlochower, 2010, “Remnant masses, spins and recoils from the merger of generic black-hole binaries,” *Class. Quantum Grav.* **27**, 114006.
- Lousto, C. O., and Y. Zlochower, 2008, “Foundations of multiple-black-hole evolutions,” *Phys. Rev. D* **77**, 024034.
- Lousto, C. O., and Y. Zlochower, 2009, “Modeling gravitational recoil from precessing highly-spinning unequal-mass black-hole binaries,” *Phys. Rev. D* **79**, 064018.
- Lovelace, G., R. Owen, H. P. Pfeiffer, and T. Chu, 2008, “Binary-black-hole initial data with nearly extremal spins,” *Phys. Rev. D* **78**, 084017.
- MacNeice, P., K. M. Olson, C. Mobarry, R. de Fainchtein, and C. Packer, 2000, “PARAMESH: A parallel adaptive mesh refinement community toolkit,” *Computer Physics Communications* **126**, 330–354.
- Madau, P., and M. J. Rees, 2001, “Massive Black Holes as Population III Remnants,” *Astrophys. J.* **551**, L27–L30.
- Marronetti, P., W. Tichy, B. Brügmann, J. A. González, and U. Sperhake, 2008, “High-spin binary black hole mergers,” *Phys. Rev. D* **77**, 064010.
- McWilliams, S. T., J. I. Thorpe, J. G. Baker, and B. J. Kelly, 2010, “Impact of mergers on LISA parameter estimation for nonspinning black hole binaries,” *Phys. Rev. D* **81**, 064014.
- Megevand, M., *et al.*, 2009, “Perturbed disks get shocked. Binary black hole merger effects on accretion disks,” *Phys. Rev. D* **80**, 024012.
- Michell, J., 1784, “On the Means of Discovering the Distance, Magnitude, etc. of the Fixed Stars, in Consequence of the Diminution of the Velocity of Their Light, in Case Such a Diminution Should be Found to Take Place in any of Them, and Such Other Data Should be Procured from Observations, as Would be Farther Necessary for That Purpose.,” *Phil. Trans. R. Soc. Lond.* **74**, 35–57.
- Miller, M. C., 2009, “Intermediate-Mass Black Holes as LISA Sources,” *Class. Quantum Grav.* **26**, 094031.
- Miller, M. C., and E. J. M. Colbert, 2004, “Intermediate-Mass Black Holes,” *Int. J. Mod. Phys. D* **13**, 1–64.
- Miller, M. C., and V. M. Lauburg, 2009, “Mergers of Stellar-Mass Black Holes in Nuclear Star Clusters,” *Astrophys. J.* **692**, 917–923.
- Milosavljević, M., and E. S. Phinney, 2005, “The Afterglow of Massive Black Hole Coalescence,” *Astrophys. J.* **622**, L93–L96.
- Misner, C. W., 1963, “The Method of Images in Geometrostatics,” *Ann. Phys.* **24**, 102–117.
- Misner, C. W., K. S. Thorne, and J. A. Wheeler, 1973, *Gravitation* (W. H. Freeman, San Francisco).
- Misner, C. W., K. S. Thorne, and W. H. Zurek, 2009, “John Wheeler, Relativity, and Quantum Information,” *Physics Today* **April**, 40–46.
- Nagy, G., O. E. Ortiz, and O. A. Reula, 2004, “Strongly hyperbolic second order Einstein’s evolution equations,” *Phys. Rev. D* **70**, 044012.
- Nakamura, T., K. ichi Oohara, and Y. Kojima, 1987, “General relativistic collapse to black holes and gravitational waves from black holes,” *Prog. Theor. Phys. Suppl.* **90**, 1–218.
- Newman, E. T., and R. Penrose, 1962, “An Approach to Gravitational Radiation by a Method of Spin Coefficients,” *J. Math. Phys.* **3**, 566–578.
- Newman, E. T., and R. Penrose, 1966, “Note on the Bondi-Metzner-Sachs Group,” *J. Math. Phys.* **7**, 863–870.
- Ohta, T., H. Okamura, T. Kimura, and K. Hiida, 1974, “Coordinate Condition And Higher Order Gravitational Potential In Canonical Formalism,” *Prog. Theor. Phys.* **51**, 1598–1612.
- O’Leary, R. M., R. O’Shaughnessy, and F. A. Rasio, 2007, “Dynamical interactions and the black-hole merger rate of the Universe,” *Phys. Rev. D* **76**, 061504(R).
- O’Neill, S. M., M. C. Miller, T. Bogdanovic, C. S. Reynolds, and J. Schnittman, 2009, “Reaction of Accretion Disks to Abrupt Mass Loss During Binary Black Hole Merger,” *Astrophys. J.* **700**, 859–871.
- Oppenheimer, J. R., and H. Snyder, 1939, “On continued gravitational contraction,” *Phys. Rev.* **56**, 455–459.
- Overbeck, J. W., and H. D. Tananbaum, 1968, “Twofold Increase of the High-Energy X-Ray Flux From Cygnus XR-1,” *Phys. Rev. Lett.* **20**(1), 24–27.
- Overbeck, J. W., E. A. Womack, and H. D. Tananbaum, 1967, “High-Energy X-Rays from Cygnus XR-1,” *Astrophys. J.* **150**, 47–56.
- Owen, B. J., 1996, “Search templates for gravitational waves from inspiraling binaries: Choice of template spacing,” *Phys. Rev. D* **53**, 6749–6761.
- Palenzuela, C., M. Anderson, L. Lehner, S. L. Liebling, and D. Neilsen, 2009, “Binary black holes’ effects on electromagnetic fields,” *Phys. Rev. Lett.* **103**, 081101.
- Pan, Y., A. Buonanno, J. G. Baker, J. M. Centrella, B. J. Kelly, S. T. McWilliams, F. Pretorius, and J. R. van Meter, 2008, “Data-analysis driven comparison of analytic and numerical coalescing binary waveforms: Nonspinning case,” *Phys. Rev. D* **77**, 024014.
- Pan, Y., A. Buonanno, L. T. Buchman, T. Chu, L. E. Kidder, H. P. Pfeiffer, and M. A. Scheel, 2010, “Effective-one-body waveforms calibrated to numerical relativity simulations: coalescence of non-precessing, spinning, equal-mass black holes,” *Phys. Rev. D* **81**, 084041.
- Pazos, E., M. Tiglio, M. D. Duez, L. E. Kidder, and S. A. Teukolsky, 2009, “Orbiting binary black hole evolutions with a multipatch high order finite-difference approach,” *Phys. Rev. D* **80**, 024027.
- Peres, A., 1962, “Classical Radiation Recoil,” *Phys. Rev.* **128**, 2471–2475.
- Peters, P. C., 1964, “Gravitational Radiation and the Motion of Two Point Masses,” *Phys. Rev.* **136**, B1224–B1232.
- Peters, P. C., and J. Mathews, 1963, “Gravitational Radiation from Point Masses in a Keplerian Orbit,” *Phys. Rev.* **131**, 435–440.
- Pfeiffer, H. P., D. A. Brown, L. E. Kidder, L. Lindblom, G. Lovelace, and M. A. Scheel, 2007, “Reducing orbital eccentricity in binary black hole simulations,” *Class. Quantum Grav.* **24**, S59–S82.
- Pfeiffer, H. P., L. E. Kidder, M. A. Scheel, and S. A. Teukolsky, 2003, “A multidomain spectral method for solving elliptic equations,” *Computer Physics Communications* **152**, 253–273.
- Pfeiffer, H. P., and J. W. York Jr., 2005, “Uniqueness and Non-uniqueness in the Einstein Constraints,” *Phys. Rev.*

- Lett. **95**, 091101.
- Phinney, E. S., 2007, “Binary black hole evolutions with moving punctures: methods and numerical codes,” bulletin of the 2007 APS April Meeting, abstract T7.00002.
- Poisson, E., 2004, *A Relativist’s Toolkit: The Mathematics of Black-Hole Mechanics* (Cambridge University Press, Cambridge).
- Pollney, D., C. Reisswig, L. Rezzolla, B. Szilágyi, M. Ansorg, B. Deris, P. Diener, E. N. Dorband, M. Koppitz, A. Nagar, and E. Schnetter, 2007, “Recoil velocities from equal-mass binary black-hole mergers: a systematic investigation of spin-orbit aligned configurations,” *Phys. Rev. D* **76**, 124002.
- Pollney, D., C. Reisswig, E. Schnetter, E. N. Dorband, and P. Diener, 2009, “High accuracy binary black hole simulations with an extended wave zone,” arXiv:0910.3803 [gr-qc].
- Portegies Zwart, S. F., and S. L. W. McMillan, 2002, “The runaway growth of intermediate-mass black holes in dense star clusters,” *Astrophys. J.* **576**, 899–907.
- Pretorius, F., 2005a, “Evolution of Binary Black-Hole Spacetimes,” *Phys. Rev. Lett.* **95**, 121101.
- Pretorius, F., 2005b, “Numerical Relativity Using a Generalized Harmonic Decomposition,” *Class. Quantum Grav.* **22**, 425–452.
- Pretorius, F., 2006, “Simulation of binary black hole spacetimes with a harmonic evolution scheme,” *Class. Quantum Grav.* **23**, S529–S552.
- Pretorius, F., 2009, “Binary Black Hole Coalescence,” in *Physics of Relativistic Objects in Compact Binaries: from Birth to Coalescence*, edited by M. Colpi, P. Casella, V. Gorini, U. Moschella, and A. Possenti (Springer, Heidelberg, Germany), 305–369, eprint arXiv:0710.1338 [gr-qc].
- Pretorius, F., and D. Khurana, 2007, “Black hole mergers and unstable circular orbits,” *Class. Quantum Grav.* **24**, S83–S108.
- Racine, E., A. Buonanno, and L. E. Kidder, 2009, “Recoil velocity at second post-Newtonian order for spinning black hole binaries,” *Phys. Rev. D* **80**, 044010.
- Redmount, I. H., and M. J. Rees, 1989, “Gravitational-radiation rocket effects and galactic structure,” *Comments Astrophys.* **14**, 165–175.
- Regge, T., and J. A. Wheeler, 1957, “Stability of a Schwarzschild Singularity,” *Phys. Rev.* **108**(4), 1063–1069.
- Reisswig, C., N. T. Bishop, D. Pollney, and B. Szilágyi, 2009, “Unambiguous determination of gravitational waveforms from binary black hole mergers,” *Phys. Rev. Lett.* **103**, 221101.
- Remillard, R. A., and J. E. McClintock, 2006, “X-ray Properties of Black-Hole Binaries,” *Annu. Rev. Astron. Astrophys.* **44**, 49–92.
- Reula, O. A., 2004, “Strongly hyperbolic systems in General Relativity,” *Journal of Hyperbolic Differential Equations* **1**, 251–269.
- Rezzolla, L., 2009, “Modelling the final state from binary black-hole coalescences,” *Class. Quantum Grav.* **26**, 094023 proceedings of 7th LISA Symposium, Barcelona June 2008.
- Rezzolla, L., E. Barausse, E. N. Dorband, D. Pollney, C. Reisswig, J. Seiler, and S. Husa, 2008a, “Final spin from the coalescence of two black holes,” *Phys. Rev. D* **78**, 044002.
- Rezzolla, L., P. Diener, E. N. Dorband, D. Pollney, C. Reisswig, E. Schnetter, and J. Seiler, 2008b, “The final spin from the coalescence of aligned-spin black-hole binaries,” *Astrophys. J.* **674**, L29–L32.
- Richstone, D., E. A. Ajhar, R. Bender, G. Bower, A. Dressler, S. M. Faber, A. V. Filippenko, K. Gebhardt, R. Green, L. C. Ho, J. Kormendy, T. R. Lauer, *et al.*, 1998, “Supermassive black holes and the evolution of galaxies,” *Nature* **395**, A14–A19.
- Rinne, O., 2010, “An axisymmetric evolution code for the Einstein equations on hyperboloidal slices,” *Class. Quantum Grav.* **27**, 035014.
- Rodriguez, C., G. B. Taylor, R. T. Zavala, A. B. Peck, L. K. Pollack, and R. W. Romani, 2006, “A Compact Supermassive Binary Black Hole System,” *Astrophys. J.* **646**, 49–60.
- Ruffini, R., and J. A. Wheeler, 1971, “Introducing the Black Hole,” *Physics Today* **January**, 30–41 (reprinted in *Physics Today*, April 2009, pages 47 - 53).
- Salgado, M., D. M. del Río, M. Alcubierre, and D. N. nez, 2008, “Hyperbolicity of scalar-tensor theories of gravity,” *Phys. Rev. D* **77**, 104010.
- Santamaría, L., B. Krishnan, and J. T. Whelan, 2009, “Searching for numerically simulated signals from black-hole binaries with a phenomenological template family,” *Class. Quantum Grav.* **26**, 114010.
- Sarbach, O., G. Calabrese, J. A. Pullin, and M. Tiglio, 2002, “Hyperbolicity of the BSSN system of Einstein evolution equations,” *Phys. Rev. D* **66**, 064002.
- Schäfer, G., 1985, “The Gravitational Quadrupole Radiation-Reaction Force and the Canonical Formalism of ADM,” *Ann. Phys.* **161**, 81–100.
- Schäfer, G., 2010, in *Mass and Motion in General Relativity*, edited by L. Blanchet, A. Spallicci, and B. F. Whiting (Springer, New York), Fundamental Theories of Physics, proceedings of the C.N.R.S. “School on Mass” in Orléans, France, June 2008, eprint arXiv:0910.2857 [gr-qc].
- Scheel, M. A., M. Boyle, T. Chu, L. E. Kidder, K. D. Matthews, and H. P. Pfeiffer, 2009, “High-accuracy waveforms for binary black hole inspiral, merger, and ring-down,” *Phys. Rev. D* **79**, 024003.
- Scheel, M. A., H. P. Pfeiffer, L. Lindblom, L. E. Kidder, O. Rinne, and S. A. Teukolsky, 2006, “Solving Einstein’s equations with dual coordinate frames,” *Phys. Rev. D* **74**, 104006.
- Schnittman, J. D., 2007, “Retaining black holes with very large recoil velocities,” *Astrophys. J.* **667**, L133–L136.
- Schnittman, J. D., A. Buonanno, J. R. van Meter, J. G. Baker, W. D. Boggs, J. M. Centrella, B. J. Kelly, and S. T. McWilliams, 2008, “Anatomy of the binary black hole recoil: A multipolar analysis,” *Phys. Rev. D* **77**, 044031.
- Schnittman, J. D., and J. H. Krolik, 2008, “The Infrared Afterglow of Supermassive Black Hole Mergers,” *Astrophys. J.* **684**, 835–844.
- Schutz, B. F., 2009, *A First Course in General Relativity* (Cambridge University Press, New York), second edition.
- Seidel, E., and W.-M. Suen, 1992, “Towards a Singularity-Proof Scheme in Numerical Relativity,” *Phys. Rev. Lett.* **69**(13), 1845–1848.
- Sesana, A., A. Vecchio, and C. N. Colacino, 2008, “The stochastic gravitational-wave background from massive black hole binary systems: implications for observations with Pulsar Timing Arrays,” *Mon. Not. R. Astron. Soc.* **390**, 192–209.
- Sesana, A., A. Vecchio, and M. Volonteri, 2009a, “Gravitational waves from resolvable massive black hole binary systems and observations with Pulsar Timing Arrays,” *Mon. Not. R. Astron. Soc.* **394**, 2255–2265.
- Sesana, A., M. Volonteri, and F. Haardt, 2007, “The imprint

- of massive black hole formation models on the LISA data stream,” *Mon. Not. R. Astron. Soc.* **377**, 1711–1716.
- Sesana, A., M. Volonteri, and F. Haardt, 2009b, “LISA detection of massive black hole binaries: imprint of seed populations and extreme recoils,” *Class. Quantum Grav.* **26**, 094033.
- Shibata, M., and T. Nakamura, 1995, “Evolution of three-dimensional gravitational waves: Harmonic slicing case,” *Phys. Rev. D* **52**, 5428–5444.
- Shibata, M., H. Okawa, and T. Yamamoto, 2008, “High-velocity collision of two black holes,” *Phys. Rev. D* **78**, 101501(R).
- Shields, G. A., and E. W. Bonning, 2008, “Powerful Flares from Recoiling Black Holes in Quasars,” *Astrophys. J.* **682**, 758–766.
- Shields, G. A., D. J. Rosario, K. L. Smith, E. W. Bonning, S. Salviander, J. S. Kalirai, R. Strickler, E. Ramirez-Ruiz, A. A. Dutton, T. Treu, and P. J. Marshall, 2009, “The Quasar SDSS J105041.35+345631.3: Black Hole Recoil or Extreme Double-Peaked Emitter?,” *Astrophys. J.* **707**, 936–941.
- Shoemaker, D. M., K. L. Smith, U. Sperhake, P. Laguna, E. Schnetter, and D. R. Fiske, 2003, “Moving black holes via singularity excision,” *Class. Quantum Grav.* **20**, 3729–3744.
- Silvestri, A., and M. Trodden, 2009, “Approaches to understanding cosmic acceleration,” *Rep. Prog. Phys.* **72**, 096901.
- Simone, L. E., S. W. Leonard, E. Poisson, and C. M. Will, 1997, “Gravitational waves from binary systems in circular orbits: Does the post-Newtonian expansion converge?,” *Class. Quantum Grav.* **14**, 237–256.
- Sintes, A. M., and A. Vecchio, 2000, in *Gravitational Waves and Experimental Gravity: Proceedings of the XXXIVth Recontres de Moriond, January 23-30, 1999, Les Arcs, France*, edited by J. T. T. Van, J. Dumarchez, S. Reynaud, C. Salomon, S. Thorsett, and J. Y. Vinet (World Publishers, Hanoi), 73–78, eprint arXiv:gr-qc/0005058.
- Smarr, L. L., 1975, *The Structure of General Relativity with a Numerical Illustration: The Collision of Two Black Holes*, Ph.D. thesis, University of Texas, Austin, Texas.
- Smarr, L. L., 1977, “Spacetimes generated by computers: Black holes with gravitational radiation,” *Ann. N. Y. Acad. Sciences* **302**, 569–604 eighth Texas Symposium on Relativistic Astrophysics.
- Smarr, L. L., A. Čadež, B. S. DeWitt, and K. Eppley, 1976, “Collision of Two Black Holes: Theoretical Framework,” *Phys. Rev. D* **14**(10), 2443–2452.
- Smarr, L. L., and J. W. York Jr., 1978, “Kinematical conditions in the construction of spacetime,” *Phys. Rev. D* **17**, 2529–2551.
- Smith, J. R. (LIGO Scientific), 2009, “The path to the enhanced and advanced LIGO gravitational-wave detectors,” *Class. Quantum Grav.* **26**, 114013.
- Sperhake, U., E. Berti, V. Cardoso, J. A. González, B. Brügmann, and M. Ansorg, 2008a, “Eccentric binary black-hole mergers: The transition from inspiral to plunge in general relativity,” *Phys. Rev. D* **78**, 064069.
- Sperhake, U., V. Cardoso, F. Pretorius, E. Berti, and J. A. González, 2008b, “High-Energy Collision of Two Black Holes,” *Phys. Rev. Lett.* **101**, 161101.
- Sperhake, U., V. Cardoso, F. Pretorius, E. Berti, T. Hinderer, and N. Yunes, 2009, “Cross section, final spin and zoom-whirl behavior in high-energy black hole collisions,” *Phys. Rev. Lett.* **103**, 131102.
- Sperhake, U., B. J. Kelly, P. Laguna, K. L. Smith, and E. Schnetter, 2005, “Black hole head-on collisions and gravitational waves with fixed mesh-refinement and dynamic singularity excision,” *Phys. Rev. D* **71**, 124042.
- Stroeer, A., J. K. Cannizzo, J. B. Camp, and N. Gagarin, 2009, “Methods for detection and characterization of signals in noisy data with the Hilbert-Huang transform,” *Phys. Rev. D* **79**, 124022.
- Szekeres, P., 1965, “The Gravitational Compass,” *J. Math. Phys.* **6**, 1387–1391.
- Szilágyi, B., L. Lindblom, and M. A. Scheel, 2009, “Simulations of binary black hole mergers using spectral methods,” *Phys. Rev. D* **80**, 124010.
- Teukolsky, S. A., 1972, “Rotating black holes: Separable wave equations for gravitational and electromagnetic perturbations,” *Phys. Rev. Lett.* **29**, 1114–1118.
- Teukolsky, S. A., 1973, “Perturbations of a Rotating Black Hole. I. Fundamental Equations for Gravitational, Electromagnetic, and Neutrino-Field Perturbations,” *Astrophys. J.* **185**, 635–647.
- Thornburg, J., 1993, *Numerical Relativity in Black Hole Spacetimes*, Ph.D. thesis, University of British Columbia, Vancouver, British Columbia.
- Thornburg, J., 2004, “A Fast Apparent-Horizon Finder for three-Dimensional Cartesian Grids in Numerical Relativity,” *Class. Quantum Grav.* **21**, 743–766.
- Thorpe, J. I., S. T. McWilliams, B. J. Kelly, R. P. Fahey, K. A. Arnaud, and J. G. Baker, 2009, “LISA parameter estimation using numerical merger waveforms,” *Class. Quantum Grav.* **26**, 094026 proceedings of the 7th International LISA Symposium, Barcelona, Spain, 16–20 June 2008.
- Tichy, W., B. Brügmann, M. Campanelli, and P. Diener, 2003, “Binary black hole initial data for numerical general relativity based on post-Newtonian data,” *Phys. Rev. D* **67**, 064008.
- Tichy, W., and P. Marronetti, 2007, “Binary black hole mergers: Large kicks for generic spin orientations,” *Phys. Rev. D* **76**, 061502(R).
- Tichy, W., and P. Marronetti, 2008, “Final mass and spin of black-hole mergers,” *Phys. Rev. D* **78**, 081501(R).
- Trias, M., and A. M. Sintes, 2008, “LISA parameter estimation of supermassive black holes,” *Class. Quantum Grav.* **25**(18), 184032 12th GWDAA (Gravitational Wave Data Analysis Workshop), URL <http://stacks.iop.org/0264-9381/25/184032>.
- Vaishnav, B., I. Hinder, F. Herrmann, and D. M. Shoemaker, 2007, “Matched Filtering of Numerical Relativity Templates of Spinning Binary Black Holes,” *Phys. Rev. D* **76**, 084020.
- van Meter, J. R., 2006, in *From Geometry to Numerics* (Institut Henri Poincaré, Paris), <http://luth2.obspm.fr/IHP06/workshops/geomnum/slides/vanmeter>
- van Meter, J. R., J. G. Baker, M. Koppitz, and D.-I. Choi, 2006a, “How to move a black hole without excision: gauge conditions for the numerical evolution of a moving puncture,” *Phys. Rev. D* **73**, 124011.
- van Meter, J. R., D. R. Fiske, and C. W. Misner, 2006b, “Excising das All: Evolving Maxwell waves beyond scri,” *Phys. Rev. D* **74**, 064003.
- van Meter, J. R., M. C. Miller, J. G. Baker, W. D. Boggs, and B. J. Kelly, 2010a, “Test of a General Formula for Black Hole Gravitational Wave Kicks,” *Astrophys. J.* **719**, 1427–1432.

- van Meter, J. R., J. H. Wise, M. C. Miller, C. Reynolds, J. M. Centrella, J. G. Baker, W. D. Boggs, B. J. Kelly, and S. T. McWilliams, 2010b, “Modeling flows around merging black hole binaries,” *Astrophys. J.* **711**, L89–L93.
- Verbiest, J. P. W., *et al.*, 2009, “Timing stability of millisecond pulsars and prospects for gravitational-wave detection,” *Mon. Not. R. Astron. Soc.* **400**, 951–968.
- Volonteri, M., 2007, “Gravitational Recoil: Signatures on the Massive Black Hole Population,” *Astrophys. J.* **663**, L5–L8.
- Wainstein, L. A., and V. D. Zubakov, 1962, *Extraction of signals from noise* (Prentice-Hall, London).
- Walther, B., B. Brügmann, and D. Müller, 2009, “Numerical black hole initial data with low eccentricity based on post-Newtonian orbital parameters,” *Phys. Rev. D* **79**, 124040.
- Weisberg, J. M., and J. H. Taylor, 2005, “Relativistic Binary Pulsar B1913+16: Thirty Years of Observations and Analysis,” *ASP Conf. Ser.* **328**, 25–32.
- Will, C. M., 2006, “The confrontation between general relativity and experiment,” *Living Rev. Relativity* **9**(3) <http://www.livingreviews.org/lrr-2006-3>.
- Wiseman, A. G., 1992, “Coalescing binary systems of compact objects to (post)<sup>5/2</sup>-Newtonian order. II. Higher-order wave forms and radiation recoil,” *Phys. Rev. D* **46**, 1517–1539.
- Yo, H.-J., T. W. Baumgarte, and S. L. Shapiro, 2002, “Improved numerical stability of stationary black hole evolution calculations,” *Phys. Rev. D* **66**, 084026.
- York Jr., J. W., 1979, “Kinematics and Dynamics of General Relativity,” in *Sources of Gravitational Radiation*, edited by L. L. Smarr (Cambridge University Press, Cambridge, England), 83–126.
- York Jr., J. W., 1999, “Conformal ‘thin-sandwich’ data for the initial-value problem of general relativity,” *Phys. Rev. Lett.* **82**, 1350–1353.
- Yunes, N., and F. Pretorius, 2009, “Fundamental theoretical bias in gravitational wave astrophysics and the parametrized post-Einsteinian framework,” *Phys. Rev. D* **80**, 122003.
- Zerilli, F. J., 1970, “Effective Potential for Even-Parity Regge-Wheeler Gravitational Perturbation Equations,” *Phys. Rev. Lett.* **24**(13), 737–738.